Application of Bennett Mechanisms to Long-Span Shelters



Nicholas O'Brien Melin

A dissertation submitted for the degree of Doctor of Philosophy in the Department of Engineering Science at the University of Oxford

Magdalen College

Trinity Term 2004

Copyright © 2005 Nicholas O'Brien Melin
All Rights Reserved

Statement of sources

The work presented in this thesis is, to the best of the candidate's knowledge and belief, original and the candidate's own work, except as acknowledged in the text. The material has not been submitted, either in whole or in part, for a degree at this or any other university.

Nicholas O'Brien Melin

Application of Bennett Mechanisms to Long-Span Shelters

Nicholas O'Brien Melin
Magdalen College
A dissertation submitted for the degree of Doctor of Philosophy in the Department of Engineering Science at the University of Oxford
Trinity Term 2004

Rapidly assembled tent structures are temporary enclosures used to house people or goods. Their uses vary to include recreation, refugee housing, and military shelters. The structural concepts applied in these shelters are as variable as their uses. Some make use of a tensioned fabric and pole system to provide structural strength. Others have a load-bearing frame with attached fabric skin. Further variants make use of inflatable arches or consist of modular containers. Analysis of a number of different types of rapidly assembled tent structures reveals an area where innovation can occur. Conflicts in the last ten years suggest that rapidly assembled shelters for both military purposes and humanitarian relief have the greatest need for innovative solutions.

Existing shelters used by the military lack the versatility and speed of deployment necessary in modern conflict. The lack of scalability in the designs makes it difficult to use an existing tent in different situations. They are slow to construct, heavy, and difficult to transport in large numbers. These problems suggest that there is a need for new shelters that better meet the needs of the military. The application of deployable structures technology meets military's needs for structures with the advantages of a small compacted volume, rapid assembly, and ease of deployment. This makes them ideal for application to shelter structures.

The aim of this dissertation was to develop a new type of deployable, long-span shelter frame based upon tiled Bennett mechanisms. An overlapping combination of

equilateral Bennett mechanisms yields a structure that opens into a half-cylinder shape, providing an enclosed space useful and applicable to the problem of deployable shelters. The specific application considered in the design portion of this process will be a long-span deployable shelter capable of housing military helicopters.

This report details the development of the Bennett Shelter concept. Its deployed and compacted geometries are explored, and a procedure for determining structural properties and dimensions is presented. The full concept for the structure, from outer covering to foundation support is then detailed. Loads affecting the structure are determined, and the process of modelling and analysing the structure is then considered. Optimisation of the structure with respect to weight and serviceability requirements is conducted using a number of different materials, and full analysis of the optimal geometries is completed. As no method exists for evaluating the effect of imperfections on the deployment of overconstrained mechanisms, a procedure is derived. The effects of manufacturing imperfections on deployment of the Bennett mechanism are then explored using the method. A full examination of the variation of energy within the Bennett Shelter during deployment provides valuable insight into the performance of the structure. With the above analysis complete, it is shown that the Bennett Shelter is viable as a long-span deployable shelter.

Keywords: Rapidly assembled tents, deployable structures, overconstrained mechanism, Bennett linkage, tiled Bennett mechanism, energy methods, structural optimisation, mathematical programming, sequential quadratic programming, imperfection analysis.

Preface

The study contained in this dissertation was carried out by the author in the Department of Engineering Science at the University of Oxford during the period from October 2001 to June 2004.

I would like to sincerely thank my supervisor, Dr. Zhong You, for his advice and support. He allowed me to pursue my interest in shelters and introduced me to the subject of deployable structures. It was his encouragement that led me to pursue a DPhil degree and his persistence that ensured I completed it. His leadership was excellent.

Appreciation also goes to my fellow research students in the Department of Engineering Science. Assistance from Kaori Kuribayashi, Yan Chen, Nguyen Dinh Giang, Nguyen Sy Lam and John Pickhaver was essential to my research. I valued their friendship and support. I am grateful to Seth Bodnar, Bradley Henderson, Ian Klaus and Rudyard Sadleir for helping me in so many ways to succeed. The advice, encouragement and good humor of Jessica Dunmore helped me to survive the rigors of the writing-up process.

Financial aid from the United States Army, the Rhodes Trust and Magdalen College for my studies at Oxford University is gratefully acknowledged. The opportunities provided to me during my studies widened my perspective and are appreciated.

I thank my family for their support. During times of stress and uncertainty they are always with me. Specifically, I thank my father Robert Melin for his excellent editorial and legal guidance. As always, he helped me when I needed it most. My love and gratefulness cannot be expressed in words.

Finally, I thank my Lord Jesus Christ for all of the blessings I have experienced in my life. All that I have is due to Him.

"The great liability of the engineer compared to men of other professions is that his works are out in the open where all can see them. His acts, step by step, are in hard substance. He cannot bury his mistakes in the grave like doctors. He cannot argue them into thin air, or blame the judges like lawyers. He cannot, like politicians, screen his short comings by blaming his opponents and hope the people will forget. The engineer simply cannot deny it. If his works do not work, he is damned… On the other hand, unlike the doctor, his is not a life among the weak. Unlike the soldier, destruction is not his purpose. Unlike the lawyers, quarrels are not his daily bread. To the engineer falls the job of clothing the bare bones of science with life, comfort and hope. No doubt, as years go by people forget which engineer ever did it, even if they ever knew. Or some politician puts his name on it. Or they credit some promoter who used other people's money… But the engineer himself looks back at the unending stream of goodness which flows from his success with satisfactions that few professions may know. And the verdict of his fellow professionals is all the accolade he wants."

President Herbert Hoover

Contents

Statement of Sources……ii

Abstract……..…..iii

Preface……v

Table of Contents……vii

List of Symbols……xi

List of Figures……xvi

List of Tables……...xx

1 Introduction……...1

1.1 Rapidly Assembled Tent Structures…….1

1.2 Deployable Structures……..8

1.3 Aim of Research……...9

1.4 Outline of the Dissertation……...9

2 Review of Existing Work……11

2.1 Existing Concepts for Large Tents…….11

2.2 Long-Span Deployable Structures…….16

2.2.1 Inflatable Structures……..……16

2.2.2 Structures made from Scissor-like Elements……....18

2.2.3 Structures Made from Overconstrained 3D Mechanisms…….24

2.3 Analysis of Deployable Structures…….33

2.3.1 General Analysis……...34

2.3.2 Buckling Analysis…….35

2.3.3 Deployment Analysis……37

2.4 Imperfections……..39

2.4.1 Underconstrained and Ideal Mechanisms…….39

2.4.2 Overconstrained Mechanisms……...40

3 Geometrical Analysis of Bennett Structures……43

3.1 Basic Structural Requirements……...43

3.2 Conceptual Development of Subsystems……...46

3.2.1 Design of Joints……46

3.2.2 Fabric Cover……48

3.2.3 Foundation Design……...50

3.2.4 Doorway System……..51

3.2.5 Connector Hallway……...53

3.3 Bennett Shelter……...53

3.3.1 Variable Definitions……..53

3.3.2 Constraints……56

3.4 Relationships among Key Geometric Parameters……..57

3.4.1 Relationship among γ, θ, φ, and α……57

3.4.2 Polygon Analogy……...58

3.4.3 Relationship between l and l'……60

3.4.4 Structure Length……61

3.4.5 Dimensions of Compacted Segment……62

3.5 Geometric Analysis of Configurations……...65

4 Structural Analysis for a Perfect Bennett Shelter……...69

4.1 Analysis Requirements and Design Methodology……..…69

4.2 Load Analysis…….……72

4.2.1 Load Combination and Application……..72

4.2.2 Dead Loads……....74

4.2.3 Wind Loads……...……75

4.2.4 Snow Loads……..……..76

4.3 Selection of Material and Sections…….77

4.4 Serviceability Analysis……...81

4.4.1 Analysis Procedure……81

4.4.2 Analysis of Bennett Shelter……...83

4.5 Stress Analysis Procedure…….……93

4.5.1 Member Stress Analysis Procedure……..93

4.5.2 Member Stress Analysis……97

4.5.3 Stress Analysis Procedure for Joints…….……99

4.5.4 Joint Stress Analysis……...102

4.6 Buckling Analysis of the Bennett Shelter…….……..104

4.6.1 Analysis Procedure……..104

4.6.2 Analysis Results…..…….107

4.7 Frequency Analysis…..……110

4.7.1 Analysis Procedure…….…….110

4.7.2 Analysis Results…..…….112

4.8 Prototype Construction……..……..113

4.9 Conclusions about the Deployed Configuration……118

5 Imperfection Analysis……...……119

5.1 Energy Methods…….……..119

5.1.1 Strain Energy and Complementary Strain Energy…..……119

5.1.2 Relationships derived from Virtual Work and Virtual Complementary Work……..……123

5.2 Application of Energy Methods to Indeterminate Structures…….……125

5.3 Validation of Energy Methods……127

5.4 Imperfection Analysis of an Imperfect Overconstrained Parallelogram Linkage……..……..131

5.5 Optimisation Techniques…….……137

5.6 Optimisation of the Simple Overconstrained Mechanism using Explicit Methods……..…….143

5.7 Approximate Expressions of Energy Functions…..……..145

6 Analysis of the Bennett Shelter with Imperfections…….……..158

6.1 Model Definition……..158

6.2 Analysis of Single Unit……164

6.3 Analysis of Two Units…….168

6.4 Discussion and Conclusions……..…170

7 Concluding Remarks……172

7.1 Achievements…..…….172

7.2 Future Work…….……175

References……...…177

Appendix 1…….……182

List of Symbols

Below is a short list of symbols representing variables used in this study.

α	Primary skew angle
α_2	Secondary skew angle
β	Central angle of regular polygon
χ	Resistance factor
δ	Member deformation
Δ	Global displacement
ε	Member strain
ε_0	Member initial strain due to imperfection
ε_{0n}	Member initial strain for the current optimisation iteration
ϕ	Kinematic variable for Kuznetsov's simple, overconstrained mechanism
γ	Angle representing the 'bend' in a Bennett segment
η	Included angle in truss cap of Kuznetsov's simple, overconstrained mechanism
θ	Deployment angle (angle between members in a Bennett Mechanism)
ϑ	Damping ratio
ρ	Material density
σ_f	Axial stress in the fibers of a composite material layer
σ_m	Axial stress in the matrix of a composite material layer
σ_{yp}	Axial yield stress
σ_1, σ_2, σ_3	Principle stresses at a point of interest
τ	Shear stress

τ_{oct}	Octahedral shearing stress
τ_{yp}	Shear yield stress
κ	Member curvature
φ	Deployment angle (angle between members in a Bennett Mechanism)
λ	The increment size used to approximate the partial derivative
λ_i	Eigenvalue of the *i*th buckling mode
μ	Included angle between bars in a Bennett segment, the supplement of φ
Π	Total energy
Π^*	Total complementary energy
υ_i	Load factor
ω_n	Undamped natural frequency
ξ	Kinematic variable for a Bennett segment
ψ^N	Modal shapes
a_i	Length of link *i*
A	Area
A_i	Transformation matrix from link *i*+1 to link *i*
A_s	Area of the structure doorway (short axis of the deployed structure)
A'	Outward area from a point of interest on member cross-section
b	Number of joints in a linkage
B	The strain displacement matrix
B_a	Number of bars in a structure
c	Stiffness constant
d	Bar diameter
d_i	offset along joint *I*

D	Constant relating stress and strain
D_e	Dead loads on structure
E	Modulus of elasticity
f	Kinematic variable in a linkage
F	Functional requirements
$F(t)$	Time varying force
F_v	Ultimate strength of the connected material
g	Intermediate relation used to determine the compatibility of structure dimensions with compacted segment dimensions
G	Shear modulus
G_e	Geometric parameters
H	Deployed structure height
I	Moment of inertia
$[I]$	Identity matrix
j	Volume fraction of fiber
k	Structure stiffness
K_0^{NM}	Stiffness matrix for degrees of freedom M and N corresponding to the base state
K_Δ^{NM}	Differential stiffness matrix due to incremental loading
l	Bennett bar length
l'	Polygon side length
l_b	Structure bar length
l_{max}	Maximum Bennett bar length useable for a given set of compacted segment dimensions

L	Deployed structure length
L_c	Compacted structure length
m	Mobility of a linkage
M	Bending moment in a member
n	Number of sides of the polygon used to model the side view of a Bennett Structure
n_i	Initial n value
n_1, n_2	Local element coordinate axes
N_i	Internal force in member i
p	Optimal performance of a structure
P	Material properties
P^N	Effects of preloads
Q_i	Load effect on the structure
Q^N	Incremental loading pattern
r	3 for planar and 6 for spatial mechanisms
r_i	Inner radius of pipe section
r_o	Outer radius of pipe section
r_s	Distance from the center of a regular polygon to the midpoint of a side
r_v	Distance from the center of a regular polygon to the intersection point of two sides
R_n	Nominal strength of the structure
s	Number of members in a linkage
S	Snow loads on the structure
t	Thickness of the member at a point of interest
T	Element transformation matrix from global to local coordinates

u	Number of units per collapsible segment
U	Strain energy
U_0	Strain energy density
U^*	Complementary strain energy
U_0^*	Complementary strain energy density
v	Number of collapsible segments in a Bennett structure
V	External energy due to applied loads
V_{max}	Maximum shearing force in a pinned joint
w_e	Tributary width for exterior load-carrying members
w_i	Tributary width for interior load-carrying members
W	Deployed structure width
W_c	Compacted segment width
W_i	Wind loads on the structure
x	System displacement
$\dot{x}$	System velocity
$\ddot{x}$	System acceleration
X_1	Component of deployed shelter length
X_2	Component of deployed shelter length
y	Distance from the center of the member to the point of interest
$\bar{y}$	Distance from the point of interest on a cross-section to the surface of the member

List of Figures

1.1 The (a) Yurt and (b) Scott Tent (Manfield, 2000)...…...…….3

1.2 Photographs of (a) the MGPTS field tent, (b) soldiers erecting the TEMPER logistics tent and (c) the LAMS (U.S. Army Soldier and Biological Chemical Command,

1999)……..…….……..6

2.1 Diamond Beam Aircraft Carrier Shelter (ABLY Shelters, 2004)……...……...……12

2.2 (a) The interior of the LANMaS airbeam shelter (Kennedy, 2001), (b) the DRASH XB Series Shelter (DHS Systems LLC, 2002), and (c) the ABLY LVRE Shelter (Ably Shelters, 2004)…….……...……...…….14

2.3 (a) The traveling exhibition pavilion for the United States Atomic Energy Commission and (b) the Fuji Group Pavilion (Gantes, 2001)…….……..17

2.4 (a) Stiffened spherical dome by Pinero. (b) Geodesic deployable x-frame dome by Zeigler (Langbecker, 2001)……...…….19

2.5 The Estran 1 Shelter with (a) cover undeployed and (b) cover attached (Hernandez, 1996)……...……...…….21

2.6 Conceptual drawings of Escrig's swimming pool cover. (a) Undeployed; (b) spread horizontally; (c) spread vertically; (d) deployed and (e) a photograph of the structure (Sanchez,

1996)……...……22

2.7 A foldable barrel vault using scissors elements (Langbecker, 2001)…...……..24

2.8 Coordinate system for two links connected by revolute joints……..……26

2.9 An equilibrium Bennett mechanism……...……28

2.10 (a) The Myard 5*R* linkage, (b) a Goldberg 5*R* linkage composed by summation (Chen, 2003)……..……..30

2.11 (a) Goldberg 6*R* linkages composed by summation and (b) subtraction (Chen, 2003)……...……31

2.12 Combination of Bennett Mechanisms yielding a cylindrical profile……...…...….32

2.13 Reticulated Shells (Gioncu, 1994)……...……...…….36

2.14 Simple overconstrained mechanism with varied bar lengths (Kuznetsov, 1991)…42

3.1 Deployment sequence of the shelter structure. (a) One folded element of the shelter structure. (b) All four elements stacked as they would be on a military pallet. (c) Structural segments laid out before connection. (d) Connected structure in folded position. (e) Structure partially deployed and (f) fully deployed. (g) Outer structural lining for the structure. (h) Inner insulation for the structure in case of cold weather…….……...…45

3.2 Swivel couplers…….…….……47

3.3 Fabric interaction with frame……...…..49

3.4 Duckbill anchor system…….……...……..50

3.5 A 3-D view of an equilateral Bennett mechanism……...…..54

3.6 Side view of a structure……...……...55

3.7 A segment of the Bennett Shelter……...…...56

3.8 Polygon approximation of a shelter doorway……....58

3.9 l and φ are independent of l'……...60

3.10 Structure length……...……..... 61

3.11 A typical Bennett segment in fully compacted configuration…..……63

3.12 Relationship between l_{max} and φ..……...…….64

3.13 Geometric design procedure……...…….68

4.1 Projection of the structure showing points where the structure carries loads…...….74

4.2 Application of wind loads to the structure……...……..76

4.3 Approximate position of analysis points for deflection…….……..…..83

4.4 ABAQUS CAE view of the initial configuration with pinned boundary conditions……...…….……..84

4.5 *Spread* in Bennett segment……...…….….86

4.6 Deflection and structure weight vs. φ for Models five to eleven….……..88

4.7 Deflection vs. φ for different steel cross-sections for Models seven to eleven……89

4.8 Deflection versus bar diameter for Model nine……..90

4.9 Analysis points on member cross-section……..94

4.10 Analysis points for bending stresses..……...……...95

4.11 Buckling Modes for the Bennett Shelter (a) Initial configuration (b) Load Cases 1,2, 3, 4, (c) 5 and (d) 6…….109

4.12 Modal Shapes for Modes (a) 1, (b) 2, (c) 3 and (d) 4……113

4.13 Pictures of the ABLY Prototype from the (a) side, (b) front and (c) compacted..116

4.14 (a) Space between the bolt and the bar in a pinned connection, (b) deformation along a bar during load-deflection testing and (c) Deformed bolts from the prototype……...117

5.1 Stress-strain diagram……120

5.2 Linear elastic stress-strain diagram with initial strain…… …….121

5.3 Simple, statically indeterminate structure……...…….128

5.4 Overconstrained parallelogram linkage……...……131

5.5 Overconstrained parallelogram linkage with truss cap……...…….134

5.6 Internal energy vs. deployment angle for a single imperfection……..136

5.7 Design space for simple mechanism with two imperfections……...……...138

5.8 Complementary strain energy through deployment……..…..…..145

5.9 Approximate sensitivities optimisation flowchart……...…149

5.10 Explicit sensitivities optimisation flowchart……..…154

6.1 One-unit Bennett segment……159

6.2 Orientation of extra bar for ξ=60 °…….……161

6.3 Test patterns…….……167

6.4 Two-unit Bennett segment……..…….……169

List of Tables

4.1 Material Indices……..……79

4.2 Material properties of interest……81

4.3 Design specifications for helicopter structure……..……..83

4.4 Deflection with CFRP cross-sections…….……84

4.5 Deflection with aluminium cross-sections…….84

4.6 Geometric specifications for analysis models……..……..87

4.7 Vertical deflection considering self-weight……...……91

4.8 Vertical Deflection for Aluminium and Steel……91

4.9 Drift for longitudinal wind loading…….……...92

4.10 Drift for cross wind loading…….……92

4.11 Model ten member stress factors of safety…….……..96

4.12 Internal forces and moments for carbon fibre composite members…….98

4.13 Bolt material properties……..102

4.14 Pin factors of safety using aluminium members and A490 bolts……...102

4.15 Pin factors of safety using steel members and A490 bolts….……103

4.16 Load Cases for Buckling Analysis……105

4.17 Results of linear buckling analysis for aluminium shelter…….……107

4.18 Results of linear buckling analysis for steel shelter…….……..107

4.19 Frequency analysis results…….……112

4.20 Design details of ABLY model……..114

4.21 Bennett Shelter component dimensions…...……..117

5.1 ABAQUS runs for each iteration of approximate sensitivities optimisation……...150

5.2 Approximate sensitivities method results……150

5.3 Explicit sensitivities method……155

6.1 Approximate sensitivities optimisation for ξ=5°……164

6.2 Approximate sensitivities optimisation for ξ=15°……164

6.3 Approximate sensitivities optimisation for ξ=30°……164

6.4 Local element internal forces for ξ=15°……165

6.5 Global forces and moments at the top and bottom of joints 2 and 7……165

1 Introduction

1.1 Rapidly Assembled Tent Structures

Rapidly assembled tent structures are temporary enclosures used to house people or goods. Their uses vary to include recreation, refugee housing, and military shelters. The structural concepts applied in these shelters are as variable as their uses. Some make use of a tensioned fabric and pole system to provide structural strength. Others have a load-bearing frame with attached fabric skin. Further variants make use of inflatable arches or consist of modular containers. These structures range in size from single-person dwellings to warehouses. The wide variations in both use and size make tent structure design a considerable challenge. Analysis of a number of different types of rapidly assembled tent structures provides a set of criteria for successful tents. It also reveals areas where innovation is desirable.

Tents are the oldest and most enduring form of housing. Early nomadic societies required housing they could move from place to place in order to find food. This often meant moving from moderate to extreme environments. Any shelter used by these people needed to be robust and flexible. One such shelter is the Yurt. Used by Turkish and Mongolian tribes, this shelter was and is the primary dwelling of the tribesmen. It is disassembled and carried across long distances. It is a frame structure, in which fabric plays no part in structural stability. The frame consists of wooden lattice sections bound together into a cylindrical wall system. A timber roof ring is attached and a band is fastened around the wall system to counteract the outward thrust of the roof, see Fig. 1.1(a). The frame is then covered with felt. The average weight of a Yurt is 250kg, which is around 50kg per occupant. It packs into five to six separate component bundles, including roof poles, lattice sections, and rolls of felt. The nomads transported these

bundles on camels or by cart. The longevity of the structure testifies to its success. It is used today in much the same way it was a thousand years ago (Manfield, 2000).

What elements of a successful tent shelter can be drawn from the Yurt? Tent structures must meet transportation requirements. The Yurt has elements that are compactable (the wooden lattice), and the structure is light enough to transport using pack animals. Rapidly assembled tents must also be simple. With only three major components, the Yurt could move often and required no special expertise. The materials used in the structure are readily available in many different areas, and the assembly process is straightforward.

A more modern use for tents is as expedition shelters. Designed for harsh conditions, these structures have very specialised requirements. Structure weight and compacted volume must meet narrower tolerances dictated by the method of transportation. Even the packing plans for these structures are dictated. The classic example of such structures is the Scott Tent, see Fig. 1.1(b). Used by Captain Robert Scott on his Antarctic expeditions, it was the first modern deployable expeditionary tent. Its intended use was for Arctic exploration, which governed its design. The sleds were small, and needed to carry all supplies for the expedition. The solution to these constraints was a frame structure consisting of four hollow aluminum poles connecting together at an apex to form a pyramid. It was then covered with lightweight fabric. Its modular packing system incorporated many other required items for the trip, which minimised total packed volume. This design has a weight of 15kg per person making it man portable (Manfield, 2000). This design was successful and is used in Antarctic expeditions today. It is important to note that transportation requirements for this type of structure make a simple design necessary. There is little area for innovation in expedition structures.



(a) (b)

Fig. 1.1 The (a)Yurt and (b) Scott tent (Manfield, 2000)

Conflicts in the last ten years suggest an increasing need for rapidly assembled shelters for both military purposes and humanitarian aid. Military actions in Somalia, Bosnia, Kosovo, Afghanistan and most recently Iraq all involved the management of large numbers of displaced people. Non-governmental organizations that provide relief in these situations include the United Nations High Council for Refugees (UNHCR) and Oxfam. The criteria for structures used in these situations are straightforward. They must be cheap to manufacture in large numbers and must meet the environmental requirements of the area. An example of these shelters is the UNHCR tent. It is a tensile structure that uses guy ropes and steel ridge poles to tension the fabric cover and support loads. This is the same structural concept used for most recreational tents. Designed for use in a wide variety of situations and climates, it is simple and cheap to manufacture. It does, however, have drawbacks. Since it weighs 25kg per occupant, the UNHCR tent is bulky when compacted. Thus, it requires a cart or vehicle to transport. Additionally, the tent lacks the structural strength to operate in extreme environmental conditions.

Efforts are ongoing to produce better shelters. Notable among these is the Oxfam Emergency Shelter developed by Peter Manfield at Cambridge University. Using PVC

pipe and commonly available fabrics, Manfield addressed many shortcomings of conventional shelters. Although issues remain with his design, such as its performance under environmental loading, his is one among many emerging refugee shelters based upon simple structural concepts.

Although non-governmental organizations manage refugees in the long term, the military often deals with their immediate needs. During the Kosovo conflict in 1999, over a million refugees fled the conflict and required aid (KFOR Online, 2001). NATO forces dealt with the difficult problem of housing a military task force and large numbers of civilians with military tents. Poor quality and inefficient shelters caused delays and complicated an already difficult mission.

Thus, the requirements for general-use military shelters are changing. Situations demand rapid deployment of military assets and a speed of execution far faster than required during the Cold War. Indeed, equipment in military inventories is being updated and redesigned to ensure that all materials necessary for a military operation can be palletised and loaded onto military transport aircraft. Shelter structures required for modern conflict must be versatile, rapidly deployable, and quickly movable to different areas of operation.

There are hundreds of different types of military shelters in use at present, with functions ranging from battlefield command center to aircraft storage hangar. Despite this variety, few structural concepts are utilised. Three representative tents are the MGPTS (Modular General Purpose Tent System), the TEMPER (Tent, Extendable, Modular, Personnel), and the LAMS (Large Area Maintenance Shelter). The MGPTS is designed for use near the front lines. This tent is erectable by four soldiers in thirty minutes. It is also modular, which allows for construction of complexes. It does, however, have problems. The structure is pole-supported, as shown in Fig. 1.2(a), which

makes it less rigid than framed structures. It is, therefore, difficult to use the MGPTS for long-term applications. The structure makes use of guy ropes, which increases its footprint and slows erection time. Also, the MGPTS is not scalable. It comes in three basic sizes, and the structural concept is not useable for large-scale tents (U.S. Army Soldier and Biological Chemical Command, 1999).

The TEMPER provides some advantages in comparison with the MGPTS, but is again a tent system designed for a specific purpose. This tent is used for base camps and supply and logistics nodes. It has a frame structure, as shown in Fig. 1.2(b), which makes it more resilient than the MGPTS. It is also modular, which allows for the erection of structural complexes. The structure, however, is quite heavy at 603kg. Soldiers cannot transport this tent without some mechanical assistance. Additionally, the TEMPER comes with lighting, heating, and cooling systems suitable for long-term applications (U.S. Army Soldier and Biological Chemical Command, 1999).



(a) (b)



(c)

Fig. 1.2 Photographs of (a) the MGPTS field tent, (b) soldiers erecting the TEMPER logistics tent and (c) the LAMS (U.S. Army Soldier and Biological Chemical Command, 1999).

The U.S. military also uses a number of large deployable shelters. In order to store and conduct maintenance on large pieces of equipment like the Apache Attack Helicopter, long-span shelters are required. The Army's current long-span shelter is the Large Area Maintenance Shelter (LAMS). It is a tensile fabric structure that utilises a system of 17 aluminium arches connected together by rain gutters, see Fig. 1.2(c). Its dimensions are 36.6m long by 23m wide by 9.5m high. This shelter has a number of problems that make innovation necessary. It weighs 12100kg, which is far too heavy to be transported using cargo aircraft. The LAMS must, therefore, be shipped by boat to its desired destination. It takes at least five days to erect the structure (U.S. Army Soldier and Biological Chemical Command, 1999). After action reviews from Operation Desert Storm reported many units left the LAMS at their home stations because it was so bulky

and difficult to erect. It is desirable to rapidly deploy aircraft like the Apache Helicopter on short notice. The required deployment and erection times for the LAMS does not match these operational requirements. There is a need for innovation with long-span military shelters.

This examination of the historical, expedition, refugee and military structures reveals a number of criteria necessary for a useful, rapidly deployable structure. Rapidly deployable shelters, whether large or small, should have the following characteristics:

- Structures should be lightweight and transportable aboard the modes of transport available for the application. For military and refugee applications, this is military cargo aircraft.

- Shelters must be cheap. Logistical equipment receives far less funding in military budgets than weapons or vehicles.

- Shelters must be resilient and easy to repair. Rapidly deployable shelters are used all over the world in harsh conditions.

- Shelters must be easily and quickly erected and struck. This is especially important for military tents. The fluid nature of the battlefield makes it dangerous to keep command and logistical centres in one place for an extended period of time. They must be able to move quickly from location to location.

- Shelters must be versatile. Organisations with large tent inventories, such as the military, require the ability to connect shelters of different size and configuration into complexes.

Among the categories of shelters reviewed above, the long-span shelter is the one that most needs innovation. The conventional frame and pole-supported structural concepts are slow to set up and heavy. For this reason, it is useful to consider deployable structures.

1.2 Deployable Structures

Deployable structures can fold into a small size for delivery and reopen to their original shape before becoming functional. The study and development of deployable structures has been primarily focused on aerospace applications. Large structures, such as antennas and spacecraft, must be packaged to fit into a launch vehicle and then expanded when reaching orbit. Deployable structures developed in response to these issues have the advantages of a small compacted volume, rapid assembly, and ease of deployment (Pellegrino, 1995). Because of these positive qualities, deployable structures are also applied on earth for retractable stadium roofs and shelters of various types (Escrig, 1996).

Deployable structures are divided into two categories: deformable structures or structural mechanisms. Deformable structures depend upon the elasticity of their members to allow mobility from the deployed to compacted shape. Examples of this category of structures include rubber balloons, tape measures, and springs. Performance of the structure is dependent on the strain level in the structure and the type of material. This limits their applicability to shelter structures, as the stressed structures are not suitable for repeated deployments.

Structural mechanisms are structures with an internal degree of mobility. Deployment does not induce any strain in structural elements. The structural members are assembled in such a way that geometric compatibility conditions are met throughout deployment. Robust performance and repeatability of deployment characterise structural mechanisms. They can also compact to a small fraction of their deployed volume. The deployment process can be controlled or terminated whenever required with the structure assuming any of the intermediate stable configurations. Most structural mechanisms are, however, very difficult to manufacture and more expensive than other conventional

structures. The advantages of structural mechanisms compare favourably to the requirements specified above for deployable tents. They deploy quickly and easily and can have a small compacted volume. These positive aspects indicate their applicability to long-span shelters.

1.3 Aim of Research

The objective of this project is to explore the feasibility of using one type of structural mechanism, the tiled Bennett mechanism, as a frame. Consideration is given to issues of geometry in deployed form and its structural capacity as a shelter frame. Imperfections in overconstrained mechanisms are explored. Analysis of energy variation through deployment of geometrically non-ideal mechanisms is conducted. It is then possible to develop a generalised procedure for determining the worst-case pattern of imperfections. The specific application considered in this study is a large deployable hangar to house an Apache Longbow Helicopter. The necessary subsystems for this hangar are a foldable frame, door system, connector hallways, versatile foundation system, and a cover. These sub-systems will be considered, and the concept of a deployable, large-scale tent structure using tiled Bennett mechanisms will be completely developed.

1.4 Outline of the Dissertation

This dissertation proceeds as follows. Chapter 2 details the existing concepts for large tents. It then examines different types of deployable structures and analysis methods. In Chapter 3, the tiled Bennett mechanism is considered. The concepts for the collapsible frame and subsystems are developed. The open, cylindrical configuration is then analysed to determine its geometrical relationships. A procedure is developed to

provide the structural properties for given shelter dimensions. Chapter 4 details the structural analysis methodology for a Bennett Shelter with ideal geometry. This methodology is applied to validate the Bennett Shelter as a structural frame. Chapter 5 explores the effect of imperfections on overconstrained mechanisms. A procedure is then developed for determining the worst-case pattern of initial imperfections for a given overconstrained mechanism. This procedure is applied in Chapter 6 to the Bennett Shelter to determine the effect of imperfections. Chapter 7 offers concluding remarks.

2 Review of Existing Work

Research and development in the area of both large-span shelters and deployable structures is ongoing. In order to understand the progress in both of these areas it is necessary to survey existing work. Section 2.1 examines existing concepts for large tents. Advantages and disadvantages of these systems are considered, as well as the structural concepts employed. Consideration will then be given to deployable structures in Section 2.2. The three subsets of deployable structures examined in this chapter are inflatable structures, structures composed of scissor-like elements and those composed of overconstrained 3-D mechanisms. Section 2.3 then details existing work in the general analysis of deployable structures and Section 2.4 covers analysis of imperfections.

2.1 Existing Concepts for Large Tents

Long-span tent structures are widely used for recreation, storage or long-term construction projects, and military applications. The robustness of the structural system utilised is generally linked to duration of its use. Recreational tents are the shortest duration structures. They are often used for social functions. These shelters use a pole and guy rope system to tension fabric and support loads (Gantes, 2001). They are not designed to withstand extreme environmental loading. A large number of companies have developed different variations of this structure, all using simple structural concepts. There is little room for innovation in this area.

Warehouse or construction shelters are often used for very long durations. They can cover projects for months or years. As such, the structural concepts utilised in these shelters must be robust. Extreme environmental loading must be considered. Additionally, the structures must have large spans in order to allow maximum storage or overhead clearance. An example of this type of structure is the ABLY Diamond Beam

Shelter system. This shelter system consists of a lightweight aluminum truss frame that can be altered to meet desired shelter dimensions. Shelters are available with up to 35m clear span widths and 20m height. Any desired length can be met and then extended in 3m increments. The largest structure built using this system was a shelter used to repaint the deck of the HMS Illustrious, see Fig. 2.1. The ship required a covered area of $4000m^2$. The structure took two weeks to completely construct, with sections completed within the first week (ABLY Shelters, 2004). Erection of these structures requires the use of cranes, and they must be fabricated on site before lifting of segments can begin.

Deployable shelters meant for long-term use, such as the ABLY Diamond Beam, make use of structural concepts used in conventional construction. The diamond beam is a truss section that can be assembled on site. The ABLY structure uses fabric cladding, which is lightweight and allows a lighter truss. Conventional structures use heavier cladding and trusses. Adaptation of conventional structural concepts and use of lightweight materials is the hallmark of long-term shelter design.



Fig. 2.1 Diamond beam aircraft carrier shelter (ABLY Shelters, 2004)

Military structures, because of their deployability and ease of erection requirements, cannot use conventional structural concepts. Loading and size

requirements make concepts used for recreational shelters unsuitable. It is necessary for soldiers to be able to construct shelters quickly and easily. As detailed in Chapter 1, the LAMS fails to meet these requirements. A great deal of work has therefore been done on replacing the shelter with more deployable alternatives. The LANMaS is the US military's newest aircraft hangar and maintenance shelter. It uses inflatable arches, as shown in Fig. 2.2(a), to support the canvas structure. This decreases the weight of the structure to 6801kg and allows it to be set up without ladders or additional equipment. Whereas the LAMS took ten soldiers seven days to set up, the LANMaS takes only two days (Kennedy, 2001). This shelter has some problems. The weight of the LANMaS is significant. The airbeams, which are made of a continuous tubular laminate surrounded by a high-strength sleeve, are complex technologically and difficult to repair. Use of airbeams is also unproven in terms of long-term durability. The structure has been in development for ten years without being fielded so no data exists on its performance. A simpler, lighter structure with a more rigid frame structure would represent a significant improvement.

Other tent systems currently fielded in the United States Army are the DRASH XB and J series tents. Designed by DHS Systems in Orangeburg, New York, they represent a significant improvement over current models used in the military. These deployable structures use a scissors structural mechanism with locking joints (DHS Systems LLC, 2002). The structural system has two degrees of mobility and folds to 2% of its deployed volume. The cover is attached to the frame, allowing for erection of the structures by two to four people in minutes. Fig. 2.2(b) shows an example. The DRASH systems are lightweight and simple to erect, but have difficulties with scalability. The J Series tent, which is designed for use as a command centre, is the largest configuration possible using the DRASH structural system. To erect it, the frame is first expanded

from the compacted configuration. A bladder is then placed under the structure and inflated. This articulates the structure until the joints lock into place. It requires, due to its size, interior portal frames in case the locking joints fail due to worst-case loading or the accumulation of snow on the structure over time. The strength of the locking mechanism in the joint controls the maximum size of DRASH structures. DRASH tent systems are currently the most expensive on the market, requiring significant funds to implement in military units. A J Shelter with trailer, heating, and cooling systems costs $90,000.00 (£59778.00). Discussions with logistical experts in Ministry of Defence, United Kingdom, and Department of Defense, United States of America, also revealed problems with long-term durability of the fabric cover of the structure and the locking joints (DHS Systems LLC, 2002).



(a) (b)



(c)

Fig. 2.2 (a) The interior of the LANMaS airbeam shelter (Kennedy, 2001), (b) the DRASH XB Series Shelter (DHS Systems LLC, 2002), and (c) the ABLY LVRE Shelter (Ably Shelters, 2004).

ABLY Shelters, the makers of the Diamond Beam shelters, also developed a deployable helicopter shelter for the UK military. The Lightweight, Very Rapidly Erected (LVRE) shelter is a mobile forward aircraft shelter designed for the Apache Longbow Helicopter, see Fig. 2.2(c). It consists of two lightweight truss arches and a system of lines running parallel to the arches that tension a fabric skin. Its deployed dimensions are 35.5m long, 15.3m wide and 7.8m tall. It weighs 6800kg. One erects the structure by assembling and attaching the arch segments to a ground beam, raising the arches and then pulling across the tensioned skin. This shelter has many advantages. A team of four soldiers can erect the structure in five hours using no cranes or lift equipment. It is transportable on military aircraft using approved container systems. It can be moved when erected and meets all environmental loading requirements (ABLY Shelters, 2004). It is important to note, however, that this structure is designed for a specific purpose, and cannot interface with other shelters. This makes it less versatile than the DRASH shelters, which have multiple uses and configurations. Also, this structure makes use of lightweight truss arches, which is a conventional structural concept.

The concepts applied in the military shelters detailed above have both advantages and disadvantages. Airbeam technology greatly speeds up the erection of large-scale structures like the LANMaS, but is complex and prone to damage. Deployable frame tents with locking joints, such as the DRASH tents, improve on many of these shortcomings but still have problems. They are inefficient, unsuitable for large-scale structures, and very expensive. The LVRE Shelter is versatile and quick to construct. It is designed, however, for a specific application and requires a complicated assembly process. A new deployable structure, able to avoid these problems and provide versatile

structure options, would certainly enhance the ability of the military to operate in a variety of situations.

2.2 Long-Span Deployable Structures

Long-span deployable structures based upon structural mechanisms are few. Research in deployable structures has focused largely on aerospace applications. Some work, however, has been done in considering the application of these structures to deployable shelters. The three areas considered are inflatable structures, deployable scissors structures and structures composed of 3-D overconstrained mechanisms.

2.2.1 Inflatable Structures

Long-span inflatable shelters have two basic structural concepts: air-supported membranes and air-inflated membranes (Dent, 1970). Air supported membrane shelters employ positive internal air pressure to support a membrane. Entrance and egress from the structure is accomplished across a pressure differential. Thus, there is a leakage of air from the building and internal air pressure must be constantly maintained. An example of this type of shelter is the United States Atomic Energy Commission travelling exhibition pavilion (Gantes, 2001). The 90m long shelter had a width of 38m and a maximum internal height of 15m. The structure consisted of an inner and outer membrane that were both tensioned by a pressure of differential of 48mm and 38mm of water pressure; see Fig. 2.3(a). It effectively withstood wind speeds of over 200km/h.

Air-inflated membrane shelters consist of closed membrane structural elements, such as columns or arches that are filled with pressurised air. They function in the same manner as elements made of conventional materials. The loss of air pressure for these structures is far less than that for air-supported shelters. Only periodic replenishment of

the internal air pressure is required. A large-scale example is the Fuji Group Pavilion for EXPO '70 in Osaka, Japan. The structure consisted of sixteen inflatable arches and had a circular plan that was 50m in diameter; see Fig. 2.3(b). Internal air pressure in the arches could be varied between 8000 and 25000Pa to withstand different wind conditions. The LANMaS is another example of an air-inflated structure.

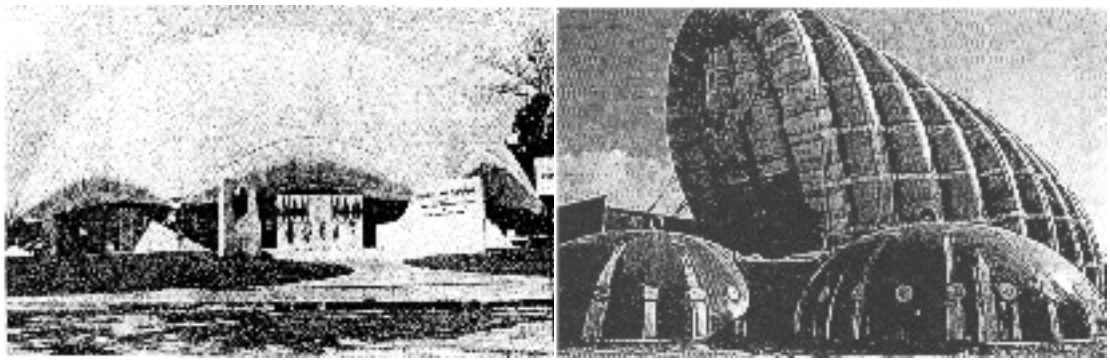


Fig. 2.3 (a) The travelling exhibition pavilion for the United States Atomic Energy Commission and (b) the Fuji Group Pavilion (Gantes, 2001)

Research into inflatable shelters has focused on experimental and numerical analysis of pressurised membrane arches as the load-bearing frames for soft-skinned shelters. These arches are modelled as circular or parabolic membrane arches with a circular cross section and internal pressure. Experimental analysis of these arches by Carradine (1998) revealed possible failure modes under service loading. Testing on 1:50 and 1:100 scale shelter models with pressurised arches at 30, 45, 60 and 90° angles from the horizontal revealed that strength, rather than serviceability or buckling, was the primary mode of failure. Arch membranes tore at mid-span under snow loading.

Numerical analysis of inflatable arches has focused on the development of analysis models that agree with experimental results. Kim (1998) numerically modelled

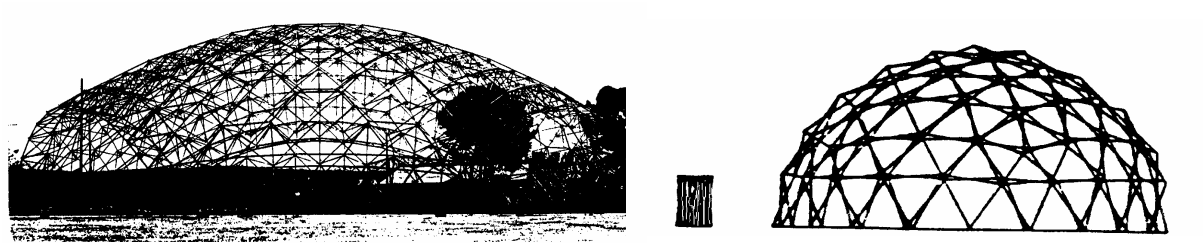
a similar shelter to Carradine consisting of six central arches and inclined arches at 20 and 40° serving as doorways using the ABAQUS finite element software. The frame structure consisted of parabolic arches with circular cross-sections composed of four node shell elements. Analysis for strength, serviceability and vibration reasonably approximated experimental behaviour. Mohan and Kapania (1998) used three node triangular elements to investigate a cantilever arch-tube under uniform external pressure and found good agreement with the four node shell element results. Goh (1998) conducted research focusing specifically on modelling the arches to be used in the LANMaS shelter. He formulated general displacement equations for the behaviour of both circular and parabolic arches based on equilibrium equations derived using total potential energy functions and compatibility equations.

2.2.2 Structures made from Scissor-like Elements

The most commonly used deployable structures applied to shelters are composed of scissor-like elements. Scissor-like elements consist of two bars connected using a hinge connection. They are combined to create shelters with internal mobility. Different configurations of scissors elements have been considered, with emphasis on repeatability of deployment, simplicity of design and cost. These structures have been researched since the 1960s, and are classified as either foldable or deformable. Foldable structures are strain-free both during deployment and in their deployed configurations. Bars or cables must be added to these structures to fix them in the desired configuration. Deformable structures are strain-free only in the compacted and deployed configurations due to geometric incompatibilities during the deployment process.

Work by Spanish architect Emilio Perez Piñero introduced the application of scissors structures to shelter design. Although previous concepts for deployable

structures existed before Piñero, his structures were the first complex deployable systems used to cover large areas (Belda, 1996). Beginning in 1961, he developed numerous structural designs to include an 8m dome for use as a travelling theatre and a large-span dome, see Fig. 2.4(a). His largest structural design, an 8,000m^2 deployable exhibition pavilion, was completely designed, manufactured and erected (Escrig, 1996). Piñero utilised three to four member structural joints in his design instead of the more commonly used scissor joint. His structures took on both flat and domical shapes, and typically had four layers. Piñero's designs utilised eccentric connections that introduced moments at the joints. These moments made larger joints and heavier members necessary. Piñero's shelters were foldable due to their strain-free deployment. Intermediate bars were added after the structures reached their desired configuration. This proved problematic for Piñero's larger structures, as temporary support for the structure was required. His work in the field of deployable structures attracted interest to the field of study and produced one of the few practical realisations of modern deployable structure design.



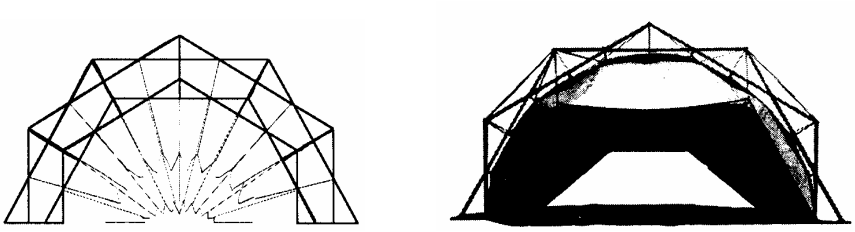
(a) (b)

Fig. 2.4 (a) Stiffened spherical dome by Piñero (Langbecker, 2000). (b) Geodesic deployable x-frame dome by Zeigler (Langbecker, 2000)

Zeigler expanded study in the field with the development of several structures, including a dome and barrel vault, see Fig. 2.4(b). His structures were deformable, with

structural members undergoing increasing strain during deployment until the structure *snaps through* to the deployed configuration (Gantes, 1991). His structures required no locking mechanisms due to this process, but problems were discovered with deformation of members during deployment and internal stresses in the final configuration of the structure. This internal strain made opening the structure only possible with the application of energy. Krishnapillai (1985) modified Zeigler's work to produce geometric designs that are stable and stress-free in the deployed configuration. These he called *clickable* structures.

The potential for rapidly deployable shelters with small compacted volumes has also attracted considerable interest from industry. Several small-scale structures have been developed for use commercially as shelters. The Estran 1 was developed for use as a small aircraft hangar (Gantes, 2001). It has two high arches with internal diameters of 16m and two low arches with diameters of 12.8m, composed of six scissors elements each. The arches are parallel and joined by 28 perpendicular arms, all of which are composed of scissor elements. Erection of this system requires a small crane. Fig. 2.5 shows how the covering is attached midway through erection of the structure (Hernandez, 1996). The Estran 1.1 improves on the Estran 1 by allowing the connection of separate shelter structures both laterally and lineally. Another prototype deployable shelter was developed at the Israel Institute of Technology. This structure is deformable, making use of the geometric incompatibility during deployment to lock the deployed structure in place. The *snap through* is accomplished with flexible fibreglass crosspieces that deform during deployment (Rosenfeld, 1993).



(a) (b)

Fig. 2.5 The Estran 1 Shelter with (a) cover undeployed and (b) cover attached (Hernandez, 1996)

The most notable application of scissor-like structures to shelter design was the development by Escrig of a deployable cover for the San Pablo Sports Centre in Seville, Spain. The aim was to develop a deployable structure to cover a swimming pool to allow use during the winter. The maximum erection and demounting time was one week (Escrig, 1996). As shown in Figure 2.6, the design used by Escrig for the cover consisted of two connected 30 x 30m foldable scissor-like structures. The structures consisted of grids of equal quadrilaterals made up of scissor-like elements and connecting at nodes (Sanchez, 1996). To minimise the difficulty of fabrication, Escrig's deployable cover was designed to use only one type of joint, structural member, and fabric covering connection. The fabric roof was connected directly to the structure so that in the deployed configuration the frame is external (Escrig, 1998). Computer design yielded 120mm member sections using aluminium, and design deflections were roughly 1:70 of the span.

Validation of the design calculations was accomplished through the construction and testing of a 1:9.5 scale model of one of the grids. Although agreement between design and experimental deflections was not good (between 24% and 847% error), the construction and testing of the model revealed that precision is absolutely required in

construction (Sanchez, 1996). It was suggested that error was caused by the differences between model and structure joints, model imperfections, and deformations associated with the deployment of the structure. In its final form, the structure had a compacted volume of 33m^3 and a deployed volume of 11,000m^3.

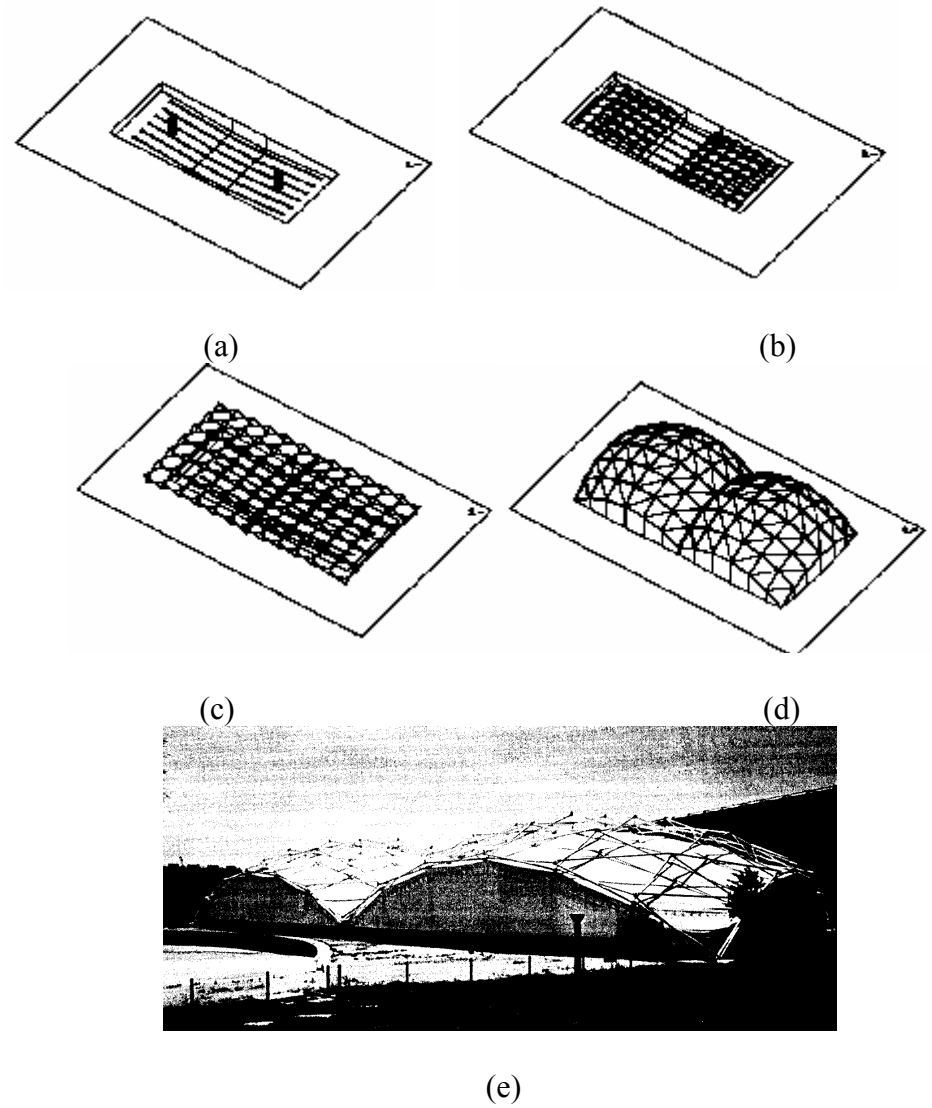


Fig. 2.6 Conceptual drawings of Escrig's swimming pool cover. (a) Undeployed; (b) spread horizontally; (c) spread vertically; (d) deployed; and (e) a photograph of the structure (Sanchez, 1996)

Although scissors structures have been applied successfully to structural problems, they have a number of shortcomings. Because numerous members must be connected together at a single joint, connections are often quite complex. In order to ensure that geometric compatibility conditions are met, these joints must also be highly accurate. Inaccuracy in fabrication introduces strain in the structure and interferes with deployment. Many scissors structures, to include the work of Zeigler, Rosenfeld and Escrig and the Estran 1 and 1.1 Shelters, are, in fact, deformable structures with strain induced in members during and after deployment. This strain must be accounted for during the design process and can lead to problems like increased susceptibility to buckling and decreased overall structural load bearing capacity (Gantes, 1991).

Foldable scissor-like mechanisms, e.g., the DRASH XB and J Series tents, have numerous members that must be connected together at a single joint. This is often quite complex. In order to ensure that geometric compatibility conditions are met, these joints must be highly accurate. Inaccuracy in fabrication introduces strain into the structure and interferes with deployment. Some of the shelters, e.g., those of Piñero and Hoberman, lack stiffness and require the addition of members or cables during the erection process. Additionally, as shown in Fig. 2.7, structures composed of scissors elements have certain depth. This means that when such structures expand the structural members create a depth among the struts that decreases the useable interior volume. It would be advantageous to develop a shelter structure with the positive aspects of structural mechanisms while avoiding those that lead to increased cost and structure weight.

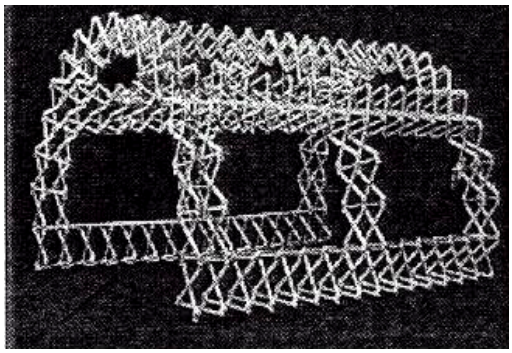


Fig. 2.7 A foldable barrel vault using scissors elements (Langbecker, 2000)

2.2.3 Structures made from Overconstrained 3-D linkages

No research has been completed up to this date on the application of overconstrained 3-D linkages to shelter structures. This is a category of structures where struts are connected by revolute hinges. Their properties suggest possible uses as shelter structures. A linkage is a specific type of mechanism consisting of interconnected components called links. The connections between links are called joints. There are a number of different types of joints used to connect links, including spherical joints, planar joints, cylindrical joints, revolute joints, prismatic joints and screw joints. When considering a mechanical device or linkage made up of links connected by joints, it is necessary to determine its mobility. Mobility is defined by the Kutzbach or Grübler equation:

$$m = r(s - b - 1) + \sum f \tag{2.1}$$

where m is mobility of an assembly consisting of s members and b joints, r is equal to three for planar or six for spatial assemblies and the $\sum f$ stands for the sum of kinematical variables in the mechanism (Kuznetsov, 1991). There are two assumptions associated with this method of determining mobility. All constraints or freedoms of the joints must be independent and the loops themselves must be proportioned with complete

geometric generality. This means that only the topology of the structure, i.e., the connectivity of links and type of connections, is considered. No other aspects of geometry or link dimensions are taken into account. When *m* equals one, the assembly is an ideal mechanism with one mobility. If greater than one, the linkage is underconstrained with more than one mobility. If *m* equals or is less than zero, the criterion renders the assembly as a statically determinate structure or statically indeterminate structure.

For a closed loop spatial mechanism, Eqn. 2.1 can be simplified to

$$m = s - 6 \tag{2.2}$$

Thus, seven members are required to achieve a single degree of mobility.

It has been found, however, that the Kutzbach criterion is not a sufficient condition for mobility. Special geometric relationships can enable an assembly to be mobile even if *m* is equal to or less than zero. This class of mechanisms is considered overconstrained. The mobility of these mechanisms is more clearly described using the Denavit and Hartenberg notation.

Denavit and Hartenberg (1955) established a standard approach to analyse linkages where geometric conditions are taken into account. They provide a method to transform the local coordinate axes of each member to the coordinate axis of adjacent members. The following parameters describe the orientation of a member in a linkage: α_i equals the twist angle between the axes of joints i and i+1, a_i equals the length of the link i, d_i equals the offset along joint i, and θ_i equals the rotation angle about joint axis i. These variables are illustrated in Fig. 2.8 below:

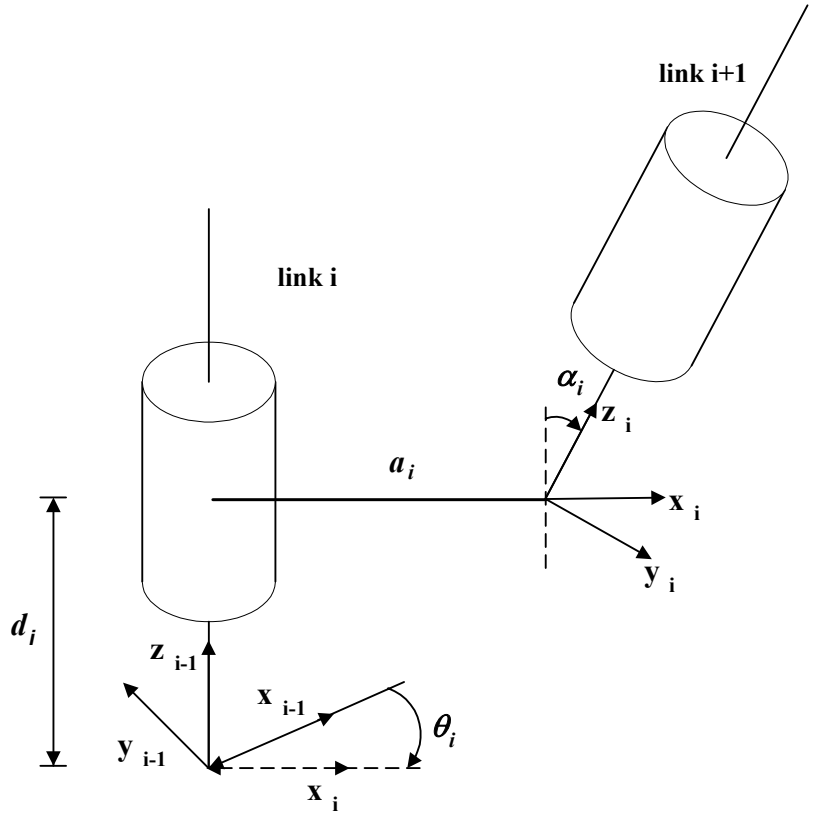


Fig. 2.8 Coordinate system for two links connected by revolute joints

The transformation from the coordinate system of link i+1 to link i is

$$[A_i]=\begin{bmatrix} \cos(\theta_i) & -\sin(\theta_i)\cos(\alpha_i) & \sin(\theta_i)\sin(\alpha_i) & a_i\cos(\theta_i) \\ \sin(\theta_i) & \cos(\theta_i)\cos(\alpha_i) & -\cos(\theta_i)\sin(\alpha_i) & a_i\sin(\theta_i) \\ 0 & \sin(\alpha_i) & \cos(\alpha_i) & d_i \\ 0 & 0 & 0 & 1 \end{bmatrix} \tag{2.3}$$

The transformation matrix from member i to member i+1 is simply the inverse of $[A_i]$. Denavit and Hartenberg derived a necessary and sufficient expression for describing the mobility of all closed loop linkages, including overconstrained ones. They pointed out that for a closed loop, the product of the transformation matrices for each member in the loop is equal to an identity matrix. This is expressed as

$$[A_1][A_2]..[A_n]=[I] \tag{2.4}$$

A four bar, closed loop mechanism has 16 Denavit and Hartenberg parameters that define its assembly configuration. These parameters can be separated into two classes: structural (α_i, a_i, and d_i) and motion (θ_i). This mechanism is immobile according to Eqn. (2.1). Special relationships between these parameters, called overconstraint conditions, can be found that make this mechanism mobile.

Numerous mechanisms have been discovered that are classified as overconstrained. The first was proposed by Sarrus in 1853. Others have been proposed by Bennett (1903), Delassus (1922), Bricard (1927), Myard (1931), Goldberg (1943) and Waldron (1967). These were summarised by Phillips (1990) and Baker (1986). The difficulty is that the complexity of the geometric relationships involved with developing these mechanisms has slowed systematic study of overconstraint. Mavroidis and Roth only recently developed a method for general classification of overconstrained mechanisms and determination of input-output curves (Mavroidis and Roth, 1995).

Overconstrained linkages have a number of useful properties. These linkages are mobile with fewer members and joints than is expected. This decrease in the number of joints and members affects cost, complexity, and structure weight. Another key advantage is that when an overconstrained linkage is fixed it becomes a redundant structure. The primary difficulty associated with overconstrained linkages is a mathematical one: the overconstraint equations that govern the mechanisms have a large number of variables. This has discouraged engineers from applying overconstrained linkages to their designs and resulted in very few practical applications.

One type of overconstrained mechanism has the potential for useful application to deployable shelters. The Bennett mechanism, which was discovered in 1903 by G.T. Bennett (Beggs, 1966), is a 3-D linkage consisting of four links and having only revolute joints. Application of Eqn. (2.1) for s=4, b=4, and $\sum f = 4$ yields m=-2. This shows that

the mechanism should have three degrees of constraint. However, it has a single degree of freedom. Fig. 2.9 below illustrates this mechanism, in which α_{AB} represents the skew angle from the axis at node A to that of node B. This is best understood as the angle between the hinge axes at node A and B. α_{BC}, α_{CD}, and α_{DA} are similarly defined.

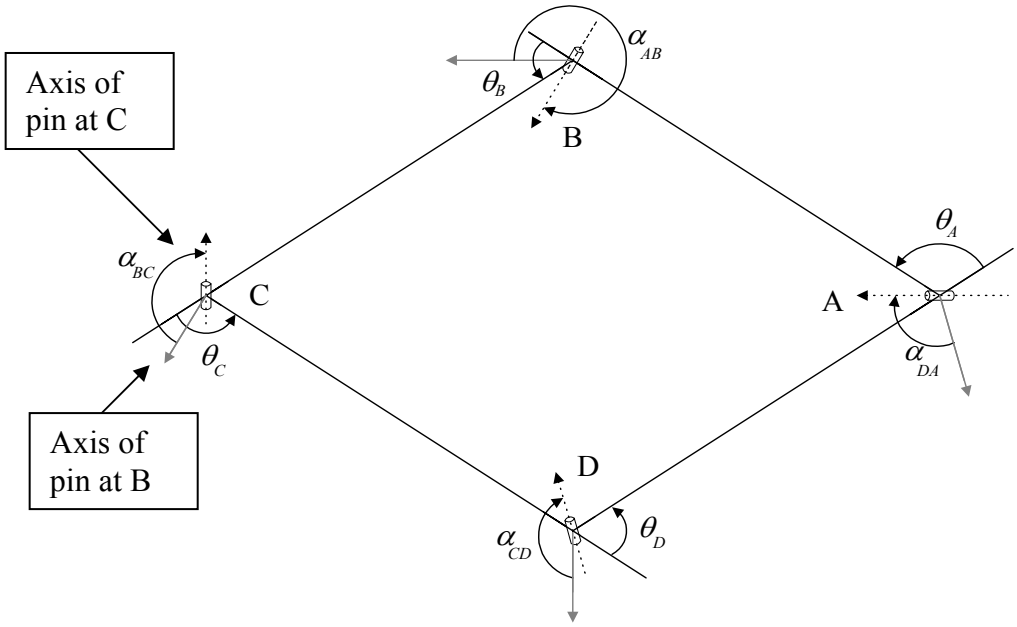


Fig. 2.9 An equilateral Bennett mechanism

The compatibility conditions for the linkage are as follows (Beggs, 1966):

- Two alternate links have the same length and twist:

$$\overline{AB} = \overline{CD} = l_1 \tag{2.5}$$

$$\overline{BC} = \overline{DA} = l_2 \tag{2.6}$$

$$\alpha_{AB} = \alpha_{CD} = \alpha_1 \tag{2.7}$$

$$\alpha_{BC} = \alpha_{DA} = \alpha_2 \tag{2.8}$$

Lengths and skew angles must also satisfy the following:

$$\frac{\sin^2(\alpha_1)}{{l_1}^2} = \frac{\sin^2(\alpha_2)}{{l_2}^2} \tag{2.9}$$

The deployment angles, i.e. the angles between the links, are denoted as θ_A, θ_B, θ_C, and θ_D. They are governed by the following equations:

$$\theta_A = \theta_C = \theta \tag{2.10}$$

$$\theta_B = \theta_D = \varphi \tag{2.11}$$

$$\tan\frac{\theta}{2}\tan\frac{\varphi}{2} = \frac{\sin\frac{1}{2}(\alpha_1 + \alpha_2)}{\sin\frac{1}{2}(\alpha_1 - \alpha_2)} \tag{2.12}$$

The special case relevant to this project occurs when:

$$\alpha_1 = \pi - \alpha_2 = \alpha \tag{2.13}$$

and

$$l_1 = l_2 = l \tag{2.14}$$

Eqn. (2.12) then becomes

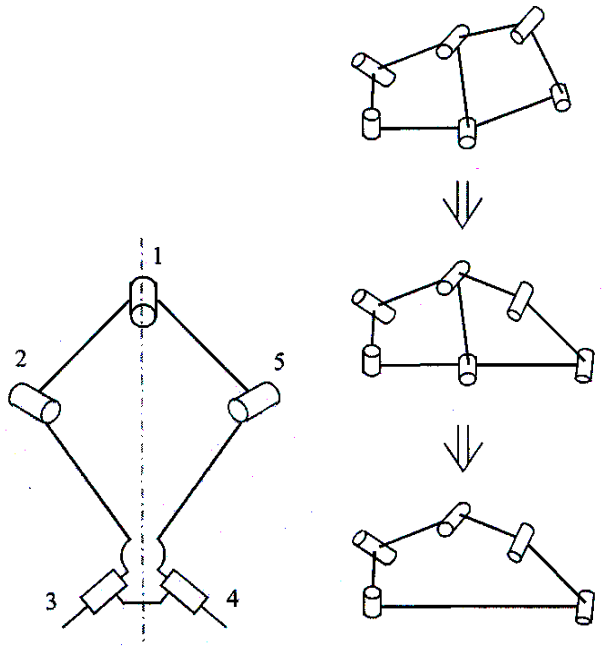
$$\tan\frac{\theta}{2}\tan\frac{\varphi}{2} = -\frac{1}{\cos(\alpha)} \tag{2.15}$$

This particular type of Bennett linkage is also called the equilateral Bennett linkage.

The Bennett linkage is the only four bar linkage with revolute connections (Waldron, 1968). As such, it has been used as a building block for spatial linkages with five or six revolute connections. They will be referred to as 5*R* and 6*R* linkages. Myard (1931) developed an overconstrained 5*R* linkage consisting of two *rectangular* Bennett linkages that are symmetrically disposed before combining them. The linkages are mirror images of each other, the mirror being coincident with the plane of symmetry of the resulting linkage (Baker, 1979). This linkage is shown in Fig. 2.10(a).

Goldberg (1943) conceived of 5*R* linkage consisting of two Bennett linkages connected in such a way that a link common to both is removed and a pair of adjacent links is rigidly attached together. This technique he refers to as summation, and is shown

in Fig. 2.10(b). He also developed a 5*R* linkage through the subtraction of a primary composite loop from another Bennett chain to form a syncopated linkage.



(a) (b)

Fig. 2.10 (a) The Myard 5*R* linkage, (b) a Goldberg 5*R* linkage composed by summation (Chen, 2003).

A number of 6*R* mechanisms have been developed. Goldberg developed four 6*R* mechanisms using the same methods as shown above. The first is a summation of three Bennett linkages (see Fig. 2.11(a)). The second found by subtracting a Goldberg 5*R* linkage from a Bennett linkage (see Fig. 2.11(b)). The third is found through the L-shaped arrangement of three Bennett linkages and the fourth by subtraction of the Goldberg L-shaped 6*R* from a Bennett linkage (Chen, 2003). Notable among the remaining 6*R* mechanisms are two of the linkages conceived of by Bricard (1927). The trihedral and line symmetric 6*R* Bricard linkages are the only other mechanism besides the Bennett linkage that can be used as a building block for other overconstrained mechanisms. They are used to compose the Wohlhart and Altmann linkages.

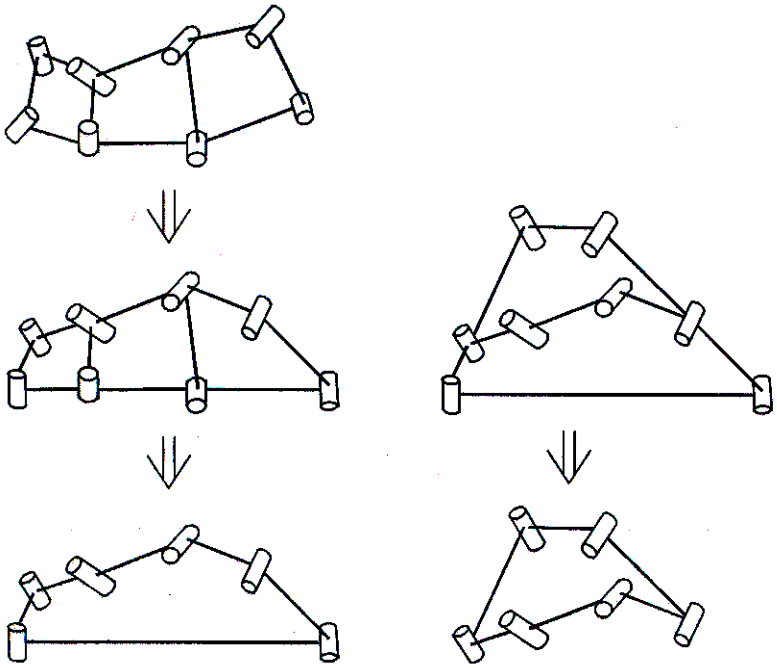


Fig. 2.11 (a) Goldberg 6*R* linkages composed by summation and (b) subtraction (Chen, 2003).

Most research has been centered on building basic mobile units rather than large structural mechanisms. Recently, work at Oxford University demonstrated that Bennett mechanisms could be tiled to develop larger, 3-D structures with the favorable properties of the Bennett linkage (Chen, et. al. 2001). The manner of connecting them varies, but it is necessary to ensure that all overlapping loops created by the connection of the linkages meet the compatibility criteria. The configuration of equilateral Bennett mechanisms pertinent to this project is shown in Fig. 2.12 below. Note that a '+' indicates a skew angle of α and '-' a skew angle of $\pi-\alpha$.

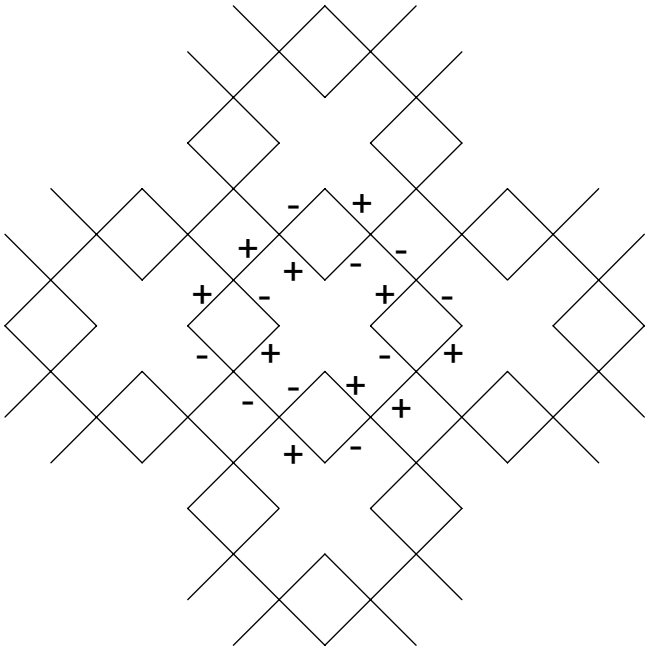


Figure 2.12 Combination of Bennett mechanisms yielding a cylindrical profile

Chen and You developed an overlapping combination of equilateral Bennett mechanisms that yields a structure that opens into a half-cylinder shape (Chen, et. al. 2001). This structural concept provides an enclosed space that is useful and applicable to the problem of deployable housing. Unlike other deployable structures, it has the following unique properties:

- The structure, itself, consists of only identical bars and hinges, which allows all members to be interchangeable.
- The structure can collapse flat and segment for compact packing.
- It has only a single layer enabling greater interior volume.
- The inter-linked frame configuration means that the weight of the system can be reduced to achieve the same structural strength.

It is this tiling of the Bennett mechanism that will be considered for this dissertation. It is important to note that Chen and You also successfully constructed large overconstrained structural mechanisms using hybrid Bricard linkages, which are

overconstrained and have a single degree of mobility. The resulting mechanisms fold from a compact bundle to a flat, triangular shape. Thus, they are not useful for the problem of deployable shelters (Chen, et. al. 2004).

2.3 Analysis of Deployable Structures

When designing deployable structures, it is necessary to take into account two different loading conditions. These are service loading in the deployed configuration and response during the deployment process. Deployment of foldable structures is ideally stress-free and requires minimum analysis. Once deployed, it is necessary to consider the optimum placement of intermediate members to provide strength and immobilise the structure. For deformable structures, response during the deployment process can be geometrically non-linear. The *snap through* buckling used to lock the structure in place is generally the governing design criterion. Deployment strain must be large enough to induce the buckling but only cause elastic deformation. This requires complicated numerical modelling. Analysis for both types of scissors structures in the deployed configuration is accomplished using standard methods.

In ideal conditions, overconstrained mechanisms are strain-free during deployment. Thus, it is only necessary to consider service loading in the deployed configuration. If initial geometrical imperfections are present, however, strain develops during deployment and requires analysis. Failure to take into account deployment response to imperfections calls the feasibility of the structure into question either due to stiff response or decreased load-bearing capacity under service loads. Work done in the area of deployable structure analysis mainly focuses on scissor-like structures. It deals with general analysis in the deployed configuration and consideration of the effects of imperfections during deployment and while deployed.

2.3.1 General Analysis

Analysis in the deployed configuration is conducted in the same manner as with conventional framed structures. The preferred analysis method is finite elements using a computer utility. Modelling the deployed configuration using this method is often computationally intensive. Considerable research has been conducted on how to simplify numerical models for scissors structures. Shan (1992) modelled a scissor-like element in 2D as two uniplets (bars) connected by a pin joint. This eliminated moments at the ends of the bars and torsional stresses through the uniplets. He generated a stiffness matrix for the scissors element by reducing the matrix for two beams. Kaveh and Daravan (1996) refined this approach by defining each uniplet using 3 nodes and three translational degrees of freedom. They then combined the matrices and eliminated the common node. Gantes (2001) further simplified preliminary analysis by proposing an equivalent continuum model for deployable flat slabs composed of scissor-like elements.

Gantes (2001), in his analysis of flat deployable slabs, determined that hinged connections in scissors-like deployable structures were small and their size could be neglected in computer models. For the larger hub connections, it was found that inclusion of discrete joint size in the model was required to ensure accurate structural stiffness.

There are three potential failure modes in the deployed configuration that require consideration: strength, stiffness, and buckling Linear analysis using finite elements may be used to determine the adequacy of the structure for both strength and stiffness. The body of work in this area for scissors-structures is robust. Notable is Langbecker's systematic study of the structural performance of different foldable frames (Langbecker, 2000). Using ABAQUS FEM software, he analysed the performance of barrel vaults

made of both Hoberman and polar units and both positive and negative curvature surfaces under service loads. Parametric analyses were performed to determine the effect of varying member sizes and structural geometry for each type of frame.

He also considered the effects of observed imperfections in experimental models. Testing showed that structures composed of scissor-like elements are susceptible to buckling out of the plane of the scissor. This decreased the strength of the structure and was not included in the numerical models detailed above. Thus, numerical and experimental results disagreed. Langbecker incorporated this into his models. He conducted linear buckling analysis to determine locations in various deployable structures of scissor-like elements susceptible to buckling. He also found the magnitude of the out-of-plane displacement due to buckling at these locations. He then introduced imperfections of equal magnitude at the same locations in the initial models. His subsequent strength and displacement analyses corresponded well with experimental results.

2.3.2 Buckling Analysis

Buckling analysis for scissors structures in their deployed configurations is straightforward. Initial analysis is conducted using linear buckling analysis. If behaviour prior to buckling failure is characterised by small deflections the results from the linear buckling analysis are considered accurate. If displacements are large, the performance of nonlinear analysis for service loading is required. Buckling analysis is included in the work of Zeigler (1976), Escrig and Valcarcel (1998), Gantes (1996), and Langbecker (2000).

Research on the buckling of deployable scissors structures provides useful guidelines for the analysis of tiled overconstrained mechanisms, but is not sufficient due

to the fact that scissors structures are double layer. Single layer structures behave differently under load, and fail due to buckling differently than double layer deployable structures. No single layer deployable structures currently exist, so the closest comparable single layer structures are reticulated shells. Reticulated shells, as shown in Fig. 2.13, are grids of members and joints used to cover large spans without intermediate supports. They have a low weight of structural material per unit area covered and are built from prefabricated units that can be rapidly assembled on site. They exhibit common features of both bar structures and solid shells. This makes them difficult to analyse and requires the use of nonlinear stability analysis to fully understand their behaviour (Gioncu, 1994). Instability in reticulated shells can arise from the following modes: member (Euler) buckling, nodal buckling, torsional buckling, line buckling, and general buckling. Coupling of two instability modes may occur when the corresponding critical loads have close values. In this case, the structure becomes very sensitive to geometrical imperfections and the buckling load can decrease dramatically.

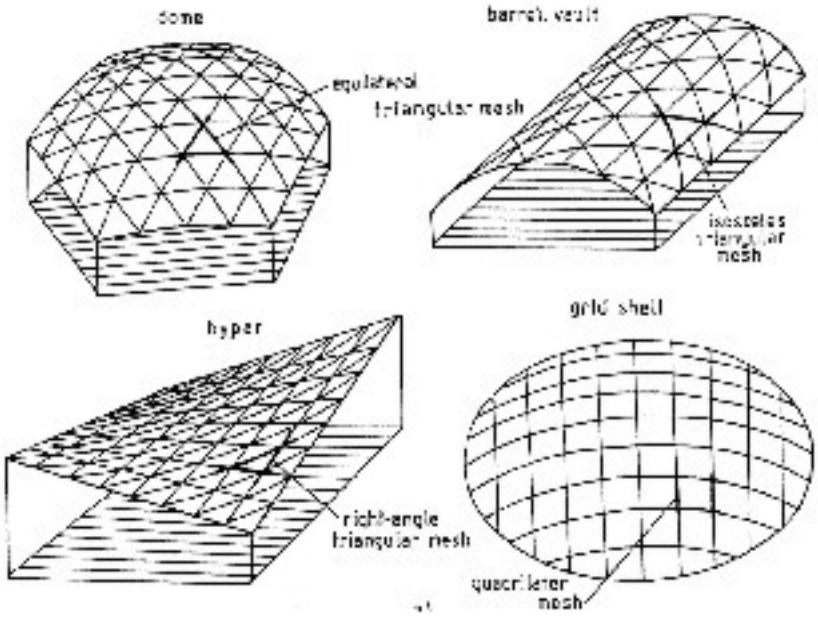


Fig. 2.13 Reticulated shells (Gioncu, 1994)

To model these instabilities accurately, one must include certain elements in the analysis. It is important to apply wind and snow loads with local and antisymmetrical effects, as these are the main loads for reticulated structures and also the ones that most often cause collapse. Because of the unstable nature of postcritical behaviour in reticulated shells, it is also important to take into account imperfections in the structure and joint rigidity during analysis. Most numerical models significantly overestimate buckling capacity by using rigid joints (Gioncu, 1994). Additionally, large joints cause torsion instability in the node. Models that do not take into account joint size miss this type of instability entirely.

The size and location of geometrical imperfections and joint rigidity are generally determined through experiment. This can be problematic, however. Scale models of reticulated shells do not provide accurate experimental results. Escrig observed this when comparing numerical and experimental results for models of his large swimming pool cover (Sanchez, 1996). It is difficult to scale bar size and joint configurations. This leads to different imperfections in models than in the actual structure and therefore unusable experimental results. Testing on full-sized models can be accurate but is not always possible. With joints, it is similarly difficult to fully replicate conditions in the full-scale structure. It is possible to do component testing, but this requires full joint design and knowledge of loading conditions.

2.3.3 Deployment Analysis

Analysis of the deployment of deformable scissors-like structures has centered on the *snap through* buckling during deployment of mechanisms using scissor-like elements. The *snap through* can be described as the gradual increase of internal stresses in one or more components of a structure during deployment until one or more

components reaches a limit point that corresponds to a critical load. The structure then spontaneously moves to a stable, strain-free equilibrium configuration. This effect is caused by geometric incompatibilities in the mechanism, and is highly non-linear. Researchers, such as Zeigler, Gantes, and Rosenfeld recognised that this effect could prove useful in deploying structures to a stable configuration (Gantes, 1991). If the *snap through* occurred with stress levels below the yield point of the members, it could be used to lock the mechanism into a deployed configuration. This would then eliminate the need for the addition of extra members or cables to immobilise the structure at the desired configuration. However, if the stress level is too high, the structure becomes either un-deployable or deployment may cause the destruction of the structure.

Rosenfeld and Ben-Ami (1993) developed a method for determining the members that have a variation in internal stress through deployment and replacing them with flexible rods that behave elastically during the *snap through.* Using iterative experimentation, it was possible to determine the size of rod and type of material necessary to achieve a *snap through* that would lock a barrel vault into a deployed configuration (Rosenfeld, 1993). Krishnapillai (1985) modified Zeigler's initial designs, making them stable and stress free in the deployed configuration. These he called *clickable* structures. Gantes (1996) expanded on this work by developing an analytical method to model changes in *snap through* by changing section sizes or geometry.

In ideal conditions, foldable structures and overconstrained mechanisms are stress-free during deployment. If imperfections are present, however, stresses will develop as the structure opens. As the Bennett mechanism is overconstrained, it is necessary therefore to examine existing work on imperfection analysis.

2.4 Imperfections

In engineering practice, the accuracy of manufacturing and fabrication of the components of a structure are generally guaranteed within some acceptable tolerance. In structural design, these standard imperfections in structural components are manageable within certain limits. Members can be deformed to meet structural requirements if the structures are statically indeterminate. This is a larger problem, however, in mechanisms.

The presence of imperfections in underconstrained or ideal mechanisms may interfere with the desired motion of deployment or the deployed shape of the mechanism. Imperfections in these types of mechanisms do not, however, cause the development of internal strain, just like statically determinate structures. For overconstrained mechanisms, they do because the geometric compatibility conditions may be violated. Energy must be input for the mechanism to deploy. Detailed analysis then becomes necessary.

2.4.1 Underconstrained and Ideal Mechanisms

Research into mechanical imperfections in deployable mechanisms has been conducted for underconstrained and ideal mechanisms (where $m \geq 1$). Prototyping and testing of underconstrained mechanisms led to the practical realisation that deviation from ideal linkage dimensions and joints orientations are sources of mechanical error. Research by Lee and Gilmore (1991) and Ting (2000) show that clearances between pin connections and the joint lead to differences between the theoretical and actual motion of underconstrained and ideal mechanisms. Further research has considered slippage in pinned connections and other practical considerations not taken into account in theoretical modelling (Hummel and Chassapis, 2000).

Deterministic and probabilistic methods are used for analysing the effects of imperfections in underconstrained and ideal mechanisms. Deterministic methods involve fixed design variable values or constraints that are used to find efficient designs for an established design criterion that include imperfections. Deterministic methods are mostly used for post-synthesis analysis, where set tolerances are used to determine worst-case position error. Research has been conducted to develop deterministic methods of evaluating how the inclusion of imperfections effects optimised designs. Mallik and Chatterjee (1987) presented a method for assessing error in a four bar underconstrained mechanism. Using a procedure based upon Lagrange multipliers with link length and clearance of hinge joints as random variables, they determined the worst-case imperfections for the deployment of the mechanism.

Statistical methods may be used for analysing tolerances during mechanism synthesis, where dimensions have a probability distribution associated with them. Dhande and Chakraboty (1973) used a probabilistic approach for error analysis of spatial linkages. A model was developed for distributing tolerance and clearances for components of a linkage to restrict output error within specified limits. This work has been used to practically apply Timoshenko's initial imperfection theories by combining them with probabilistic analysis. Instead of looking at the worst-case effect of imperfections, this method determines a mean imperfection effect to be expected in any four bar mechanism.

2.4.2 Overconstrained mechanisms

The effect of initial imperfections on overconstrained mechanisms is largely uninvestigated up to this point. The complexities of the relationships that govern overconstrained mechanisms make them difficult to consider systematically. Only

recently has a governing method for proving overconstraint and determining input-output relationships been developed (Mavroidis and Roth, 1995). When considering overconstrained mechanisms as deployable shelters, it is necessary to examine both the deployed configuration and the deployment process itself. When fully deployed, the effects of imperfections on overconstrained mechanisms are the same as in conventional, statically indeterminate structures. Analysis of initial waviness lightweight trusses showed that decreased structural strength accompanied imperfections (Crawford and Hedgepeth, 1975). Structural optimisation techniques could still, however, be applied to find minimum weight solutions. The effect of imperfections on optimisation of structures was investigated by Rosen, who found that small imperfections changed the optimal design by causing a variation in the distribution of material (Rosen, 1981).

Some consideration has been given to the deployment of overconstrained mechanisms with imperfections. Analysis of the trajectory of path-generating mechanisms, which may be overconstrained, has been limited to the determination of actual paths of motion with imperfections as opposed to theoretical solutions (Raghavan and Roth, 1990). The most relevant research to this report is that of Kuznetsov. In his systematic study of the motion of mechanisms, he addressed overconstrained mechanisms as a special case. Using a simple example, he examined the effect of imperfections on mobility of overconstrained mechanisms (Kuznetsov, 1991). Kuznetsov proposed adding an extra bar to an ideal planar mechanism to achieve overconstraint, see Fig. 2.14 (a). Kinematical transformations of this system were studied using a statical-kinematical approach. The global strain energy expression for the mechanism was derived, and a statically possible stress state applied. Kuznetsov evaluated the mobility of the linkage for different bar lengths.

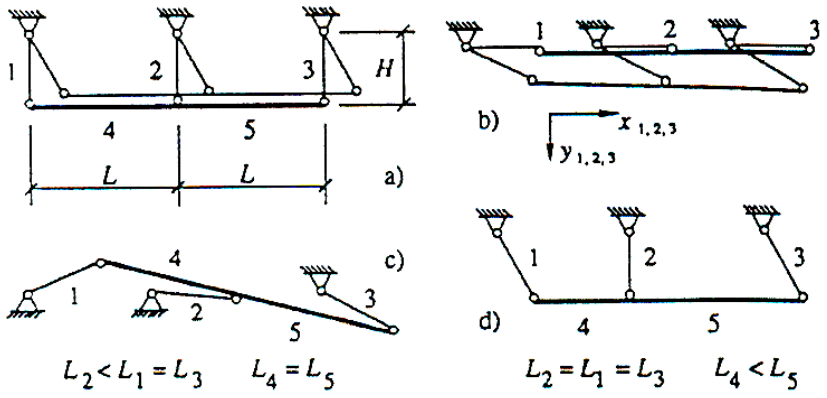


Fig. 2.14 Simple overconstrained mechanism with varied bar lengths (Kuznetsov, 1991)

From this analysis, Kuznetsov found that globally statically indeterminate mechanisms possess kinematical mobility only as an idealisation. Any component deformation or departure from nominal member sizes leads to either elastic interference or self-stress. As shown in Fig. 2.14 (c) and (d), the system becomes geometrically invariant and elastically resists loads for all possible member sizes and orientations but the one presented in Fig. 2.14 (a). Thus, the system remains mobile after the addition of an extra bar only if strict geometric compatibility conditions are met. The introduction of any variation in geometry to this special case induces a self-stress. Kuznetsov showed using energy methods that the system will spontaneously move to the configuration where energy is minimised and acquire elastic resistance to any displacements, see Fig. 2.14(b). This resulting elastic resistance is directly proportional to the initial strain caused by the pre-stress.

3 Geometry of the Bennett Shelter

This chapter deals with the development of a geometric design procedure for a large shelter using overlapping Bennett mechanisms. Section 3.1 outlines the basic structural requirements for a large military shelter structure. It then shows the concept for a shelter based upon tiled Bennett mechanisms (to be referred to as a Bennett Shelter from here forward). Section 3.2 conceptually develops subsystems for the shelter. Section 3.3 details variables and constraints, and the key geometric parameters for the Bennett Shelter are derived in Section 3.4. Section 3.5 then defines the geometrical design procedure for given structural frame dimensions.

3.1 Basic Structural Requirements

In order to develop the military structure, it was first necessary to determine the requirements that a finished structure must meet to be used in the military. Using the MGPTS specification, as published by the United States Army, it was possible to determine the load conditions that military tents must withstand in order to be purchased by the U.S. Army (Performance Specification, 2001). The specification also included ergonomic requirements relating to the function of the tent structures when handled by soldiers. It was also necessary to determine pallet and container dimensions for both the U.S. and U.K. military (Airlift Planners Course, 1995). The compacted dimensions of the structure had to conform to these sizes. A complete summary of design information is included in Appendix 1.

Large shelter structures are commonly used in the military to house helicopters. They require a deployed structure height of 5.5m at minimum. The structure must be 11m wide at a height of 3.4m in order to accommodate the main rotor of the helicopter.

The total length of the structure must be 18.3m at minimum in order to fit the helicopter from nose to tail rotor.

The properties of the Bennett Shelter detailed in Section 2.2.3 make it ideal for use in military structures. Because of the foldable nature of the structure, it is easily packed and prepared for airdrop. As shown in the Fig. 3.1 below, the folded structure can be segmented for the purpose of stacking on military pallets. These segments provide flexibility in constructing shelters of various sizes. One needs only to connect the segments and the structure can be expanded to its deployed configuration with ease. Once deployed, it is necessary to secure the structure to the ground and attach the appropriate fabric covering and insulation. The fact that the structure consists of identical bars and hinges allows for cheap fabrication of parts and maintenance. Because the structure is single-layer, it has no wasted interior volume. The inter-linked frame configuration means that the weight of the system can be reduced to achieve the same structural strength. The structure is overconstrained, which allows it to withstand failure of one or more structural elements.

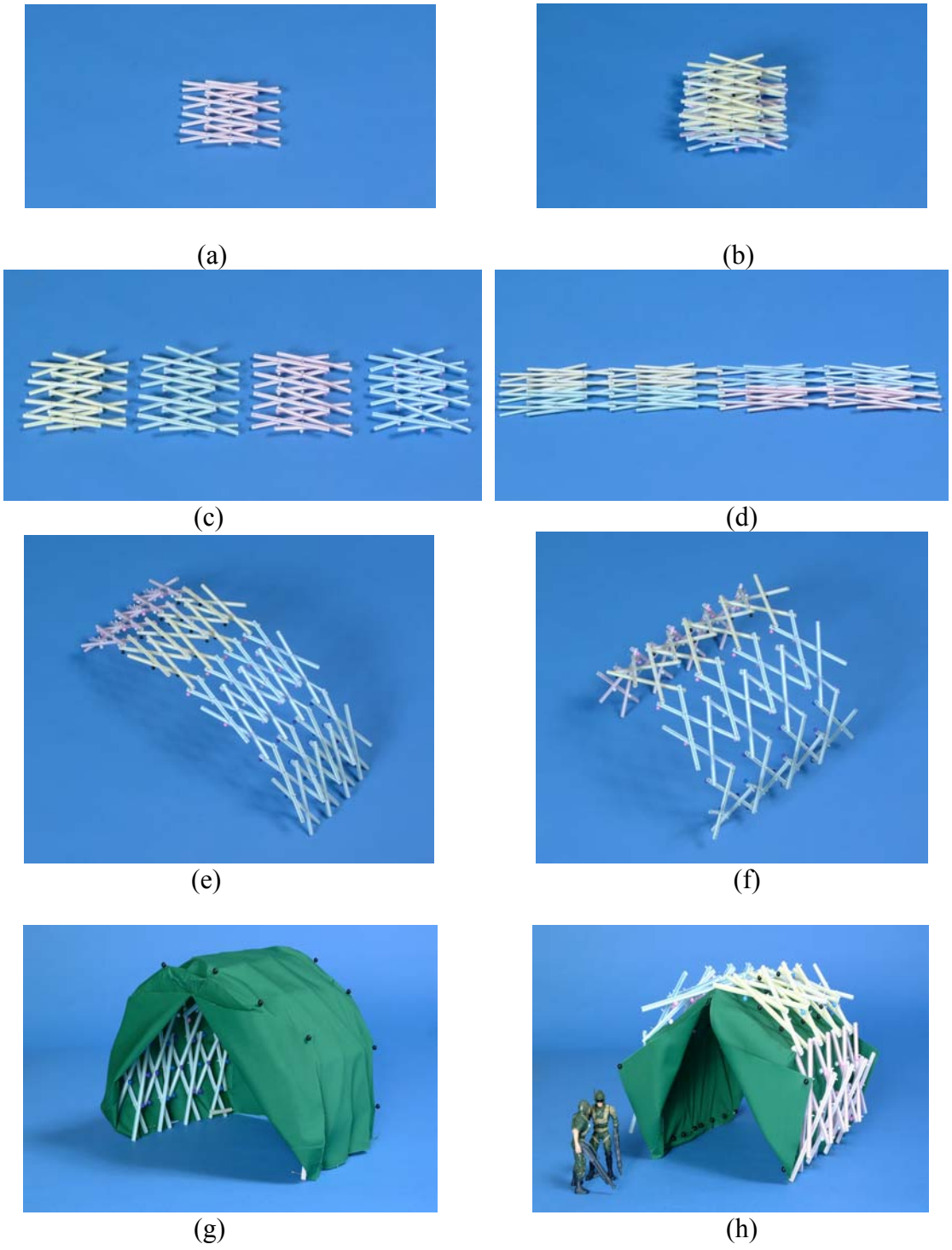


Fig. 3.1 Deployment sequence of the shelter structure. (a) One folded element of the shelter structure. (b) All four elements stacked as they would be on a military pallet. (c) Structural segments laid out before connection. (d) Connected structure in folded position. (e) Structure partially deployed and (f) fully deployed. (g) Outer structural lining for the structure. (h) Inner insulation for the structure in case of cold weather.

3.2 Conceptual Development of Subsystems

With the concept for the frame defined, it is useful to consider other portions of the shelter structure. The major subsystems are the structure joints, fabric cover, foundation system, doorway system and connector hallway. Analysis of these systems will provide additional constraints on the structural analysis of the frame.

3.2.1 Design of Joints

The joints used in the Bennett Shelter are mechanically simple. The connections are revolute, allowing rotation only about the pin axis. The complexity of the joints is in their placement along each structural member and the angle between the pin axes (α and α_2). The development of joints for the Bennett Shelter is further complicated by usage-related constraints. The structure must be collapsed and configured in a number of different shapes. The application considered in this study, the helicopter shelter, requires permanent connections for all joints in each segment and joints that can be disconnected to allow for storage and transport of the structural frame.

The aforementioned structural and usage criteria can be accomplished in a variety of ways. It is possible to use removable pins for the inter-segment connections. This method has the advantage of simplicity, but also has some drawbacks when used with carbon fibre composite pipes. Drilling holes in these pipes can cause cracking along the length of the member and greatly decreases its failure strength. Use of drilled pin connections is therefore problematic with this material. It is necessary to consider the possibility of alternative connections. Any connection used would have to provide accurate skew angles between joints and allow 360-degree rotation about the pin axis. A connection capable of meeting these specifications is the swivel coupler (shown in Figure 3.2 below).

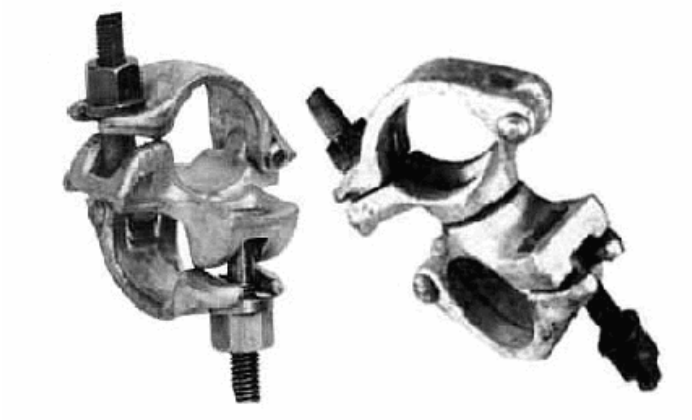


Fig. 3.2 Swivel Couplers (British Standard BS1139, 1991)

This type of connection is generally used to secure diagonal bracing in independent-tied scaffolding. The connection makes use of friction provided by adjustable sleeves to secure the two members it connects. There is no need to drill holes in the member to use this coupler, and it provides full rotation about the pin. The necessity for accurate joint alignment can be solved by a small alteration of the coupler and member. Marking the bar to ensure correct placement of the couplers is straightforward. Sanding flat the sides of the bar such that the flattened portions of the bar are parallel to the desired pin axis and ensuring the coupler sleeves have flattened portions parallel to the lug connector between the sleeves allows for the coupler to be oriented correctly. Analysis and design of both pin and swivel coupler connections is necessary to determine the optimal solution. Both solutions must also be considered during prototyping of the Bennett Shelter.

3.2.2 Fabric Cover

Fabric design is an area in which a great deal of research and development has been done. DHS Systems, maker of DRASH tents, designs its own fabric, as do most military tent designers. Research is also underway at Cambridge University concerning the development of cost-effective shelter fabrics for refugee camps (Manfield, 2000). Fabrics used for shelter covers must meet a number of criteria. Shelters must be able to maintain comfortable internal temperature in extreme weather. In order to avoid detection, no light can escape from the shelter during use (this is often referred to as blackout capability). Fabric strength is an obvious criterion for design, as well as water resistance. Integrated shelter and ground covers that keep pests out of shelters are the current industry standard. The use of single or dual-layer fabric systems is also considered. Dual layer systems make use of the air space between layers to decrease thermal conductance. These systems, however, have problems when wind gets between the layers. Interior fabric coverings are not designed to withstand wind abrasion, and wear quickly when exposed to wind loading. Premature wear is a major disadvantage of DRASH tents.

Attachment of fabric covers to structures is also an important factor considered in design. The MGPTS, LAMS, LANMaS and TEMPER tents use separate covers. The DRASH systems, however, have pre-attached covers. DRASH frames compact in two directions, reducing to a small compacted volume without any disassembly of the structure. Fabric does not hinder the expansion of the frame to its deployed configuration, and attaching a cover to the structure only requires a method of folding the cover when the frame is compacted (DHS Systems LLC, 2002). Pre-attached covers speed up the erection of shelter structures, but can introduce maintenance and durability issues. Another consideration involved with fabric covering attachment is pooling. Flat

areas on shelter structures gather water and introduce additional loads to the structure. Pooling can also cause leakage over long periods of time.

The Bennett Shelter makes connection of a fabric cover somewhat complex. In order to have a taut cover, the fabric cover must conform to the deployed structural dimensions. During compaction, however, the structure elongates from an arched vault to a long, flat bundle (see Fig. 3.1). The compacted length of the structure is greater than the length of fabric required to cover the deployed structure. Any fully pre-attached cover would, therefore, provide restraint and immobilise the structure. The possibility of partially attaching the fabric and then completely securing it after deployment exists, but requires further study. The interaction of the fabric cover with the frame is shown in Fig. 3.3 below. It is obvious that the ridgeline of the structure has a flat portion. This could introduce the problem of pooling. Development of a ridge segment that creates a peaked ridgeline is a possible solution. Attachment of covers is less problematic. The structure can easily accommodate either a single or dual-layer cover.

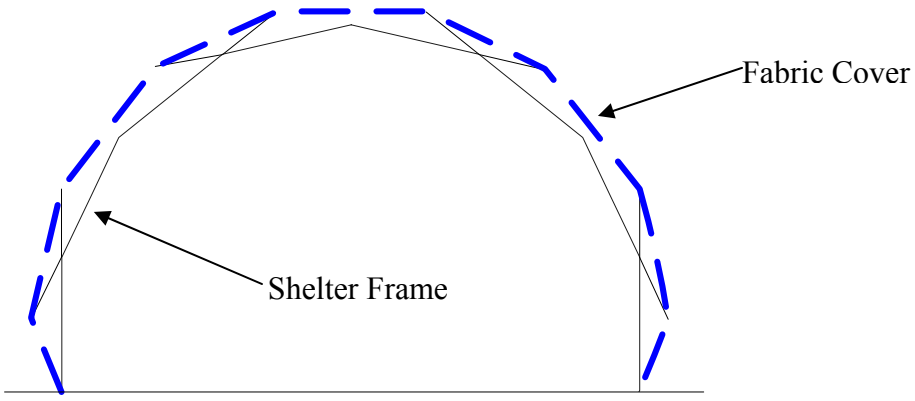


Fig. 3.3 Fabric interaction with frame

Because of the complexities associated with the development of fabric covers and the excellent solutions already available, the cover for the Bennett Shelter will be adapted from existing solutions.

3.2.3 Foundation Design

Development of ground attachment for the Bennett Shelter must differ with size by necessity. Deployable structures currently used by the military (DRASH tents) and other new designs avoid the use of guy lines for structural support. These lines slow down the erection of the structure, and require a large footprint. DRASH tents use base plates and stake support for all tents (DHS Systems LLC, 2002). The current large-scale structures in use in the Army, to include the LAMS and the LANMaS, make use of duckbill anchors for foundation support. As shown in Fig. 3.4, duckbill anchors are pushed into the ground to a prescribed depth and then ratcheted up until the long axis of the anchor is perpendicular to the steel attachment cable (Melin, 2000).

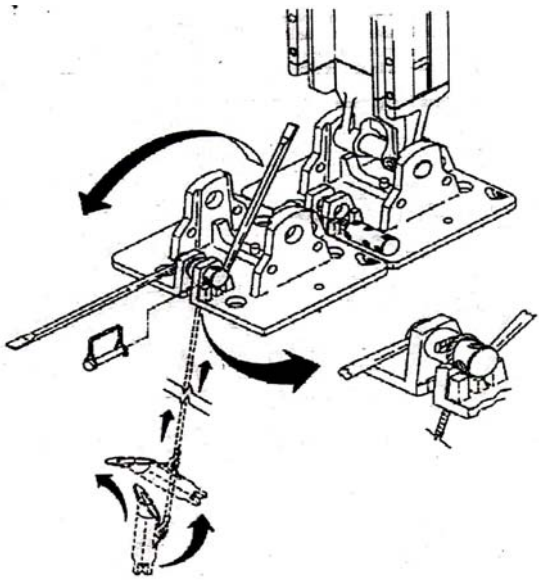


Fig. 3.4 Duckbill anchor system (Melin and Workman, 2000)

Difficulties occurred with this method of foundation support, however, when applied in the Bosnia and Kosovo military campaigns. Due to rain and soil composition, large amounts of mud were present in areas where large-scale structures were constructed. The duckbill anchor relies on the stiffness of the soil to provide foundation support. It works best with a gravelly base. These anchors were useless in muddy conditions. The solution developed by Melin and Workman involved the design of pile caps and screw anchor foundation systems for muddy conditions (Melin and Workman, 2000).

Development of foundation support for the Bennett Shelter consists simply of adapting existing foundation support used for the LAMS. For the helicopter shelter, the use of duckbill anchors will be sufficient for most conditions. The hardware necessary for installation is already developed and fielded in the U.S. Army. In poor ground conditions, screw anchors and pile caps will be used. For smaller structures, stakes can be used as with the DRASH XB and J Series tents.

3.2.4 Doorway System

Doorway design is important due to issues of modularity and the functionality of large-scale structures. Structures like the MGPTS, TEMPER, and DRASH tents have doorways that are designed to interface with each other. Connecting the shelters together allows users to decide the size and shape of the shelter they desire. The TEMPER, MGPTS, and DRASH tents accomplish this by simply designing fabric covers that can attach to each other. DRASH also has special fabric doorways, called bootwalls, which are designed to attach military vehicles to shelters. These allow for the construction of command posts that make use of military technology and provide versatility.

For large-scale structures, such as helicopter shelters, the design of functioning doorways is a prime consideration. The openings in shelters designed for storing

equipment are quite large, and require doors with separate frame structures. The opening and closing of these doors is accomplished using an electric powered winch. Structures like the LANMaS and LAMS make use of clamshell doorways. These structures consist of four arches next to each other and connected by fabric. The base plates are connected together, and a set of two winches is used to articulate the structure (Melin, 2000). Another door configuration used with large-scale structures is the hard shell door. This type of doorway consists of two curved pieces mounted on wheels that open outwards from the center either manually or using a motor. The hard shell doorway is heavy and difficult to transport. Although it does not impart additional loads onto the structural frame, it is slow to construct and has difficulty when used on uneven ground. The clamshell door can have problems with shifting of base plates on uneven ground. Because only a rain gutter is used to tie arches together, shifting of base plates due to opening and closing of the clamshell door causes damage to the electric winches (Melin, 2000).

Design of doorway structures for the helicopter structure requires examination of current designs. Because of the inter-linked frame of the Bennett Shelter, the problem of shifting base plates would not occur if a clamshell door was used. The use of a hard shell door would not work with the Bennett Shelter because of the difficulty of transporting it and the increased weight. The door structure must conform to all specifications for weight, speed of erection and transportability defined above. Doorway design is not included in this study.

3.2.5 Connector Hallway

It is desirable to connect shelters both laterally and lineally. This allows the construction of large shelter complexes for various uses. The Bennett Shelter is modular. It is possible to connect structures of the same type (same design details) end-to-end so that the structures have one continuous frame. It is not possible, however, to connect shelters perpendicular to the long axis. There are a number of solutions to allow the construction of shelter complexes. Development of an intermediate structure connecting two Bennett Shelters composed of tiled Bennett mechanisms is possible. This, however, would necessitate considerable design. A better solution is to examine the removal of a unit from the bottom segment of a frame and development of a connector hallway between two structures. Connection between the hallway and structure frames is not required. This can be accomplished using a fabric connection. All that is required, therefore, is additional structural analysis to ensure that components are designed to withstand changes in loading caused by the exclusion of a structural unit in the ground level segments.

Development of the full concept of the structure provided additional constraints to the frame design process. Ruling out the use of guy ropes, determining that doorway weight would be carried separately, and deciding to analyse the structure missing units in segments adjacent to the ground provided information necessary to conducting load and structural analysis.

3.3 Bennett Shelter

3.3.1 Variable Definitions

In order to develop a versatile shelter structure, it was necessary to develop a method of designing structures to meet the criteria of the Bennett linkage. Potential

users of the structure can only be expected to provide desired structure length, width and height. A procedure is necessary to take these dimensions and translate them into design details, such as bar length and primary skew angle. The first step to accomplishing this goal is describing the geometry of the structure in deployed and compacted configurations. To do this, it is useful to first determine the variables that describe the structure, any relationships between these variables, and constraints that affect the structure.

The variables describing the equilateral Bennett Shelter are shown in Fig. 3.5.

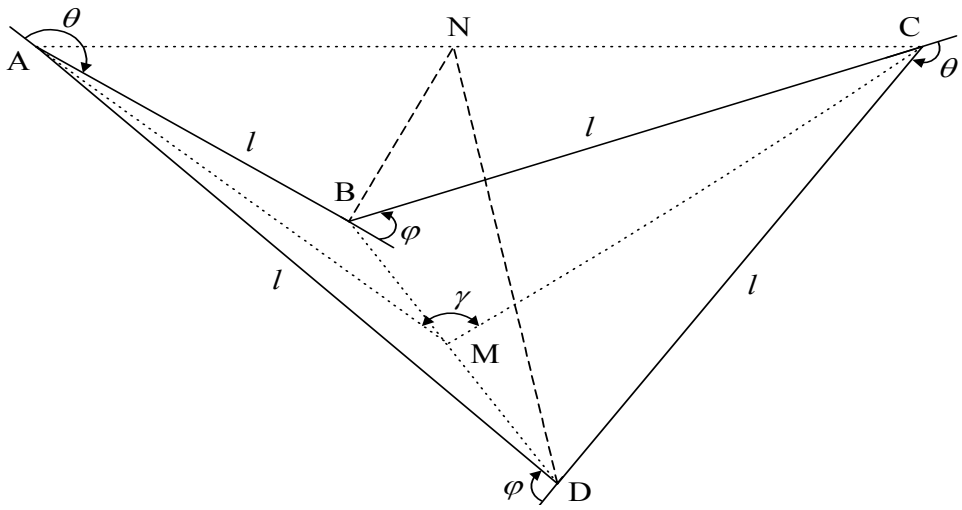


Fig. 3.5 A 3-D view of an equilateral Bennett mechanism

Angle γ represents the *bend* in the Bennett mechanism at any point in deployment. The Bennett bar length is represented by l. The angles between adjoining bars are represented by θ and φ respectively. The angle between adjacent pins, as shown in Fig. 2.6, is represented by α. Furthermore, since the mechanism is equilateral, triangles BCD, ABD, BCA, and DCA are isosceles. We also know that triangles DNB and AMC are isosceles because the perpendicular bisectors of isosceles triangles with equal legs are equal. Fig. 3.6 shows a side view of a Bennett Shelter made from identical, equilateral

Bennett linkages. H and W designate height and width, respectively. The side length of the structure when viewed from the short axis is defined as l'. This length becomes important when drawing an analogy between the short axis and a regular polygon, which is done in Section 2.4.2.

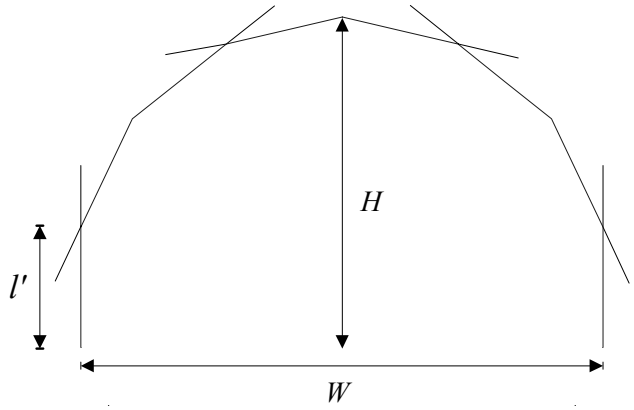


Fig. 3.6 Side view of structure

As the structure is segmented for transport, it is necessary to define the segmented sections of the structure. As shown in Fig. 3.7, the number of segments the structure is broken down into for transport is defined as v. The number of four bar units in each segment is defined as u.

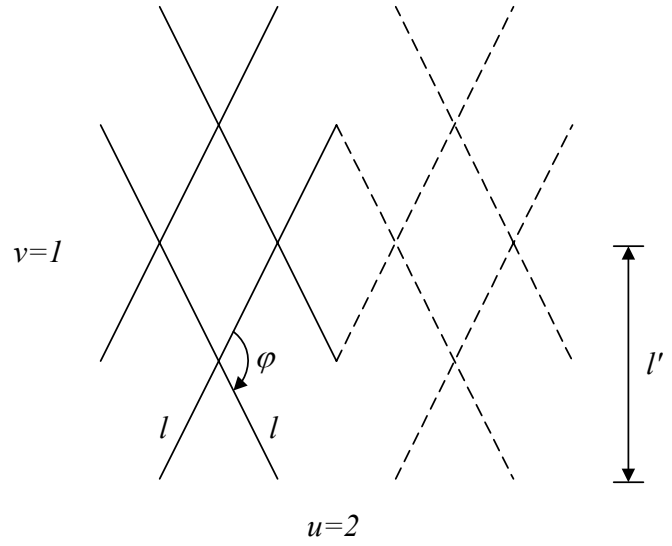


Fig. 3.7 A Segment of the Bennett Shelter (additional unit shown in dashed lines)

With variables designed, it is necessary to establish relationships and constraints between them.

3.3.2 Constraints

The Bennett Shelter is governed by a number of conditions. First, the structure is composed of equilateral Bennett mechanisms and therefore compatibility equations (2.13-15) apply. Because the structure is being used as a shelter, the configuration of the structure that provides maximum space is when the ends of the structure are perpendicular with the ground. This allows for easy connection to foundation systems. Further, an interesting condition is established. As shown in Fig. 3.6, when the ends of the structure are perpendicular to the ground the structure takes on the shape of a portion of a regular polygon. Relationships governing the dimensions of a regular polygon, therefore, apply to the deployed configuration of the structure.

The uses of the structure provide a number of constraints. As shown in Fig. 3.1, the frame is segmented before placement on pallets. These segments must conform to

the dimensions of the transportation pallets or shipping containers used to deliver them to an area of operations. The compacted length and width of the shelter segments are, therefore, restricted.

3.4 Relationships among Key Geometric Parameters

3.4.1 Relationship among γ, θ, φ, and α

Fig. 3.5 shows an equilateral Bennett mechanism. Applying the law of cosines and Eqns. (2.5) and (2.6) it can be found that

$$\overline{BD}^2 = l^2 + l^2 - 2l^2\cos(\pi - \theta) = 2l^2\left(1 + \cos(\theta)\right) \tag{3.1}$$

Likewise, it can be determined that

$$\overline{AC}^2 = l^2 + l^2 - 2l^2\cos(\pi - \varphi) = 2l^2\left(1 + \cos(\varphi)\right) \tag{3.2}$$

Applying the Pythagorean Theorem, it can be determined that

$$\overline{CM}^2 = \overline{BC}^2 - \left(\frac{1}{2}\overline{BD}\right)^2$$

$$\overline{CM}^2 = l^2 - \frac{l^2}{2}\left(1 + \cos(\theta)\right) \tag{3.3}$$

In order to determine γ, we next look at ΔAMC. Applying the law of cosines, we find

$$\overline{AC}^2 = \overline{AM}^2 + \overline{MC}^2 - 2\overline{AM} * \overline{MC} * \cos(\gamma)$$

Combining Eqns. (3.1), (3.2), and (3.3), we can define γ:

$$\gamma = 1 - 2\frac{1 + \cos(\varphi)}{1 - \cos(\theta)} \tag{3.4}$$

This equation relates the deployment angles φ and θ to γ, the bend in the Bennett mechanism. Eqn. (2.12) relates α, φ, and θ. We have two equations and three

unknowns. By combining these two equations, we can cancel θ and solve for α. The result is

$$\alpha = \cos^{-1}\left(\frac{1}{-\tan\left(\frac{1}{2}\cos^{-1}\left(1-2\frac{1+\cos(\varphi)}{1-\cos(\gamma)}\right)\right)\tan\left(\frac{\varphi}{2}\right)}\right) \tag{3.5}$$

The next step in the analysis is to examine more closely the modelling of the structure using a regular polygon.

3.4.2 Polygon Analogy

As the side of the structure when deployed can be related to a portion of a regular polygon, it is useful to define equations relating to polygons. A regular polygon is shown in Fig. 3.8.

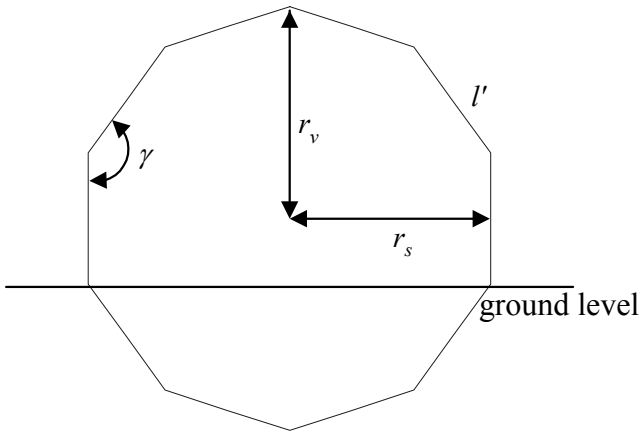


Fig. 3.8 Polygon approximation of a structure doorway

For a regular polygon, the distance from the center of the shape to the midpoint of a side (as defined in Fig. 3.8 as r_s) is defined. The width of the shelter structure is twice this distance. The width, therefore, is defined as

$$W = 2r_S = \frac{l'}{\tan\left(\frac{\pi}{2n}\right)} \tag{3.6}$$

where n equals the number of sides of the polygon and l' equals the length of one side of the regular polygon. The distance from the center of a regular polygon to the intersection of two sides (as defined in the above figure as r_v) is equal to the height of the structure plus one half of the side length. The height of the structure is, therefore, defined as

$$H = r_V + \frac{l'}{2} = \frac{l'}{2}\left(\frac{1}{\sin\left(\frac{\pi}{2n}\right)} + 1\right) \tag{3.7}$$

The structure height and width can be related directly to each other with the following equation

$$\frac{W}{H} = \frac{2\cos\left(\frac{\pi}{2n}\right)}{1+\sin\left(\frac{\pi}{2n}\right)} \tag{3.8}$$

We recognise from examination of the Bennett Shelter that the included angle between adjacent sides of the regular polygon is equal to γ. The equation for γ is

$$\gamma = \left(\frac{n-2}{n}\right)\left(\frac{\pi}{2}\right) \tag{3.9}$$

The relationship between n, the number of sides of the regular polygon used to model the shelter, and the number of collapsible structural segments, v, can be further deduced. It is

$$n = 4v - 2 \tag{3.10}$$

From this analysis, expressions for the height and width of the structure are determined. It is also evident that height and width are related to each other. Additionally, Eqn. (3.9) provides a method of determining γ.

The polygon relationship shows that if the height or width of the structure is given, the other dimension and l' are fixed. They are not affected by the skew angle, α, deployment angle, φ, or Bennett bar length, l. This is illustrated in Fig. 3.9. For a given value of l', a number of values of l and φ are possible. It is still necessary to determine the relationship between l' and l, the length of the structure and given variables, and the effect of packaging constraints.

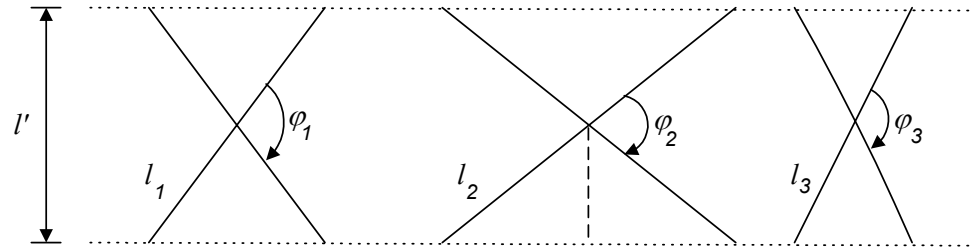


Fig. 3.9 l and φ are independent of l'

3.4.3 Relationship between *l* and *l'*

As shown in Fig. 3.9, an isosceles triangle is formed at the intersection of bars in each Bennett segment with legs of length l. The perpendicular bisector of this triangle equals half the polygon side length. Using the Pythagorean Theorem, it is possible to solve for the Bennett bar length, l.

$$l'^2 = 4l^2 - 2l^2(1+\cos\varphi)$$

or

$$l = \frac{l'}{\sqrt{4-2(1+\cos\varphi)}} \tag{3.11}$$

3.4.4 Structure Length

The length of the structure is a user-defined option. Additional units, u, can be added in order to meet any length requirement. It is necessary to express the number of units in terms of the structure length, L, deployment angle, φ, and bar length, l. As shown in Fig. 3.10, the length of the structure can be broken down into multiples of two separate lengths, X_1 and X_2. The length can be described as

$$L = (u-1)X_2 - (u-3)X_1 \tag{3.12}$$

where u is equal to the number of Bennett units used in the structure. Using the law of cosines, it is possible to determine that

$$X_1^{\,2} = 2l^2(1+\cos\varphi)$$

$$X_2^{\,2} = 18l^2(1+\cos\varphi)$$

Substituting these equations into Eqn. (3.12) and solving for u yields

$$u = \frac{L}{2.828l\sqrt{1+\cos\varphi}} \tag{3.13}$$

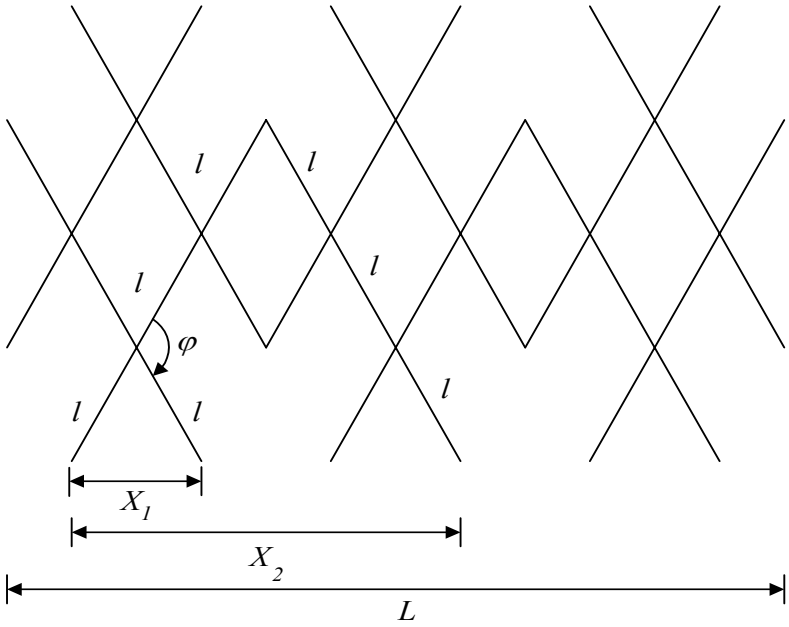


Fig. 3.10 Structure length

At this point in the analysis of the structure, the height, width, and length of the structure are all defined in terms of the deployment angles, primary skew angle, α, Bennett bar length, l, and polygon side length, l'. The goal is to develop a system of equations that provides design details with the input of the length of the structure and either the desired height or width. The difficulty is that it is necessary to specify either the deployment angle or primary skew angle to solve for the key structure variables. An examination of constraints introduced by the packing of the segmented structure is, therefore, necessary.

3.4.5 Dimensions of Compacted Segment

When a Bennett segment is completely compacted, the 'bend' in the Bennett segment, γ (see Fig. 3.5), approaches π and the segment is flat. Although the segment is spatial during deployment, in this configuration all bars of the segment effectively lie in the same plane. In this configuration, it is possible to develop relationships to define the fully compacted length and width of the segment.

As shown in Fig. 3.11, the perpendicular distance between two adjacent bars in the segment when compacted is defined as d. The included angle between two members of the segment, as shown, is defined as μ. In the fully folded position, d equals the width of the bar. It is possible to solve for μ in terms of d and l.

$$\mu = \sin^{-1}\left(\frac{d}{l}\right) \tag{3.14}$$

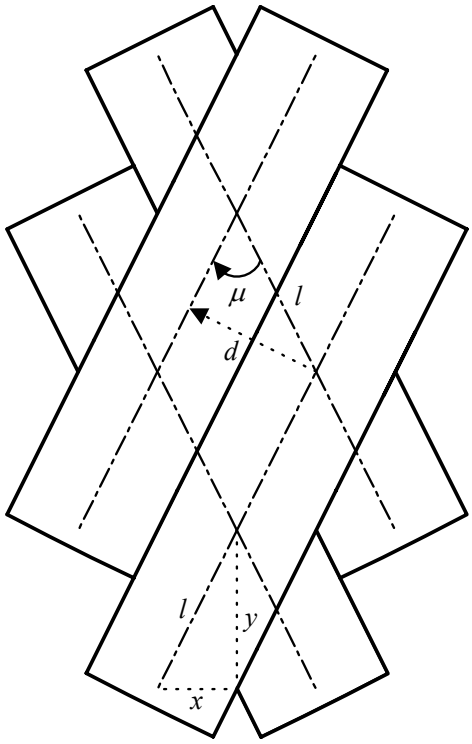


Fig. 3.11 A typical folded Bennett segment when the physical dimensions of the links are considered

Next, it is useful to determine the length of x and y, as shown in Fig. 3.8, and substitute in Eqn. (3.14).

$$x = l\sin\left(\frac{1}{2}\sin^{-1}\left(\frac{d}{l}\right)\right)$$

and

$$y = l\cos\left(\frac{1}{2}\sin^{-1}\left(\frac{d}{l}\right)\right)$$

Knowing the width of one component of the segment length, it is possible to factor in the full width of the unit and the number of units to determine the compacted structure width (W_c)

$$W_c = 4ul\sin\left(\frac{1}{2}\left(\sin^{-1}\left(\frac{d}{l}\right)\right)\right) \tag{3.15}$$

It is similarly possible to determine the compacted length of the segment

$$L_c = 4l\cos\left(\frac{1}{2}\left(\sin^{-1}\left(\frac{d}{l}\right)\right)\right) \tag{3.16}$$

This expression can be simplified. If the Bennett bar length (l) is large compared to the bar diameter (d), then μ is approximately equal to zero. Eqn. (3.16) simplifies to

$$L_c = 4l$$

If the maximum compacted length of the segment is established for the purpose of packaging the structure for delivery, the maximum Bennett bar length for a given structure geometry is, therefore, equal to

$$l_{\max} = \frac{L_c}{4} \tag{3.17}$$

As shown in Fig. 3.12, a relationship exists between l and φ. If l is limited by the pallet length, it follows that φ must be limited as well.

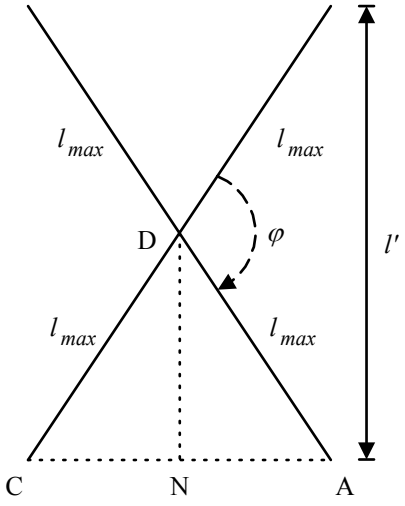


Fig. 3.12 Relationship between l_{max} and φ

Using right triangle trigonometry, it is possible to determine the limiting value of φ to be

$$\varphi = -2\left(\cos^{-1}\left(\frac{\frac{1}{2}l'}{l_{\max}} \right) \right) + \frac{\pi}{2} \tag{3.18}$$

A problem with this relationship is that when $\frac{\frac{1}{2}l'}{l_{\max}}$ is greater than one, the equation is undefined. When this occurs, the segment length does not meet the pallet constraint. This indicates that the structure defined for the desired deployed structure dimensions cannot meet packaging constraints. Defining an intermediate variable, *g*, provides a convenient method of determining the compatibility of structural and constraint dimensions.

$$g = \frac{\frac{1}{2}l'}{l_{\max}} \tag{3.19}$$

If *g* is greater than or equal to one, the structure does not meet the pallet constraint. If less than one,

$$\varphi = -2\left(\cos^{-1}(g)\right) + \frac{\pi}{2} \tag{3.20}$$

This set of equations provides a value for φ, and, along with Eqn. (3.11), provides the final relationships necessary to develop a design procedure.

3.5 Geometric Analysis of Configurations

In order to develop dimensional tables, there must be a deterministic process that supplies structure dimensions for a requested structure height, length, and width. The user must provide desired structure dimensions and determine whether height or width is the controlling dimension. The reason for this is that height and width are related directly to each other. The user must next specify the compacted length, L_c, and

compacted width, W_c, requirements for the packaged structure. From L_c, the Bennett bar length can be calculated using Eqn. (3.17). The user then inputs the diameter of the bars used in the structure.

The next step is to determine an initial n value. By rearranging Eqn. (3.8), it can be found that

$$n_i = \frac{\pi/2}{2\tan^{-1}\left(\frac{-2W+4H}{2W+4H}\right)} \tag{3.21}$$

Inputting user-defined structure height and width yields an approximate n value. It is necessary to ensure the n value is compatible with a whole number of segments. Rearranging Eqn. (3.10) yields

$$v = \frac{n_i + 2}{4} \tag{3.22}$$

Using this value, after rounding up to the nearest whole number, in Eqn. (3.10) yields the n value for the shelter structure. The next step is to solve for the polygon side length (l'). Rearranging Eqns. (3.6) and (3.7) yields

$$l' = W\tan\left(\frac{\pi}{2n}\right) \tag{3.23}$$

$$l' = \frac{2H}{\frac{1}{\sin\left(\frac{\pi}{2n}\right)}+1} \tag{3.24}$$

If the user specified structure width as the defining dimension, Eqn. (3.23) is used to calculate l'. If height was specified, Eqn. (3.24) is used. Eqns. (3.6) and (3.7) are then used to calculate the other dimension.

With the possible structure height and width defined, the next step is to determine γ using Eqn. (3.9). It is then possible to calculate φ using Eqns. (3.18), (3.19) and (3.20).

If the compacted structure does not fit within the constraint dimensions, it is necessary to restart the design procedure with different dimensions or altered constraints. With all dependent variables defined, it is next possible to calculate the primary skew angle, α, using Eqn. (3.5). The Bennett bar length is then determined using Eqn. (3.11). The next step is to find the number of units per segment. Applying Eqn. (3.13), an initial u value is calculated. It is necessary to round this value up to the nearest whole number and apply the following equation to find the length of the structure

$$L = 2.828ul\sqrt{1+\cos\varphi} \tag{3.25}$$

To determine whether the structure length meets the constraint dimension, it is necessary to calculate the compacted width of the structure using Eqn. (3.15). If the compacted width is greater than the constraint dimension, the length of the structure must be changed to meet the constraint. The final steps of the design process are to calculate the structure bar length and the number of bars used in the structure. The structure bar length (l_b) is simply three times the Bennett bar length. The number of bars in the structure equals

$$B_a = 4uv \tag{3.26}$$

Displayed in Fig. 3.13 is a flow chart showing the design procedure. This provides a method for calculating design information for the Bennett Shelter.

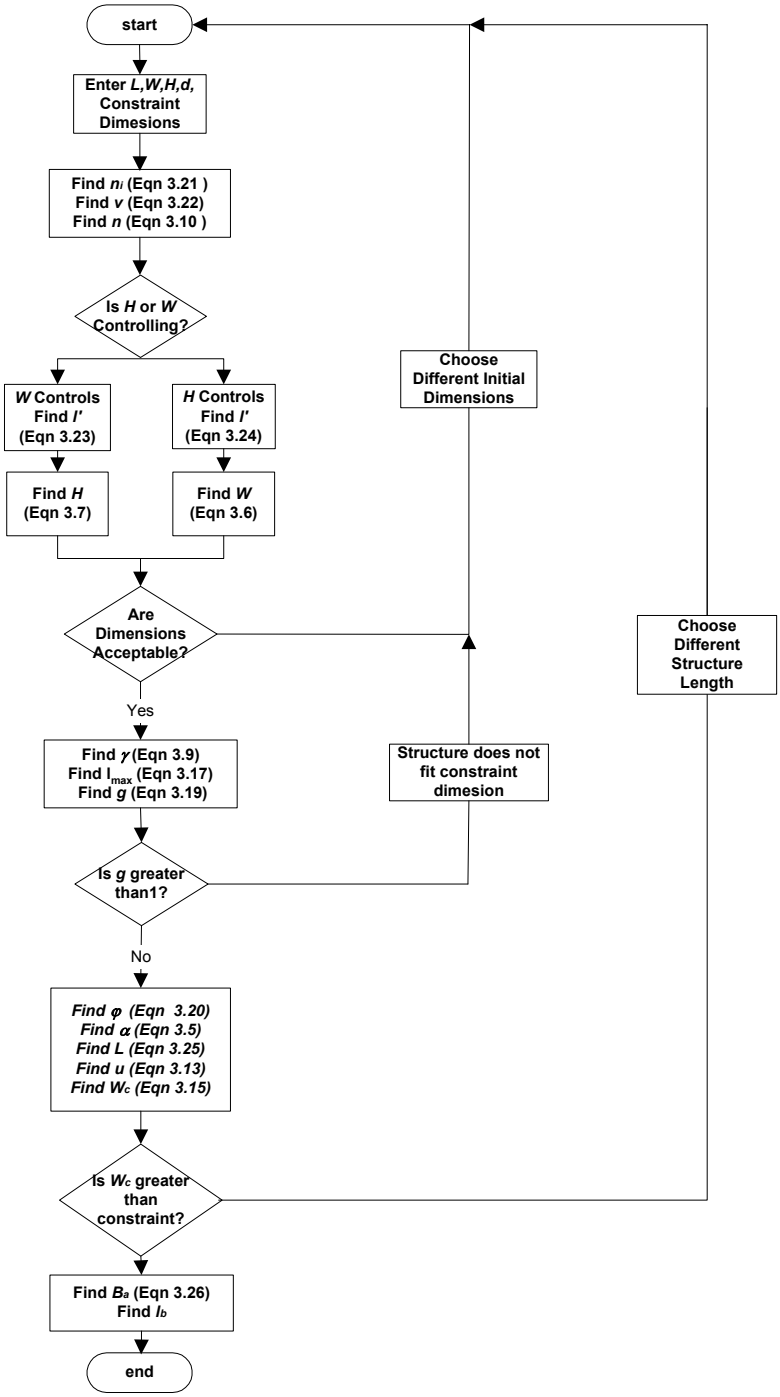


Fig. 3.13 Geometric design procedure

4 Structural Analysis for a Perfect Bennett Shelter

With a geometrical analysis completed, it is possible to determine the performance of the Bennett Shelter under load. Because it is 3-D, thought must be given to the design methodology applied to the structure, the proper method for factoring loads and applying them, and the magnitude of the loads and materials to be used during analysis. With the model defined, an analysis methodology is developed for the deployed shelter. The ultimate limit states considered are member and joint internal stresses and buckling. The serviceability limit states analysed are deflection under load and frequency analysis. The layout of this chapter is as follows: Section 4.1 defines analysis requirements and design methodology for the Bennett Shelter. The application of service loads to the deployable frame and their factoring are considered in Section 4.2. Materials used in the frame are chosen in Section 4.3. Section 4.4 addresses serviceability analysis and Section 4.5 covers stress analysis. Buckling and frequency analyses are detailed in Sections 4.6 and 4.7 respectively. Prototype construction is then detailed in Section 4.8 and some conclusions are presented in Section 4.9.

4.1 Analysis Requirements and Design Methodology

When conducting a structural analysis, a number of factors must be addressed. The structure's geometry, the boundary conditions of the model and the type of analysis being conducted using ABAQUS should be determined. The design methodology for the structure and the manner in which loads on the structure are factored also requires consideration. It is then necessary to find where combined stresses reach a critical value in the structure and determine factors of safety versus failure due to internal stress and buckling.

The configuration of the Bennett Shelter to be analysed is fully open with ground-level units excluded to allow for the attachment of connector hallways (as detailed in Section 3.2.4). The structure is pinned at all ground-level connections. The finite element software used for the structural analysis is ABAQUS. It is a versatile utility that can analyse complex, 3-D mechanisms both statically and dynamically. A computer routine, written using Matlab, is used to generate ABAQUS input programs for any set of Bennett Shelter dimensions. Joints are modelled using the multi-point constraint connection. This allows free rotation around the axis of the joint. Frame elements are used to model structural members. This allows the outputting of internal forces along the length of the element. Additionally, elastic-plastic analysis is possible using frame elements. Elastic response is governed by Euler-Bernoulli beam theory. Plastic response is lumped at element ends and accounts for kinematic hardening (Hibbitt et. al, 2002). When using the plastic defaults option, all required response parameters are generated based upon the material yield stress.

Design of the Bennett Shelter requires consideration of both strength and serviceability limit states. For long-span shelters, the controlling design criterion is often serviceability. It is necessary to determine the member cross-sections and joint sizes necessary to keep deflection within limits specified by codes. Then, both the members and joints are designed to withstand stresses under ultimate limit states. This analysis considers the structure's performance under load both elastically and plastically. A separate buckling analysis is conducted using asymmetrical loading to verify that failure does not occur due to load patterns not accounted for in stress analysis. The combined effects of stress and buckling are then considered. Finally, frequency analysis is conducted as part of the serviceability limit state to ensure that the natural frequencies of

the structure do not correspond to those caused by wind and other machinery such as a helicopter.

Before beginning structural analysis, a design methodology must be chosen. The two methodologies used in structural design are Allowable Stress Design (ASD) and Load Resistance Factor Design (LRFD) (AISC, 1998).

ASD is expressed by the following relationship

$$\sum Q_i \leq \frac{R_n}{F.S.} \tag{4.1}$$

where $\sum Q_i$ equals the total load effect on the structure, R_n equals the nominal strength of the structure, and *F.S.* equals the factor of safety against structural failure. When using ASD, the effects of loading are directly totaled and then a single factor of safety is used to provide load-carrying capacity above the required minimum.

LRFD provides the uniform reliability for steel or aluminium structures under variable loading. It is expressed by the inequality below,

$$\sum \upsilon_i Q_i \leq \chi R_n \tag{4.2}$$

where υ_i equals the load factor, Q_i equals the effect of a load, χ is the resistance factor, and R_n is the nominal strength of the structural member. It incorporates probabilistic factoring of service loads as calculated by the American National Standards Institute (ANSI). A statistical study on structural loading showed that in situations of combined loading it is highly improbable for more than one type of loading to reach its maximum value (AISC, 1998). ANSI developed probability-based load factors that set one source of loading at its maximum lifetime value while the others assume arbitrary point-in-time values. LRFD factors each load on a structure depending upon its frequency and severity within a certain geographic region.

Both design methodologies have advantages and disadvantages. Use of ASD allows for analysis of complex loading using classical stress analysis methods. A number of different theories of failure can be applied to analyse a structure or component. Additionally, ASD is useable with any linear elastic material. This includes carbon fibre composites, which behave elastically until reaching a failure stress. These advantages make ASD the preferred method for mechanical design. The disadvantage of this methodology relates to the direct summation of load effects. When considering environmental loading, this method is overly conservative.

LRFD is less conservative than ASD due to the application of probabilistic load factors. This leads to smaller, more realistic load effects and more efficient structural designs. Also, empirical design aids exist for both aluminium and steel. Because LRFD develops resistance factors only for materials commonly used in construction, however, it cannot be used for special materials. Carbon fibre composites, a material often used in tent shelters, are designed for specific loading conditions. Thus, material properties vary from application to application and general resistance factors for different failure modes cannot be determined (AISC, 1998).

Though LRFD is considered the standard design methodology for conventional structural design, ASD provides a more general approach. It is applicable to any proposed material type, and more than one failure theory can be applied for a given state-of-stress. Thus, ASD is used in this study.

4.2 Load Analysis

4.2.1 Load Combination and Application

Loads affecting the Bennett Shelter are wind, snow, and self-weight. They are found using procedures from *American Society of Civil Engineers 7-95, Minimum*

Design Loads for Buildings and Other Structures (*ASCE 7-95*, 1996). Code specifies that loads must be adjusted to take into account variation in environmental effects and the type of analysis conducted. Serviceability limits states involve visually objectionable deformations, repairable cracking, or other effects caused by consistent loading over a long period. These loads may not be the largest that the structure will have to carry. The suggested load combination for deflection analysis with no live loading is

$$D_e + 0.5S \tag{4.3}$$

The load combination used for analysing lateral drift is

$$D_e + 0.7W_i \tag{4.4}$$

where D_e is the dead load, S is the snow load, and W_i is the wind load (either crosswind or longitudinal wind loading). Stress analysis considers the ultimate limit state during the entire lifetime of the structure. Duration is not important. The load combinations for this analysis are:

$$D_e \tag{4.5}$$

$$D_e + S \tag{4.6}$$

$$D_e + W_i \tag{4.7}$$

$$0.75\left(D_e + W_i + S\right) \tag{4.8}$$

Complete analysis for the Bennett Shelter requires the running of three load combinations for serviceability and six different load combinations for stress analysis. Dead loading is combined singly with snow and wind loading both parallel and perpendicular to the long axis of the building. Design code permits, for the combination of dead, wind and snow loading, the application of a reduction factor of 0.75. This is due to the improbability of having both wind and snow loading at full magnitude at the same time. Load combinations for buckling will be addressed in Sections 4.6.

The Bennett Shelter's fabric cover interacts with the frame at specific points. Loads applied to the fabric cover, assuming it is taut, transfer from the fabric to the structure through these points, which are illustrated in Fig. 4.1. The dashed lines represent the fabric cover, to include the separation of the cover into tributary areas. Highlighted portions of the figure designate points at which the fabric attaches to the frame. Exterior and interior bar ends carry different loads, due to the fact that they have different tributary areas ($l'\times w_i$ or w_e).

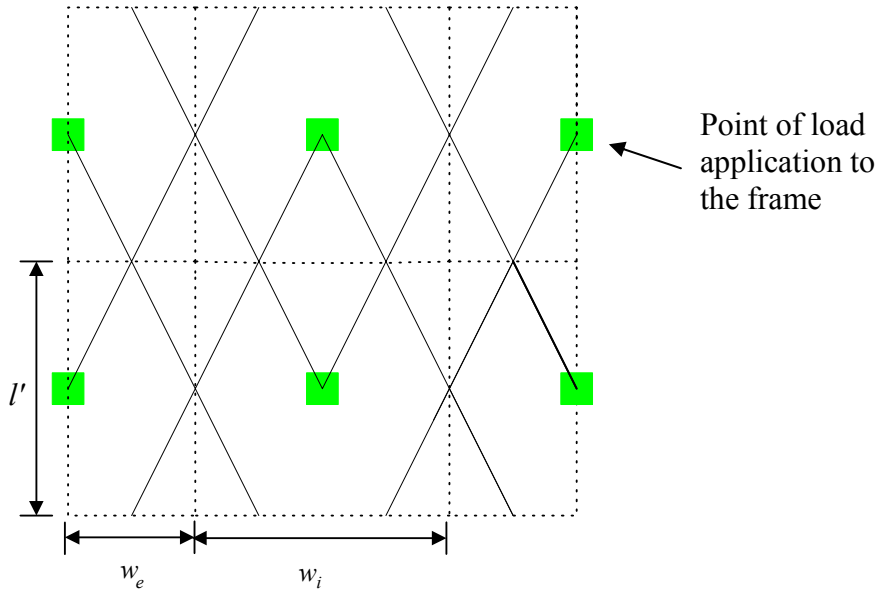


Fig. 4.1 Projection of the structure showing points where the structure carries loads

4.2.2 Dead Loads

Calculation of dead loads requires the determination of the load caused by the frame, the fabric cover, standard joint weight, and a lighting or duct allowance. Analysis initially uses standard scaffolding tubes because of their availability. Cross-sectional dimensions are changed to meet serviceability and strength requirements during the analysis. The frame weight is determined by calculating the weight per meter of pipe

and then multiplying by the total length of pipe in the structure. Averaging the weight of a number of different models of scaffolding joints provides a standard joint weight of 10.8N. The weight per square meter of fabric is found using a sample from a Ministry of Defense (MOD) shelter. Discussions with shelter designers revealed that the wet weight of the fabric should be used as a worst-case scenario.

When calculating the area of the fabric cover, it is assumed that a separate frame will carry the weight of fabric used for the doorways. Thus, calculation of the area of fabric requires only the determination of the area of fabric on the frame. An approximation for the length of fabric covering one deployed segment of the structure is *2l'*. From this, an expression for the width of the fabric cover is determined and the area of the fabric structure found by multiplying by the deployed length of the structure.

$$A = 2vL\sqrt{2l^2(1+\cos\varphi)} \tag{4.9}$$

Multiplying by the unit weight of the fabric yields the weight of the outer cover. In order to incorporate the weight of an inner lining, a weight equal to 2/3 of the outer cover is added. A lighting and ductwork allowance of 500N is added as well along the crest.

4.2.3 Wind Loads

The Bennett Shelter is composed of multiple segments which, when opened, approximate an arched roof. Wind load calculation, therefore, uses the code for an arched roof springing from ground level. Loading on both the long and short axes of the structure is considered. As specified in code, wind blowing into the long axis of the structure causes pressure on the windward quarter of the structure, and suction pressures on the center half, leeward quarter, and sidewalls. Wind blowing into the short axis of the structure causes pressures similar to long, flat roofed structures. This consists of

pressure on the windward wall of the structure, graduated suction pressures along the long axis, and suction pressures on the leeward wall and the sidewalls (*ASCE 7-95*, 1996).

Application of the loads to the shelter is simplified by the polygon assumption. As shown in Fig. 4.2, pressure loads are calculated for each polygon side, resolved into point loads using the tributary areas mentioned in Section 4.2.1, and applied to the ends of the structural members (like the one highlighted below).

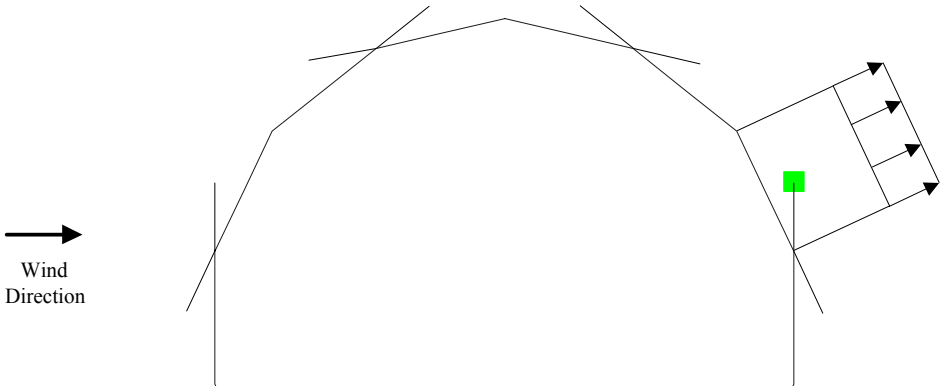


Fig. 4.2 Application of wind loads to structure

Application of pressures on the doorway of the structure requires the calculation of the doorway area. The area of the door is half the area of a regular polygon plus the area of a rectangle with dimensions of the structure width and half the polygon side length.

$$A_s = \frac{(l')^2}{2\tan\left(\frac{\pi}{2n}\right)}\left(\frac{n}{4}+1\right) \tag{4.10}$$

4.2.4 Snow Loads

As specified in Appendix 1, design snow load for the structure is 478.8N/m^2. For a barrel vault structure, *ASCE 7-95* states that portions of curved roofs having a slope exceeding 70° are considered free of snow load. After calculating the slope of each

segment, it is possible to determine the structural segments carrying snow and then find the loading using code. Assumptions made in the calculation of snow loading are that the roof is cold and has an unobstructed slippery surface. Application of loads to the structure requires the determination of projected polygon side widths. This allows calculation of the projected area carrying snow loading and translation of the loads onto the member ends.

4.3 Selection of Material and Sections

Choosing materials for use in the analysis of any structure or component requires consideration of several different criteria (Ashby, 1999). They are

- Function of structural component
- Materials available and their properties
- Shape and size of the component
- Process used to manufacture the component
- Cost and Availability

These criteria cannot be considered separately. The manufacturing process, for example, is influenced by the materials used in the structure. It also interacts with shape, size, required precision of manufacture, and cost. Each variable affects and is affected by the other variables. Thus, any attempt to optimise one criterion is complicated by the consideration of the other criteria. The more sophisticated the design, the more interrelated the criteria become and the more difficult to separate and evaluate. For this reason, a process for systematically considering the effects of material, geometry and performance has been developed. The optimal performance of any structure (p) can be related as

$$p = f\left[\begin{pmatrix}\text{Functional}\\ \text{Requirements},F\end{pmatrix},\begin{pmatrix}\text{Geometric}\\ \text{Parameters},G_e\end{pmatrix},\begin{pmatrix}\text{Material}\\ \text{Properties},P\end{pmatrix}\right] = f\left(F,G_e,P\right) \tag{4.11}$$

where p describes some aspect of the performance of the component. Optimal design either maximises or minimises p based upon requirements. Manipulation of this relationship often shows that one or more of the variables can be separated from the rest. A separated variable can be optimised independently. In the case of materials, this variable is called the material index. The advantage of optimising using this method is that it is unnecessary to completely solve the design problem to find the optimal material for the application (Ashby, 1999).

For the Bennett Shelter, the most essential material criteria are weight and stiffness. As the structure deploys rapidly, weight is critical. Additionally, long-span structures must be stiff to avoid excessive deflections. To model these criteria in simple terms, it is useful to view a member from the structure as a simply supported beam that must be both light and stiff. This is an accurate approximation of the behaviour of a member in the Bennett Shelter because all members in the structure have pinned joints. Finding the material index requires definition of a system of equations relating stiffness, weight, and geometry. Material variables are then separated. The maximum deflection at mid-span due to a point load is defined as

$$\Delta = \frac{PL^3}{48EI} \tag{4.12}$$

For a circular pipe, the moment of inertia, I, is defined as

$$I = \frac{\pi}{4}\left(r_o^4 - r_i^4\right)$$

and mass as

$$M = L\left(\pi\left(r_o^2 - r_i^2\right)\right)\rho$$

where ρ equals the density of the material. To find an expression for mass in which all material variables are separated, it is necessary to substitute the expression for I into Eqn. (4.12), solve for r_o^2-r_i^2 and substitute into the mass equation. It is

$$M = \left(\frac{P}{12\Delta}\right)^{\frac{1}{2}} \left(\pi L^5\right)^{\frac{1}{2}} \left(\frac{\rho^2}{E}\right)^{\frac{1}{2}} \tag{4.13}$$

From this expression, the material index is $\left(\frac{\rho^2}{E}\right)^{\frac{1}{2}}$. Minimising this index provides the most lightweight, stiff material for the Bennett Shelter. Table 4.1 shows common material values for this index.

Table 4.1 Material Indices (Ashby, 1999)

Material	**Material Index**
Steel	0.55
Polyurethane foam	0.41
Concrete	0.36
Aluminium	0.32
GFRP	0.31
Wood	0.17
CFRP	0.09

As the indices show, the most efficient material to use is carbon fibre reinforced plastic (CFRP). It is, also, the most expensive. Wood is not a realistic option due to long-term durability issues, and graphite fibre reinforced plastic is as expensive as CFRP without the large increase in performance over conventional materials. Obviously, the use of concrete or polyurethane foam is not realistic for this application. Thus, the three most logical construction materials for the Bennett Shelter are CFRP, aluminium, and steel. Analysis will evaluate the performance of these materials.

Determination of the necessary material properties for aluminium and steel is straightforward. Their behaviour when subjected to loading is linear elastic up to the

yield strength of the material, after which the materials deform plastically and eventually rupture. CFRP material properties are, however, more variable. Composite laminates usually consist of carbon, graphite, or ceramic fibres suspended in a polymer matrix (usually epoxy, polyester or plastic). The elastic modulus of the polymer matrix is usually quite low, but it ties together the fibres and is easily molded into different shapes. The in-plane elastic modulus of fibre used in these sorts of composites is very high (around 3000GPa), while the modulus perpendicular to the fibre plane is far lower (around 35GPa). Because of the great disparity in moduli in and out-of-plane, it is common to construct components with composite reinforced matrix layered in different orientations. The method of layering the composite is dictated by the size and orientation of loads on the structure. Both the fibre and polymer matrix are brittle materials and behave elastically up to the failure stress. The stress in a layer of composite is expressed using the rule of mixtures

$$\sigma_1 = j\sigma_f + (1-j)\sigma_m \tag{4.14}$$

where j is the volume fraction of fibre in the composite, σ_f is the stress in the fibre and σ_m is the stress in the matrix. Failure in the composite can occur when the matrix fails and load is transferred completely to the fibres, when the matrix fails partially and the fibre cannot carry the full load, or when the fibre fails before the matrix. With carbon/epoxy systems, the fibres make a contribution to the failure stress at fibre contents above 2.5%. As most fibre composites have fibre volume fractions between 30-70%, fibre strength is dominant in determining the axial strength of the composite (Derby, 1992).

Initial analysis of the Bennett Shelter showed that worst-case loading on the structural members required both a large modulus of elasticity and shear modulus. To

conduct the design, it is, therefore, not necessary to consider the actual layering of composite to achieve these material properties. Rather, a general modulus of elasticity and shear modulus for the composite members is applied. An elastic analysis is run using representative values for the elastic modulus and shear modulus to find worst-case member internal forces and moments. This information can be used by manufacturers to design the CFRP cross-section. Table 4.2 shows the material properties of interest for this study.

Table 4.2 Material properties of interest

	Density (kg/m3)	Tensile Yield (MPa)	Shear Yield (MPa)	Elastic Modulus (GPa)	Shear Modulus (GPa)
Carbon Fibre/Epoxy	1600	N/A*	N/A*	126.8	30.31
6061-T6 Aluminium	2710	240	140	70	26
ASTM-A36 Steel	7860	250	145	200	77
ASTM-A242 Steel	7860	345	205	200	77

* Tensile and shear yield stresses are not required for elastic analysis.

With material definition complete, it is next necessary to define the initial cross-section of the members. Because the bars require drilled pin connections or use of scaffolding couplers, it is necessary to use a pipe cross-section. As scaffolding pipes are widely available in both aluminium and steel, it is advantageous to use the standard pipe dimensions. These are 48.3mm diameter with 4.47mm wall thickness. To meet design criteria, both the diameter of the pipe and wall thickness will be varied.

4.4 Serviceability Analysis

4.4.1 Analysis Procedure

Serviceability analysis requires the determination of whether or not the maximum vertical displacement and horizontal drift meets the serviceability criteria set out by code

or the potential user. The serviceability criteria in conventional structures are prescribed in *American Society of Civil Engineers 7-95, Minimum Design Loads for Buildings and Other Structures*. Acceptable deflections for roof members of a permanent structure are generally $1/240$ of the span. This prevents any difficulties with doors or sliding partitions. Drift limits are on the order of $1/600$ to $1/400$ of building or story height for permanent structures (ASCE 7-95, 1996).

These criteria are for permanent structures. The potential applications for the Bennett Shelter are different. It is a temporary structure and has no internal partitions. Some drift and deflection is, therefore, acceptable so long as it is elastic and does not affect the entry and exit of the helicopter. Knowing the critical dimensions of the Apache Longbow Helicopter, as defined in Section 3.1, it is possible to develop deflection and drift criteria for the shelter based upon its potential use as an aircraft shelter. Deflection limits are set so as to avoid contact between the structure and both the top of a helicopter and main rotor during loading. If this clearance is large, then the vertical deflection will be kept below 2.5% of the structure span. Drift limits are set to avoid contact between the main rotor and the frame during loading. Analysis points for the structure are shown in Fig. 4.3. Point D corresponds to the height of the main rotor of an Apache Longbow helicopter. Points A, B, and C run along the crest of the structure, and correspond to the height of the helicopter's radar assembly.

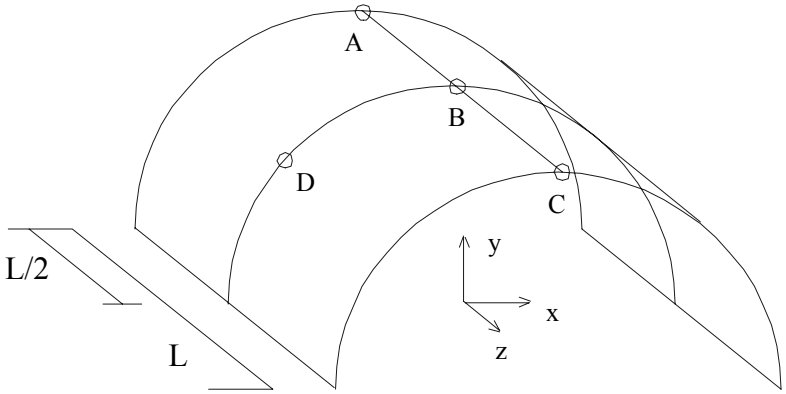


Fig. 4.3 Approximate position of analysis points for deflection

4.4.2 Analysis of the Bennett Shelter

The first step to designing the Bennett Shelter was application of the geometric design procedure detailed in Section 3.4 to meet user requirements. This yielded a configuration with properties listed in Table 4.3. Its deployed configuration with boundary conditions is shown in Fig. 4.4.

Table 4.3 Design specifications for helicopter structure

Structure Height (H)	6.7m (22ft)
Structure Width (W)	12.433m (40ft 9.5in)
Structure Length (L)	18.458m (60ft 6.7in)
Bar Length (l_b)	2.44m (8ft)
# of Collapsible Segments (v)	11
# of Units per Segment (u)	7
Primary Skew Angle (α)	3.02 radians (173°)
Secondary Skew Angle (α_2)	0.1222 radians (7°)
Bend in Bennett Segment (γ)	2.992 radians (171.42°)
Limiting Deployment Angle (φ)	1.29 radians (73.91°)
Polygon Side Length (l')	0.932m (3ft 0.7in)
Collapsed Segment Length (L_c)	3.1m 10ft 2in
Collapsed Segment Width (W_c)	0.356m (1ft 2in)
Corridor Height	1.854m (6ft 1in)
Corridor Width	1.778m (5ft 10in)
Number of Bars in Structure (B_a)	308
Total # of Joints	604
Total Bar Length	746.9m (2450ft 6in)

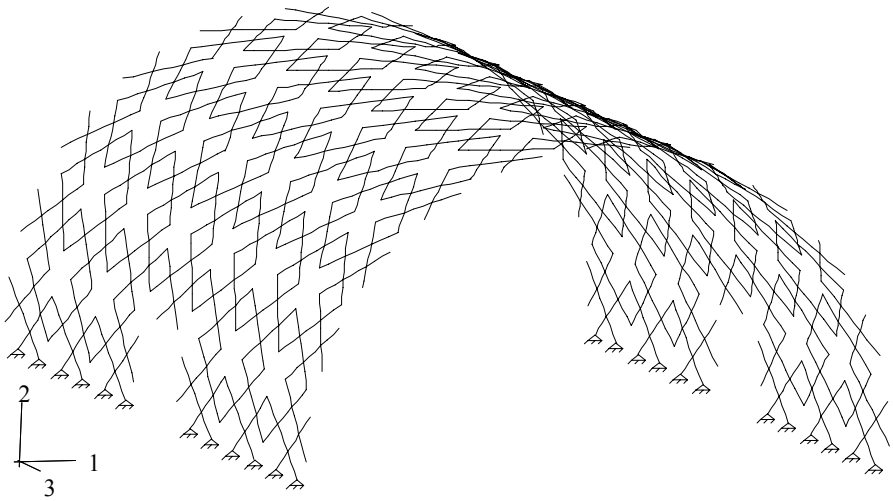


Fig. 4.4 ABAQUS CAE view of initial configuration with pinned boundary conditions

Using pipe member cross-sections defined in Section 4.3, it was possible to complete serviceability analysis. Environmental loading was factored using Eqns. (4.3-4.4). As clearance between the helicopter and the shelter was fairly large (1.21m for the initial configuration), a deflection limit of 2.5% of the structure span was used. The results of this analysis are shown in Tables 4.4 and 4.5.

Table 4.4 Deflection with CFRP cross-sections

Cross-Section	Deflection (m)	% Deflection (d/span)
114.3mm x 6.35mm	-0.3041	-2.45
127mm x 3.25mm	-0.3423	-2.75
127mm x 6.35mm	-0.2256	-1.81
0.1397m x 6.35mm	-0.1734	-1.39

Note: Cross-sections are listed in outer diameter x wall thickness

Table 4.5 Deflection with aluminium cross-sections

Cross-Section	Deflection (m)	% Deflection (d/span)
127mm x 6.35mm	-0.4706	-3.79
139.7mm x 6.35mm	-0.3359	-2.70
0.1524m x 3.25mm	-0.4922	-3.96

It was found that the structure failed for all materials. Deflection exceeded the limit and plastic deformation occurred in the members and joints. It was, therefore, necessary to increase the bar diameter and thickness. Use of steel was quickly ruled out during this process because of the increase in weight. For a 127mm diameter bar with a wall thickness of 6.35mm the structure weight using steel was 15253kg. This was heavier than all conventional solutions used by the United States Army. Analysis of CFRP and aluminium cross-sections also yielded solutions incompatible with potential applications. As shown in Tables 4.4 and 4.5, carbon fibre cross-sections met deflection requirements, but both CFRP and aluminium required cross-sections of at least 127mm in diameter. A cross-section of this size was too large for use in military applications.

It was obvious that the Bennett Shelter was not behaving ideally. There are two potential causes for this discrepancy. It is possible that the deployed dimensions of the initial configuration are simply too large to achieve acceptable deflections. If this is true, the Bennett Shelter is only useful for smaller structures. It is, also, possible that the shelter is not sufficiently *arch-like*. The longer the segment is in the global z-axis, the larger the flexural stresses in the members and smaller the axial stresses become. The variable that describes the *spread* of the Bennett segment is the deployment angle φ, as shown in Fig. 4.5 below.

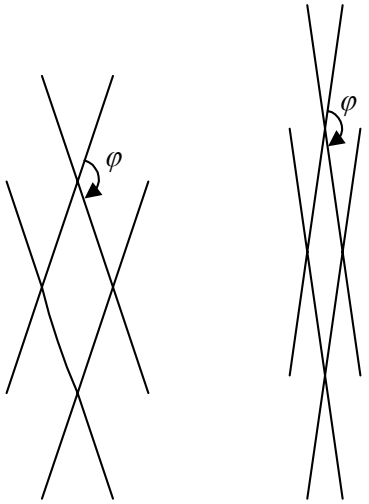


Fig. 4.5 *Spread* in a Bennett segment

Increasing the value of φ decreases the *spread* in the segment. This also decreases the magnitude of flexural stresses in the member and increases the portion of the load transmitted to the supports through axial compression. Thus, the Bennett Shelter behaves more like an arch as φ increases. Structure weight is also affected by φ. If a fixed deployed length is desired, increasing φ decreases the z-axis length of each unit of the segment. More units are required, and structure weight increases as a result.

The most efficient configuration for the Bennett Shelter is defined, therefore, by two variables: weight and mesh density. The initial configuration of the structure was designed to optimise structure weight but had unacceptable deflections. It is useful to generate a number of structural geometries that meet the user requirements with different values for φ. The most efficient configuration for the shelter can then be found by determining the weight and mid-span deflection for each model. If analyses of these configurations show that for all mesh densities deflections are unacceptable, then the Bennett Shelter cannot be used as a large-span structure.

Developing a series of models with different values of φ required iteration using the geometric design procedure and slight variations of the height and width of the structure in order to get different configurations. Thus, the models shown in Table 4.6 had a maximum variation of 0.5m in width or height. Bar length was kept constant and skew angles within a 0.02 radian tolerance.

Table 4.6 Geometric specifications for analysis models

Model	1	2	3	4	5	6	7	8	9	10	11	12	13	14	15
H (m)	6.5	6.59	6.7	6.7	6.7	6.95	6.7	7.1	6.90	7	7.15	6.9	6.94	7	7.06
W (m)	12.51	12.6	12.74	12.52	12.43	12.8	12.22	12.95	12.43	12.61	12.88	12.226	12.3	12.4	12.5
L (m)	18.83	21.5	21.0	19.26	18.46	19.25	20.29	20.90	19.52	20.55	20.91	19.93	20.3	20.38	20.08
l_b (m)	2.44	2.44	2.44	2.44	2.44	2.44	2.44	2.44	2.44	2.44	2.44	2.44	2.44	2.44	2.44
v	21	18	16	12	11	10	9	9	8	8	8	7	7	7	7
u	6	7	7	7	7	8	9	10	11	12	13	21	23	26	30
α (rad)	3.02	3.02	3.037	3.02	3.02	3.037	3.02	3.037	3.02	3.02	3.037	3.02	3.02	3.02	3.02
α_2 (rad)	0.122	0.122	0.105	0.122	0.122	0.105	0.122	0.105	0.122	0.122	0.105	0.122	0.140	0.122	0.122
γ (rad)	3.065	3.052	3.04	3.005	2.992	2.976	2.957	2.957	2.932	2.932	2.932	2.9	2.9	2.9	2.9
φ (rad)	0.629	0.747	0.86	1.17	1.29	1.507	1.637	1.77	2.006	2.05	2.123	2.558	2.6	2.662	2.733
l' (m)	0.48	0.566	0.646	0.856	0.932	1.061	1.132	1.2	1.307	1.325	1.353	1.484	1.493	1.506	1.518
B_a	504	504	448	336	308	320	324	360	352	384	416	588	644	728	840

Note: Model Five is the initial analysis configuration.

The models were analysed considering dead and snow loading. Loading was kept constant in order to compare vertical deflections directly. Deflections were measured at mid-span, and dead loads took into account the fabric cover and frame weight. The material used for this analysis was ASTM-A36 steel. Excessive deflection quickly eliminated Models One through Six from consideration as possible configurations for the Bennett Shelter.

Examination of the variation of weight was also useful. Model Five minimised the structure weight. This was the initial configuration. As this configuration had unacceptable deflections, it was necessary to consider configurations of the Bennett

Shelter with weights above the minimum. Models Twelve through Fifteen had deflections less than 0.34m and a minimum weight of 6870kg. Considering that some increase in bar diameter would be required to meet strength requirements, the minimum weight would certainly increase and be too large for military use. Analysis revealed that Models Seven through Eleven were the only ones with acceptable weights and mid-span deflections. The analysis results for Models Five through Eleven were graphed against each other, as shown in Fig. 4.6 below.

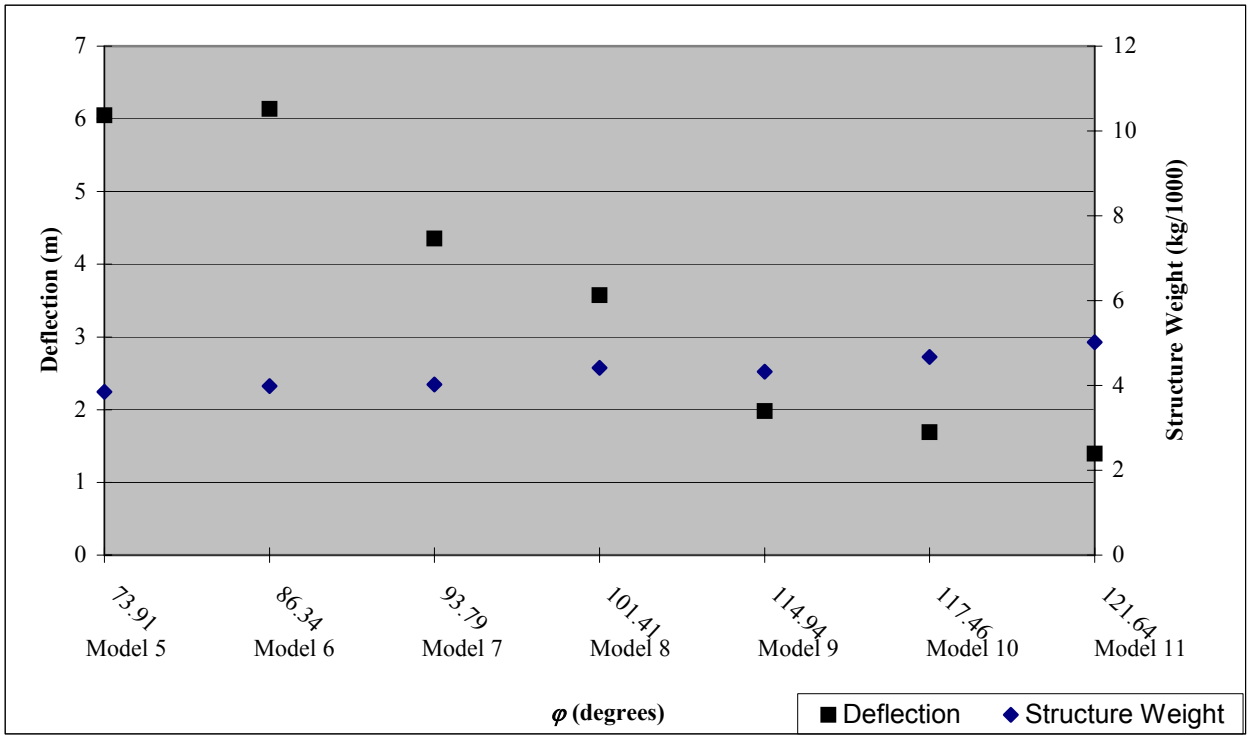


Fig. 4.6 Deflection and structure weight vs. φ for Models Five to Eleven

The above figure illustrates the tradeoff between weight and mesh density. It can be seen that as φ increases, vertical deflection at mid-span decreases but weight increases. The graph also shows that Models Nine to Eleven has the most acceptable deflection values and weights. Increasing the bar diameters of these models and conducting new analyses allows the determination of the required bar diameter for each

model to meet deflection requirements. These analyses were conducted using steel sections, and are shown in Fig. 4.7.

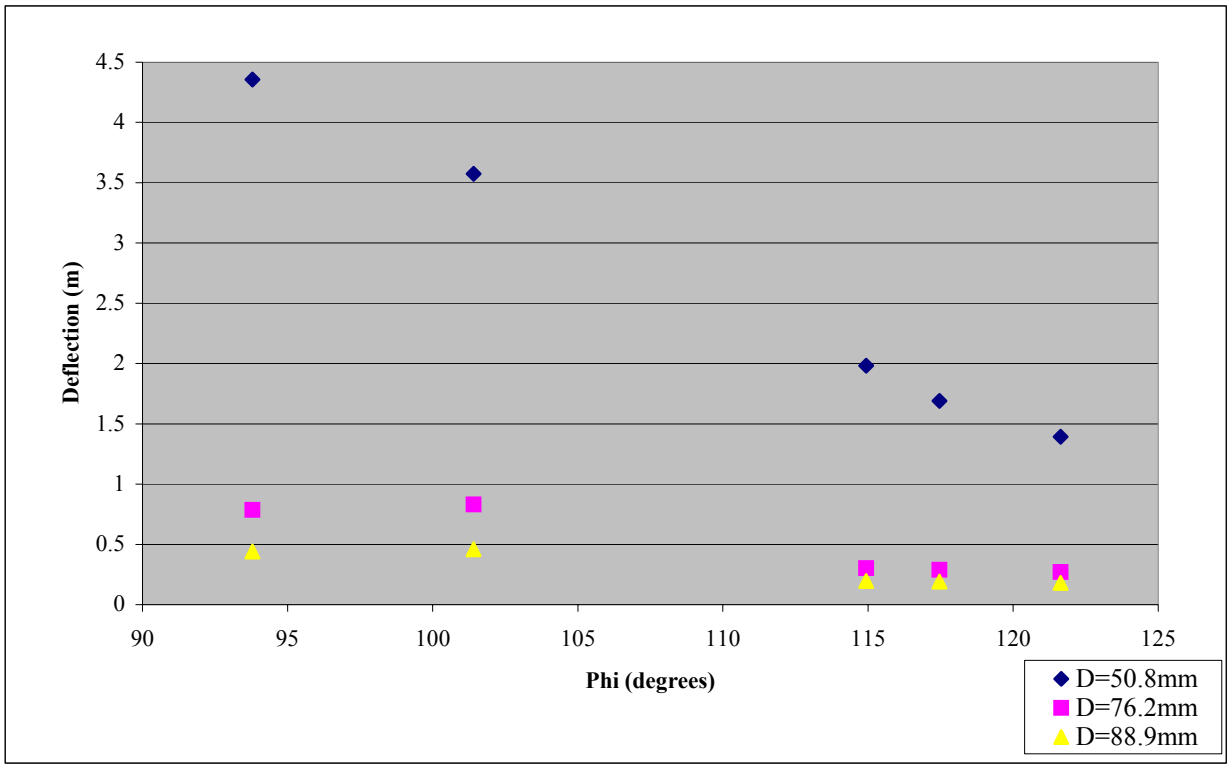


Fig. 4.7 Deflection vs. φ for different steel cross-sections for Models Seven to Eleven

Acceptable deflections were achieved in Models Nine, Ten, and Eleven for bar diameters of 76.2mm and 88.9mm and a constant wall thickness of 4.47mm. The next step was to consider all viable material types for the Bennett Shelter. Analysis considering different materials was conducted using Model Nine. If it met deflection limits when aluminium and CFRP were used, then it could be deduced that Model Ten and Eleven would also be acceptable. A graph of deflection versus bar diameter for different materials is presented in Fig. 4.8 below.

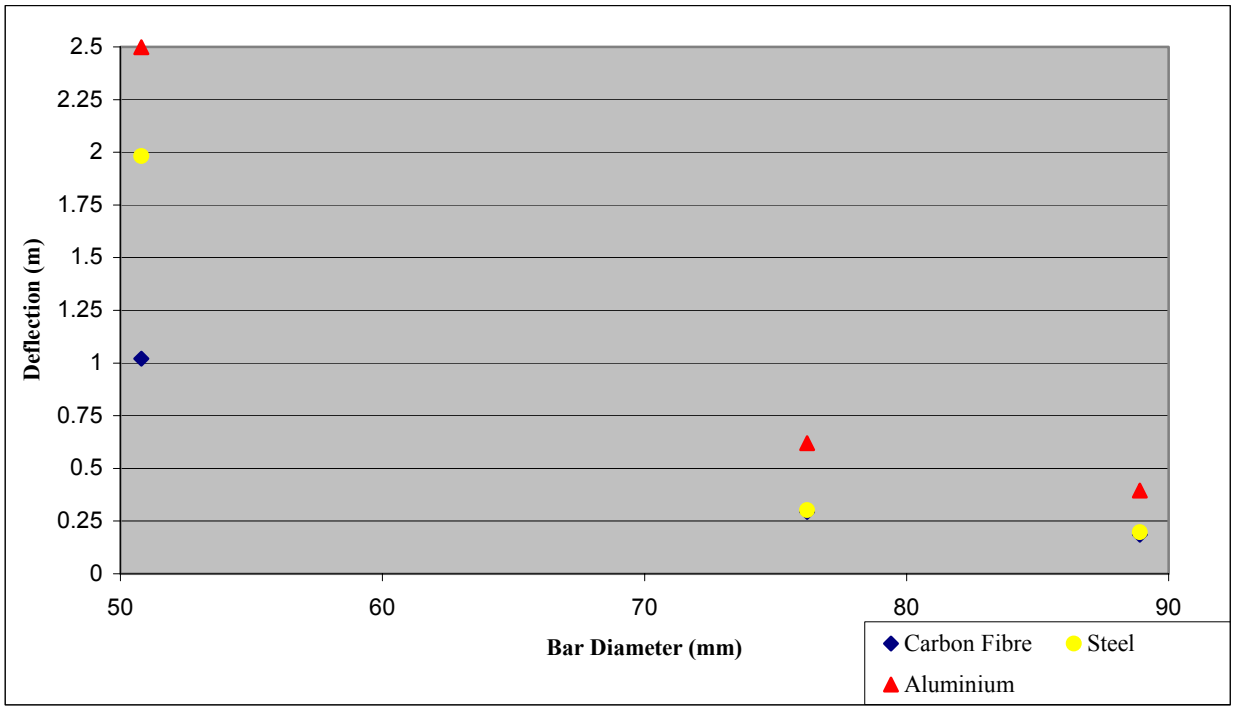


Fig. 4.8 Deflection versus bar diameter for Model Nine

Model Nine had acceptable deflections for all three materials when using 76.2 and 88.9mm member diameters. Mid-span deflections for both steel and CFRP were well below the 2.5% deflection limit. Aluminium met deflection requirements for the 88.9mm bar diameter, and had a mid-span deflection of 0.62m for a 76.2mm diameter. Although this was 4.9% of the structure span, it was still well within the deflection limit set by the required clearance above the radar assembly of the Apache Longbow Helicopter. The conclusion of the optimisation process was, therefore, that Model Nine had the minimum mesh density necessary to meet design requirements for the Bennett Shelter. A preliminary stress analysis determined, however, that Model Nine failed due to member internal stresses. Full serviceability analysis was, therefore, completed for Model Ten, which satisfied the preliminary stress analysis.

The maximum allowable vertical deflection at rotor height for Model Ten is 0.43m, and the maximum drift at rotor height is 0.37m (see Fig. 4.3 for an illustration).

The maximum vertical deflection at the crest is 1.5m. As vertical deflection limits at both the crest and rotor height are large, the critical criterion is the 2.5% limit.

It was useful to first know the deflection caused only by structure self-weight. This provided information about the performance of the structure under ideal conditions. Deflection values and percentage deflection with respect to the structure span are shown in Table 4.7 below.

Table 4.7 Vertical deflection considering self-weight

Cross-Section	Vertical Deflection (m)		% Deflection (d/span)	
	Rotor Height	Crest	Rotor Height	Crest
0.0889m x 8mm Aluminium	-0.02	-0.09	-0.12	-0.73
0.0889m x 5mm ASTM-A242 Steel	-0.01	-0.08	-0.11	-0.67

Vertical deflections considering self-weight were well within all serviceability limits. The structure performed adequately with this loading condition. It was necessary to determine the vertical deflection under the load condition described in Eqn. (4.3). The results are presented below.

Table 4.8 Vertical Deflection for aluminium and steel

Cross-Section	Vertical Deflection (m)		% Deflection (d/span)	
	Rotor Height	Crest	Rotor Height	Crest
0.0889m x 8mm Aluminium	-0.033	-0.23	-0.26	-1.82
0.0889m x 5mm ASTM-A242 Steel	-0.023	-0.15	-0.18	-1.19

The structure met all criteria for vertical deflection at both the crest and at rotor height. From the above analyses, it can be seen that vertical deflection in the structure will not interfere with its function.

Consideration of structural drift due to wind loading is, also, necessary using load conditions described in Eqn. (4.4). Excessive drift could impede the entry and exit of the Apache Longbow Helicopter, as well as cause problems if a number of shelters are attached together. Although there is no set drift limit for the long axis of the structure, the limit for the short axis (0.37m) is used for both structure directions. Results for long and short axes, as well as percentages of the aforementioned drift limit, are listed in Tables 4.9 and 4.10 below.

Table 4.9 Drift for longitudinal wind loading

Cross-Section	Longitudinal Wind (m)		% of Drift Limit at Rotor Height	
	short axis	long axis	short axis	long axis
88.9mm x 8mm Aluminium	0.26	0.08	70.27	21.62
88.9mm x 5mm ASTM-A242 Steel	0.1	-0.15	27.03	-40.54

Table 4.10 Drift for cross wind loading

Cross-Section	Cross Wind (m)		% of Drift Limit at Rotor Height	
	short axis	long axis	short axis	long axis
0.0889m x 8mm Aluminium	-0.1	0.31	-27.03	83.78
0.0889m x 5mm ASTM-A242 Steel	-0.07	0.15	-18.92	40.54

Both long and short axis drift met serviceability criteria. Attachment of guy ropes to minimise drift is unnecessary for both aluminium and steel sections. Completion of the above analyses verifies the sufficiency of the structural design for serviceability.

4.5 Stress Analysis

4.5.1 Member Stress Analysis Procedure

It is next necessary to check whether internal stresses are within tolerance. To do this, one must find the location of the worst-case loading, determine the 3-D state-of-stress from the internal forces in the member and calculate the factor of safety using theories of failure for ductile materials

The finite element models used for all analyses have over 3000 elements and 4000 nodes. Frame elements are used for the structural members. Unfortunately, ABAQUS will not output member internal stresses when using frame elements. It does, however, list the maximum internal forces and moments along with the elements where they occur. By analysing elements that have a force or moment component that is the maximum for the whole model, it is possible to find the worst-case loading. It is, also, necessary to check that the set of forces and moments in the element are the maximum combination in the structural member of which the element is a part. This method does not check every element in the model, but allows for determination of worst-case member loading.

Once the element with the maximum internal loading is located, the point of maximum stress on the member cross-section must be found. The Bennett Shelter uses pipes with a circular cross-section. As shown in Fig. 4.9, points on the interior of the pipe (b) and at the outer fibres (a) are considered. Calculation of the 3-D states-of-stress at these points takes into account the distribution of stresses in the cross-section.

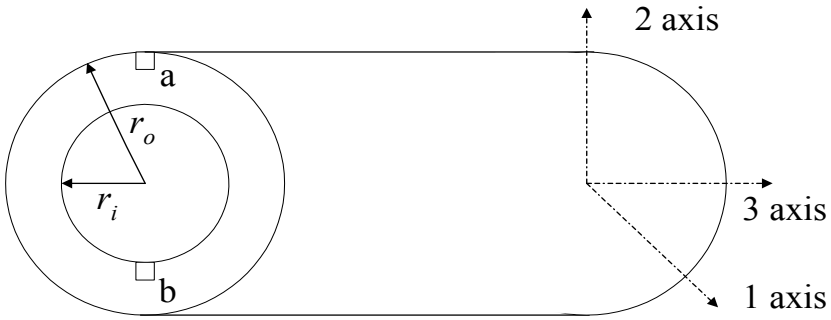


Fig. 4.9 Analysis points on member cross-section

Typical loading for an element in the structure is two shear forces, an axial force, two bending moments about the cross-sectional axes and torsion along the member. Conversion of the axial force, shear forces and torque to stresses is straightforward. Shear stresses are maximum at (b) and zero at (a). Shear stress due to torque and the stress due to the axial force are constant across the cross-section.

Determination of the point of maximum stress due to the bending moments is more complex. The sign and magnitude of bending stresses vary across the cross-section and depend upon the axis of application. Consideration of stress at points along each cross-sectional axis (as shown in Fig. 4.10) shows that no combination of moments results in both moments acting at full magnitude at a point. In fact, the maximum bending stress at a point along one cross-sectional axis is equal to the stress caused by the bending moment about that axis.

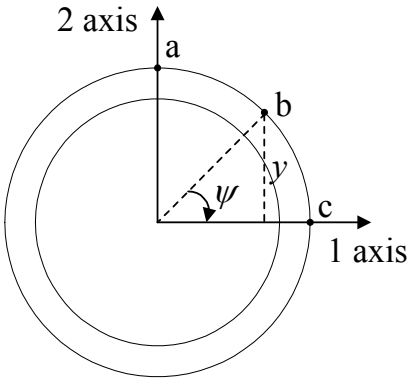


Fig. 4.10 Analysis points for bending stresses

It is possible that the combination of bending stresses between the two axes is greater than the maximum stress due to a single moment. When considering the stress at points between axes, only resultant stresses greater than those caused by each moment individually are important. The midpoint between the two axes was chosen as the analysis point for combined stresses. This may underestimate the maximum combined stress in the cross-section, but results indicate that the difference between the calculated and maximum stress is small and does not affect the analysis. The expression for the stress at the midpoint is

$$\sigma_{3_b} = \pm\frac{M_1 y}{I} \pm \frac{M_2 y}{I} \tag{4.15}$$

Knowing that ψ equals $\pi/4$ radians, it is possible to determine that y equals $0.7071r$ (either outer or inner radius depending upon the point of interest) using right triangle trigonometry. It is only necessary to examine cases where the signs in Eqn. (4.15) are the same. Considering all possible sign combinations of bending moments on the cross-section, it is possible to determine that the signs in Eqn. (4.15) are only the same when the signs of the bending moments about the two cross-sectional axes are different.

Given the relationships determined above, a number of considerations are required when determining the point of maximum bending stress on the member cross-section using internal moments found using ABAQUS. If the signs of the two outputted bending moments are the same, the maximum stress occurs at the outer fibres of the cross-section along the axis of the largest moment. If the signs of the bending moments are different, it is necessary to check the combined stress at a point midway between the cross-sectional axes using Eqn. (4.15) against the stress caused by the largest moment at the outer fibres.

Once the point of largest bending stress on the cross-section is determined, the state-of-stress can be fully expressed in the following form:

$$\begin{bmatrix} \sigma_1 & \tau_{12} & \tau_{13} \\ \tau_{21} & \sigma_2 & \tau_{23} \\ \tau_{31} & \tau_{32} & \sigma_3 \end{bmatrix}$$

The principal stresses are equal to the eigenvalues of the state-of-stress matrix. Using these stresses, it is then possible to determine the factor of safety of the section using the octahedral shearing stress theory of failure. Failure occurs when changes in geometry due to loading are no longer entirely reversible. This theory predicts failure by yielding when the octahedral shearing stress at a point achieves a particular value. This value is determined by the relationship between τ_{oct} and σ_{yp} in a simple tension test, which is

$$\tau_{oct} = \frac{\sqrt{2}}{3}\sigma_{yp} \tag{4.16}$$

This can be calculated in using principle stresses with the following equation

$$\tau_{oct} = \frac{1}{3}\left[(\sigma_1 - \sigma_2)^2 + (\sigma_2 - \sigma_3)^2 + (\sigma_3 - \sigma_1)^2\right]^{\frac{1}{2}} \tag{4.17}$$

Determination of the factor of safety of the component only requires dividing the Eqn. (4.16) by Eqn. (4.17) (Ugural and Fenster, 1995).

4.5.2 Member Stress Analysis

The materials used when analysing Model Ten were 6061T-6 aluminium and ASTM-A242 steel. Because they are linear elastic materials one can use classical stress analysis to determine the maximum state of stress in the material due to load conditions. The results of the analysis are presented in Table 4.11 below.

Table 4.11 Model Ten member stress factors of safety

	D_e	D_e+S	$0.75(D_e+W_i+S)$ cross	$0.75(D_e+W_i+S)$ long	D_e+W_i cross	D_e+W_i long
Aluminium						
88.9mm x 4mm	5.35	1.05	1.025	1.11	1.13	0.689
88.9mm x 7mm	5.63	1.51	1.536	1.64	1.71	0.924
88.9mm x 8mm	5.55	1.61	1.66	1.76	1.87	1.13
ASTM-A242 Steel						
88.9mm x 5mm	3.02	1.29	1.39	1.47	1.91	1.24

Note: D_e stands for dead loads, W_i stands for wind loads and S stands for snow loads.

From serviceability analysis conducted in Section 4.4.2, it was determined that the maximum allowable outside member diameter is 88.9mm. It was necessary to consider different wall thicknesses to attain acceptable factors of safety. There was, however, a tradeoff with structure weight that occurs when bar thickness is increased. A 1mm increase in bar thickness resulted in a weight increase of 569kg for aluminium and a 1620kg for steel. Taking this into account, successive analyses were run for both steel and aluminium, increasing the bar thickness each time. The overall factors of safety for the structural members using aluminium and steel were 1.13 and 1.24 respectively.

When measuring the ability of a member to withstand loading using a factor of safety, the required factor is a function of the usage of the structure and the necessity of preventing failure. As covered in Section 4.1, ASD has inherent redundancy due to the fact that one factor of safety is used for a number of different loading conditions. When

determining the factor of safety for the Bennett Shelter, it is clear that the loading conditions are conservative. Additionally, the structure is temporary, making comparisons with factors of safety for permanent structures difficult. Factors of safety for Model Ten were well over one, and further increase in bar thickness would lead to unusable structures due to weight. Thus, these cross-sections were chosen for the structural design. During prototyping of this structure, it will be necessary to test the members against failure for representative loading conditions related to the potential applications of the structure.

Carbon fibre composites provide the possibility of decreasing weight and increasing the factor of safety. Because composites are not homogenous and have specifically engineered strengths in different directions, it was not possible to conduct a stress analysis using CFRP tubing without knowing the layering and material properties of the composite. It was possible, however, to run analyses with representative dead loads and determine the maximum internal forces and moments due to the load cases. They are shown in Table 4.12 below.

Table 4.12 Internal forces and moments for carbon fibre composite members

Load Case	Internal Forces (N)			Internal Moments (N*m)		
	1	2	3	1	2	3
D_e	777.4	157.8	-1684	122.3	1305	0
D_e+S	3844	-608.6	-6741	-471.7	5224	0
0.75(D_e+W_i+S) cross	7583	340.6	-6684	263.9	5180	0
0.75(D_e+W_i+S) long	5986	391.8	-6210	303.7	4813	0
D_e+W_i cross	3514	833.8	1735	4074	-2305	1942
D_e+W_i long	-8682	-1222	11431	-946.9	-8859	0

Member stress analysis produced some noteworthy results. Analysis of all six load cases for steel and aluminium showed that the magnitude of the worst-case bending moment in the structure controlled the design. The effects of axial and shear forces were

negligible. Structural members around the missing ground-level units experienced the largest flexural stresses. If these units are not removed, the factor of safety for internal stresses will increase.

The effect of increasing member cross-sectional diameter was also interesting. As cross-sectional dimensions increased, so too did the factors of safety for load cases with wind pressures. This was due to the dead loads counteracting the uplift pressures on the structure. Load cases that considered dead loading or dead plus snow loading had decreasing factors of safety with increased diameter. This was especially noticeable with steel sections, due to the high density. It is probable that carbon fibre tubing, because of the low density, will be especially susceptible to uplift pressures, with load cases that consider wind being the controlling cases for the material.

With member stress analysis completed for steel and aluminium sections and a table of internal forces and moments for carbon fibre tubing compiled, it was possible to analyse structural joints.

4.5.3 Stress Analysis Procedure for Joints

For standard, single-bolted connections, the possible failure modes are shearing of the bolt, tensile failure of the bolt and bearing failure of the connected material around the bolt hole. The joints in the Bennett Shelter only allow rotation about the tangent axis of the joint. Thus, one must also consider yielding due to bending stresses about the other two local pin axes. The procedure used for analysis of the joints in the Bennett Shelter is to first check combined loading, as done with the structural members, and then bearing in the connected material around the pins.

When using the multi-point constraint option, joints are modelled as perfectly rigid with no length. ABAQUS does not, therefore, output joint internal forces directly.

Rather, equilibrium must be applied using member end forces from each of the connected elements to find the internal forces in the joint. Member end forces outputted by ABAQUS are expressed in each element's local coordinate system. In order to determine the internal forces and moments in the joint, it is necessary to complete the following steps:

- Translate connected member internal loads from local to global axes.
- Sum forces and moments at the top and bottom of the joint.
- Determine joint loads and moments in the global coordinate axis.
- Translate joint loads and moments from the global axis to the joint axis.

To do this, however, it is necessary first to understand how ABAQUS defines the local coordinate axes. The local tangent vector is determined from the two nodes of the element. ABAQUS defines an approximate n_1 vector for each element. The approximate n_1 vector for elements in ABAQUS models for this study is <0,-1,0>. The n_2 vector is equal to the cross product of the tangent vector and the approximate n_1 vector. The n_1 vector is then found by taking the cross product of the n_2 vector and the tangent vector (Hibbitt et. al, 2002).

Knowing the orientation of the local coordinate axis for each element in terms of the global axis allows translation of loads into the global axis. Summation of forces at the top and bottom of the joint and calculation of the joint forces and moments is then easily completed. In order to translate the forces into the pin axis, it is necessary to find the pin tangent vector. This is found using the nodal location of the joint and the reference node used to define the multi-point constraint (MPC). Determination of the n_1 and n_2 vectors is then possible using the procedure detailed above. As each joint is modelled as a pin, rotation about the pin should not be restrained. If there is a moment about the pin axis the method of calculation is incorrect. Once joint internal loading is

determined, the stresses in the pin can be found and factors of safety calculated using the procedure for members.

Analysis of bearing strength of the connected material around the bolt requires consideration of both the yielding of the connected material and the possibility of the bolt tearing out of the member. For structural design, the accepted minimum distance between the bolt and the edge of the connected material to avoid the problem of connections tearing out is 1.5 bolt diameters. This is taken into account in the bars of the Bennett Shelter by the addition of an extra edge distance from the connection to the end of the bar. The bearing strength of a single-bolted connection, according to the *Manual of Steel Construction: Allowable Stress Design*, is

$$V_{\max} \leq 3dtF_U \tag{4.18}$$

where V_{max} is the maximum shearing force in the pin, d is the diameter of the pin, t is the thickness of the member, and F_U is the ultimate strength of the connected material. Taking into account the fact that hollow circular sections are used in this design changes the equation to

$$V_{\max} \leq 6(r_o - r_i)dF_U \tag{4.19}$$

From this relationship, a factor of safety for bearing can be determined.

Use of scaffolding swivel couplers as joints requires additional analysis. Swivel couplers have three major failure criteria, which are shear failure of the pin, failure of the coupler due to bending stresses, and slip failure of the coupler. Standard maximum loads for these modes of failure are detailed in British Standard BS1139. It states that the maximum slip load is 12.5kN and the maximum shear load is 17kN (British Standard BS1139, 1991). Yielding failure due to bending stresses is calculated in the same manner as for pinned joints. The cross-section of the coupler when considering yielding

due to bending stresses is not equal to that of the lug connecting the two parts of the swivel coupler. The swiveling faces are smooth and in sufficiently close contact to avoid bending stresses in the pin alone. The cross-section considered is, therefore, the diameter of the swiveling face. The ability of a swivel coupler to withstand design loads is determined in this manner.

4.5.4 Joint Stress Analysis

For analysis of pinned joints, the pins themselves were modelled as structural bolts. The three most commonly used bolts in structural design are A307 steel bolts and A325 and A490 high strength steel bolts (AISC, 1998). The material properties and range of bolt diameters available are listed in Table 4.13 below.

Table 4.13 Bolt material properties (AISC, 1998)

Bolt Type	Sizes (mm)	Density (kg/m3)	Tensile Yield (MPa)	Shear Yield (MPa)	Tensile Ultimate (MPa)	Elastic Modulus (GPa)	Shear Modulus (GPa)
A307	6.35 - 101.6	7860	250	160	400	200	77
A325	12.7 – 38.1	7860	635	290	724	200	77
A490	6.35 - 38.1	7860	896	414	1034	200	77

The first step to analysing the pinned joints was to check the joints against the combination of bending, tensile and shear stresses. This analysis considered loading in the pins for all load cases and aluminium and steel members. Analysis showed that both bolt strength and maximum bolt diameter made A490 bolts the best type for use in the Bennett Shelter. A307 bolts, which allow a wide range of bolt sizes, provided factors of safety against yielding that were less than one for all bolt diameters that were compatible with the structural members (diameters less than 50.8mm). A325 and A490 pins restricted the maximum allowable bolt size to 38.1mm. Analysis of A325 bolts

considering this limitation provided factors of safety below one as well. Only A490 bolts provided acceptable factors of safety for a bolt diameter of 38.1mm. The results of analysis for both aluminium and steel members are presented in Tables 4.14 and 4.15.

Table 4.14 Pin factors of safety using aluminium members and A490 bolts

Load Case	diameter	FS	Internal Forces (N)			Internal Moments (N-m)		
	(mm)		1	2	3	1	2	3
D_e+S	38.1	1.76	1502.4	383.2	-460.3	-1363.3	2533.6	0
0.75(D_e+W_i+S) cross	38.1	2.4	8541.9	-4708.3	-1088.8	375.2	-1986.3	0
0.75(D+W_i+S) long	38.1	2.32	1614.7	1196.8	1374.0	-161.8	-2084.3	0
D_e+W_i cross	38.1	1.29	2779.4	-81.9	3288.2	424.8	-3775.7	0
D_e+W_i long	38.1	3.67	-4654.3	2169.9	1869.9	986.8	1302.9	0

Table 4.15 Pin factors of safety using steel members and A490 bolts

Load Case	diameter	FS	Internal Force (N)			Internal Moments (N-m)		
	(mm)		1	2	3	1	2	3
D_e+S	38.1	2.22	12988.1	-5114.6	-1657.1	509.5	-2126.2	0
0.75(D_e+W_i+S) cross	38.1	2.13	10430.4	5459.9	-1301.1	-448.9	-2235.7	0
0.75(D+W_i+S) long	38.1	1.89	60.2	467.6	-380	1269.8	2372.4	0
D_e+W_i cross	38.1	6	11794.3	-5257.5	853.7	-756.6	-280.5	0
D_e+W_i long	38.1	3.82	8287.2	-6191.9	-1040.2	-242.0	1232.6	0

It should be noted from the above results that uplift pressures affected the factor of safety for pins in the aluminium shelter. Smaller dead loads counteracted less of the suction forces along the roof of the shelter and resulted in larger internal bending moments. As flexural stresses controlled both member and joint designs, the factor of safety for the aluminum structure was less than that for steel. Worst-case loading in the joints occurred in joints in ground-level segments at the corners of the structure.

Determination of the factor of safety against shear was included in the analysis of combined loading. The point of maximum shear in the cross section (the interior of the pipe) was considered as a possible point of maximum stress. The final check necessary for the pinned joints was bearing failure of the connecting material. Applying Eqn.

(4.19) yielded a maximum allowable shear loading of 548kN for steel members and 475kN for aluminium members. This was far more than the maximum shear loads of 3.29kN for aluminium members and 6.19kN for steel members. Thus, 38.1mm diameter A490 bolts were sufficient for use in the Bennett Shelter.

The checks required for determining whether swivel couplers could be used with the Bennett Shelter were similar to those for the pinned joints. Yielding due to combined loading could be determined in the same manner as for the pin. Because the lug does not carry the bending stresses, but rather the swiveling surface, it was reasonable to assume that the diameter of the swiveling surface of the coupler would be greater than or equal to 38.1mm, the bolt diameter determined above. The maximum shearing forces for both aluminium and steel members were less than both the 12.5kN slip limit and the 17kN distortion load limit. Thus, swivel couplers can also be used as joints for the Bennett Shelter.

4.6 Buckling Analysis of Bennett Shelter

4.6.1 Analysis Procedure

Instability analysis for the Bennett Shelter requires the determination of the critical buckling load for a variety of different loading conditions that correspond to service loading of the structure. Additionally, it is necessary to consider the combined effects of buckling and internal stresses on the structure.

Using ABAQUS, it is possible to conduct buckling analysis for a number of different load cases. Design for both strength and serviceability ensures that displacements due to loading are minimised and that stresses within the structure stay in the elastic range. It is, therefore, possible to classify the Bennett Shelter as *stiff*. This allows the use of linear buckling analysis. In ABAQUS, a base-state loading pattern P^N

is applied to the structure and K_0^{NM}, the stiffness matrix with degrees of freedom *M* and *N* corresponding to the base state, is derived. An incremental load, Q^N is then applied to determine K_Δ^{NM}, the differential stiffness matrix due to incremental loading.

ABAQUS then defines the linear buckling problem as follows

$$\left(K_0^{NM} + \lambda_i K_\Delta^{NM}\right) v_i^M = 0 \tag{4.20}$$

where v_i is the *i*th buckling mode shape and λ_i is the eigenvalue corresponding to it. Loads that cause Eqn. (4.20) to become singular are critical buckling loads. These loads can be expressed as

$$P^N + \lambda_i Q^N \tag{4.21}$$

An eigenvalue λ outputted by ABAQUS can be best understood as the multiplier of the incremental load in the buckling load equation corresponding to a specific buckling mode. Only smallest eigenvalue for each load case, which corresponds to the smallest buckling load, is of interest. Additionally, outputted eigenvalues can be negative. Presence of these values indicates that reversing the load direction would lead to buckling. Consideration of the other eigenvalues for each load case is useful in determining the sensitivity of the structure. Structures with closely spaced eigenvalues are often considered imperfection sensitive. Post-buckling analysis is required for these structures. Buckling mode shapes, v_i, can be understood as normalised vectors of structure response due to corresponding critical buckling loads. They can be used to predict likely failure modes of the structure.

It is necessary to develop a number of load cases to take into account different possible loading conditions. The load cases considered in this study are listed in Table 4.16 below.

Table 4.16 Load Cases for Buckling Analysis

Load Case	Base State Loading	Incremental Loading
1	Dead Load	Full Snow Load
2	Dead Load	Snow Load on ½ of Structure
3	Dead Load	Full Crosswind
4	Dead Load	Full Longitudinal Wind
5	0.75(Dead Load)	0.75(Snow Load)+0.75(Crosswind)
6	0.75(Dead Load)	0.75(Snow Load)+0.75(Longitudinal Wind)

Analysis of the buckling of reticulated shells, as detailed in Section 2.3.2, emphasises the importance of considering asymmetric loading conditions and imperfections in the analysis of the Bennett Shelter. Load cases 1 and 2 consider both symmetric and anti-symmetric snow loading. As both longitudinal and crosswind loading are anti-symmetric, these loading conditions are applied directly in cases 3-6. The actual susceptibility of the structure to buckling under service loads is determined by setting the base state load equal to the dead loads experienced by the structure and the incremental loads equal to the full live loading. If the minimum eigenvalue outputted by ABAQUS is less than one for a load case, then the structure will buckle under the full service loading. The value of the eigenvalue is, in effect, a factor of safety against buckling for a specific load case.

Because no experimental data on its performance under load exists, the inclusion of geometric and manufacturing imperfections in the buckling analysis of the Bennett Shelter is difficult. Observations of structural behaviour and likely modes of failure can not be used to alter the numerical analysis. It is possible, using ABAQUS, to include the stresses and deformations due to base state loading in the incremental analysis through

the use of the NLGEOM command. Buckling analysis incorporating manufacturing imperfections is not covered in this analysis.

Consideration must also be given to the combined effect of buckling and internal stresses. In most design codes this is accomplished through the application of a strength reduction factor that is empirically determined for different material types. As the analysis of the Bennett Shelter is conducted using non-material specific methods, the following relationship is applied.

$$\frac{1}{F.S._{Stress}} + \frac{1}{F.S._{Buckling}} < 1 \tag{4.22}$$

If the sum of the inverse of the factors of safety for member stress and buckling is less than one for each load case, then the structure is sufficient in combined buckling and stress.

4.6.2 Analysis Results

The eigenvalues resulting from the analysis of the load cases presented in Table 4.16 are shown in Table 4.17 and 4.18 below.

Table 4.17 Results of linear buckling analysis for aluminium shelter

Load Case	Eigenvalues			
	1	2	3	4
1	3.110	10.548	10.849	12.268
2	6.152	20.259	21.345	23.772
3	-2.296	-6.025	-6.393	-7.800
4	-3.145	-6.059	-8.155	-9.606
5	-11.433	-11.459	-11.862	-21.034
6	-16.332	-19.587	-20.137	23.095

Table 4.18 Results of linear buckling analysis for steel shelter

Load Case	Eigenvalues			
	1	2	3	4
1	6.412	21.334	21.973	24.766
2	12.678	40.929	43.215	47.998
3	-4.733	-12.143	-12.880	-15.819
4	-6.486	-12.292	-16.509	-19.143
5	-23.049	-23.143	-24.237	-42.562
6	-33.142	-39.721	-40.520	46.591

These results showed that the Bennett Shelter would not fail only due to buckling for any load case. The smallest eigenvalue was –2.2964, more than double the service load for crosswind that the structure had to carry. Load case 5 had closely spaced eigenvalues. This indicated imperfection sensitivity was insignificant due to the fact that buckling occurred at eleven times the service load for the aluminium structure and twenty three times the service load for the steel structure. Load cases 3 to 6 had negative eigenvalues. As these cases considered wind loading, it was likely that the negative signs indicate that switching wind load direction would lead to buckling.

The mode shapes corresponding to the lowest eigenvalue for each load case are shown in Fig. 4.11 below. It can be seen that wind loading on the long axis of the shelter caused the minimum buckling load. The shape indicates that ground-level members buckled due to wind loading. Mode shapes for load cases 5 and 6 show that suction pressures due to wind loading along the roof caused buckling. For case 5, members at the crest buckled. Buckling of ground-level members at the end of the shelter occurred in case 6. The smoothness of all mode shapes indicates that the dominant buckling mode was member buckling. This was due both to the fact that the structure is similar to a reticulated shell in its behaviour and rigid joint modelling.

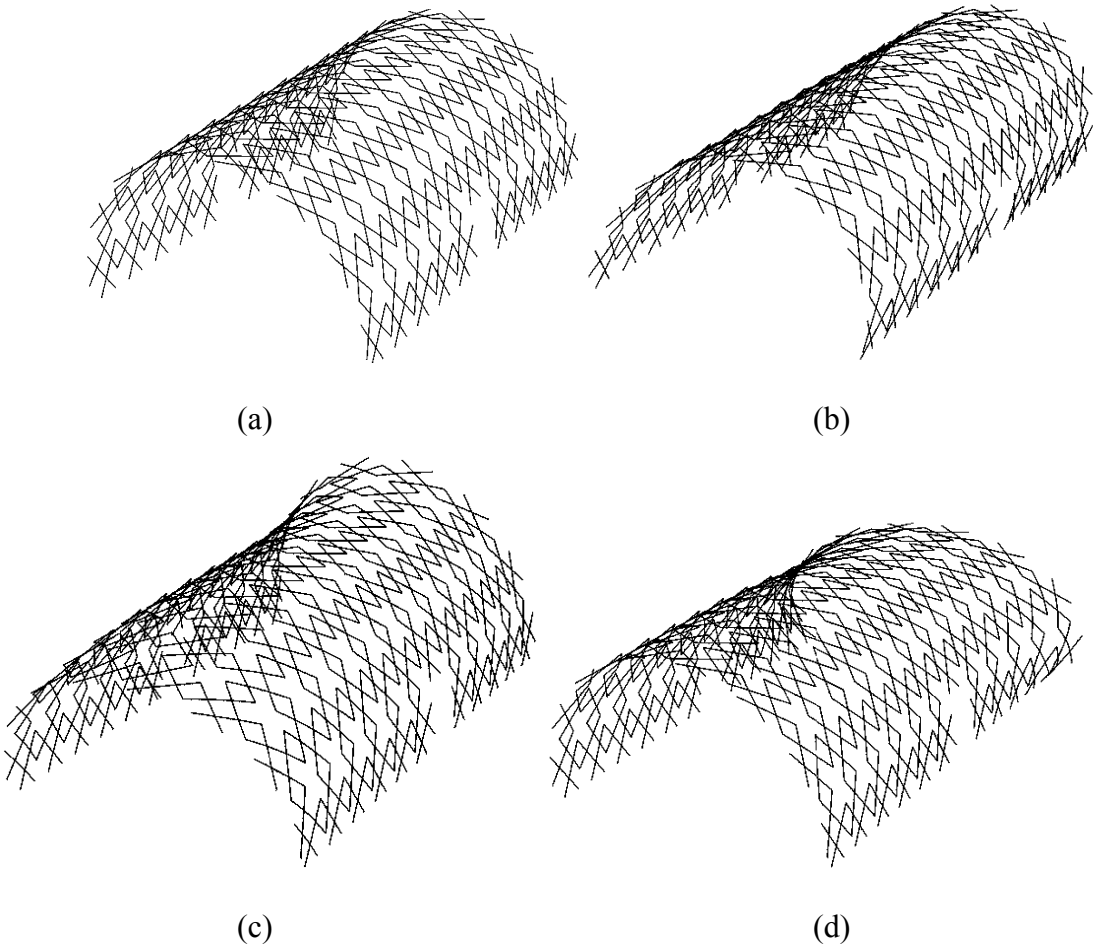


Fig. 4.11 Buckling Modes for the Bennett Shelter (a) Initial configuration (b) Load Cases 1,2, 3, 4, (c) 5 and (d) 6.

The model used for analysis of the Bennett Shelter does not take into account the effects of joint size and rigidity on node and torsion buckling modes. Although this makes it difficult to gauge the susceptibility of the structure to nodal and torsional buckling, it is realistic to assume that these buckling modes would not control the design. The joints used in the Bennett Shelter are simple swivel connections. In analysis of scissors structures, pivotal connections are generally modelled using two nodes with identical coordinates and restricted degrees of freedom. Only the larger, multi-member connections are modelled using separate elements (Gantes, 2001). The Bennett Shelter uses pivotal connections exclusively, and makes similar assumptions about the

importance of joint size for these types of connections. Without prototyping and component analysis, it is not possible to include real joint rigidities in the model. Careful design of joint connections, as detailed in Section 4.5, should account for the effects of torsion on the joint.

Application of Eqn. (4.22) to consider the combined effects of buckling and stress provided interesting results. The critical load case for stress was Eqn. (4.7) with wind directed along the long axis of the structure. Combination of factors of safety for this load case resulted in a value of 0.96 for aluminium members and 1.2 for steel. Thus, only steel members were sufficient for combined stress. An increase in the thickness of the aluminium cross-section to 9mm was required to satisfy Eqn. (4.22).

4.7 Frequency Analysis

4.7.1 Analysis Procedure

Frequency analysis, consisting of the determination of the natural frequencies, modal shapes, and damping characteristics, describes a structure in terms of its natural, dynamic properties. The natural frequency of a structure is defined as frequency of application of a force with constant maximum amplitude to a structure that elicits the maximum response. Modal shapes are the pattern of response in the structure (the deformed shape) that results from the application of load at the natural frequency. It is possible for a structure to have a number of natural frequencies. In fact, the number of natural frequencies is theoretically equal to the number of degrees of freedom in the system.

To determine the vibratory characteristics of a structure, its equation of motion must be defined. The Bennett Shelter, as most large-scale structures, is a multi-degree-of-freedom system. It is most easily analysed as a lumped-parameter system

(assemblage of discrete masses and springs). This facilitates the use of matrix methods of analysis. The system equation of motion can be expressed as

$$M\ddot{X} + KX = F \tag{4.23}$$

where M is the mass matrix, K is the global stiffness matrix, F is the load vector, X is the displacement vector and $\ddot{X}$ is the acceleration vector. As the damping ratio is less than 10% for most civil engineering structures and it is difficult to determine damping, the damping matrix, C, is not included. Determination of the natural frequencies and modal shapes is accomplished by setting F equal to zero (free vibrations) and assuming a displacement of

$$X = \psi \sin(\omega_n t) \tag{4.24}$$

Substituting into Eqn. (4.23) yields

$$\left(-\omega_n^2 M^{MN} + K^{MN}\right)\psi^N = 0 \tag{4.25}$$

where M and N are the degrees of freedom of the structure and ψ^N are the modal shapes. This is an eigenvalue problem. Solving Eqn. (4.25) yields n eigenvalues that are equal to the squares of the circular frequencies. These can be converted to the natural frequencies, in cycles per second, by dividing by 2π (Drabble, 1990).

For civil engineering applications, it is desirable to ensure that the natural frequencies of the system do not coincide with the frequency of any dynamic loads on the system. The most obvious dynamic loading for most structures is loading due to human occupants. Human occupants impart dynamic forces to a floor at frequencies in the range of 2 to 6 Hz. The general rule is that the natural frequency of any structural element should be two times the frequency of any steady-state excitation to which the element may be subjected.

The Bennett Shelter experiences no live loading due to human occupants. The potential sources of dynamic loading are environmental wind loading and wind loading due to helicopter take-off. Design code for wind loads in *ASCE 7-95* takes into account load magnification effect caused by gusts in resonance as well as vibrations of flexible buildings and other structures. Thus, the effect of dynamic loading is already factored into the structural analysis. Because of the large loads imparted to existing shelters due to helicopter take-off, it is standard operating procedure for helicopters to take-off at a safe distance from shelters. Frequency analysis for the Bennett Shelter is, therefore, straightforward. Using ABAQUS, it is possible to conduct frequency analysis to provide the natural frequencies of the shelter and the mode shapes. Though the design code accounts for vibrations, knowing the natural frequencies of the structure and seeing the mode shapes at these frequencies provides insight into the behaviour of the Bennett Shelter.

4.7.2 Analysis Results

Frequency analysis was completed for the Bennett Shelter. The first four natural frequencies were determined and are listed, along with the corresponding eigenvalues, in Table 4.19 below:

Table 4.19 Frequency analysis results

Mode Shape	Aluminium		Steel	
	Eigenvalue	Natural Frequency (Hz)	Eigenvalue	Natural Frequency (Hz)
1	18.085	0.67682	19.404	0.70107
2	123.90	1.7715	133.59	1.8395
3	128.96	1.8074	138.98	1.8762
4	181.10	2.1418	194.41	2.2191

The shapes corresponding with the modes detailed in Table 4.19 are shown in Figure 4.12.

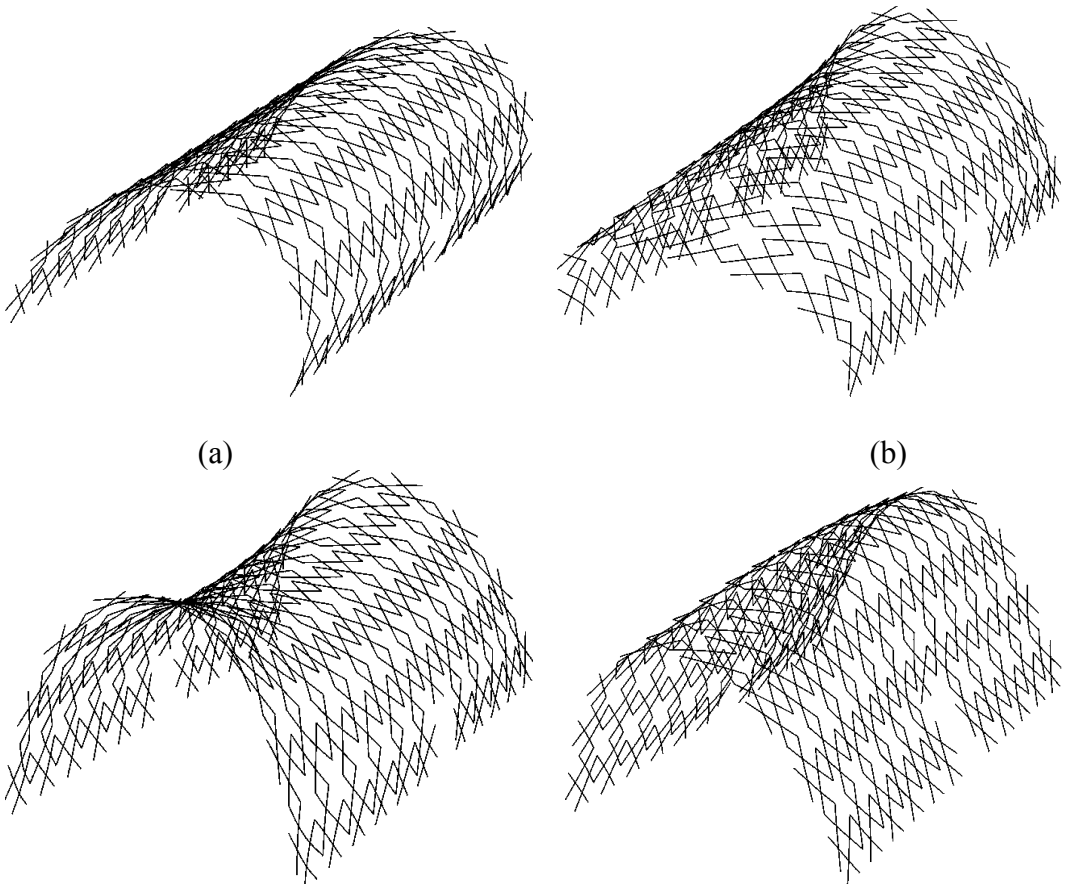


Fig. 4.12 Modal Shapes for Modes (a) 1, (b) 2, (c) 3 and (d) 4

Unacceptable vibration due to environmental loading for the Bennett Shelter is unlikely. It is interesting to note that the lowest natural frequency for both aluminium and steel are well below the frequency imparted by human occupants. The low natural frequency indicates that the shelter is quite flexible. This could have effects on different applications for the frame that experience vibratory loading. It is useful to note that, as with the buckling analysis, structural response mirrors that of shell structures.

4.8 Prototype Construction

The geometrical and structural design procedures detailed above require validation through the construction of models. If prototype mechanisms constructed

using the geometrical design procedure are mobile, the method is valid for development of large deployable shelters. Comparison of the design dimensions calculated using the geometrical procedure and those of experimental models also validates the accuracy of the method derived in Chapter 3.

Comparisons can also be made between the behaviour of the model under load and the results of numerical analysis. If the deflections of the model under load are comparable to numerical results, then the design procedure is valid and applicable to the design of long-span shelters. As covered in Chapter 2, scale models do not always provide accurate results for deployable structures. If loads and structural dimensions are not proportioned accurately, the failure mode that controls for a scale model may be different than those for the full-sized structure. Additionally, the fabrication of complicated connections for the smaller models may not be possible. Thus, the larger the model is in comparison to the actual structure, the more accurate the results of any experimental testing.

Construction of a model provides an opportunity to conduct more accurate numerical modelling. Experimental determination of joint rigidities allows one to eliminate infinitely rigid joints in the numerical model and more accurately model the actual behaviour of the structure under load. Also, structural behaviour not captured in numerical analysis can be found through experimentation. This can then be integrated into the numerical model to increase its accuracy.

No model of the Apache Longbow Helicopter Shelter detailed above has been constructed. ABLY Shelters has, with the assistance of Oxford University, built a large model to test the viability of the tiled Bennett mechanism. The intent of the model was to illustrate the method of deployment to executives at the company, as well as to collect

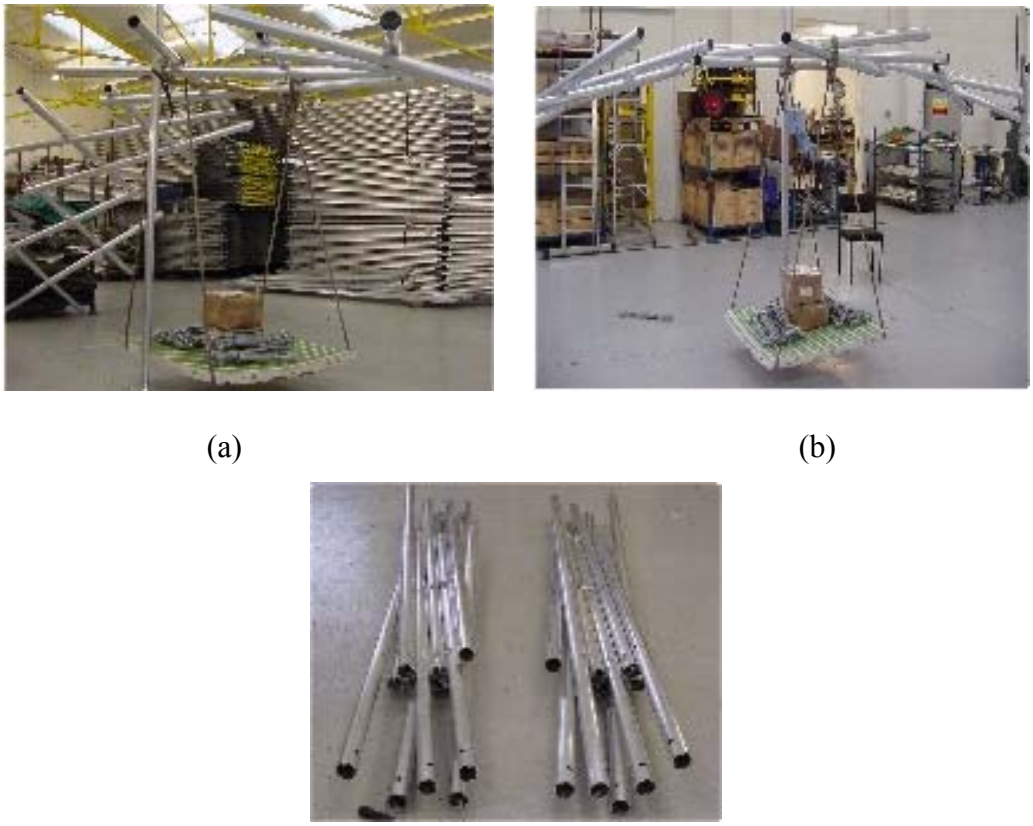
some rudimentary information pertaining to the performance of the shelter under load. The design details are shown in Table 4.20.

Table 4.20 Design details of ABLY model

Structure Height (H)	3m
Structure Width (W)	8m
Bar Length (l_b)	1.905m
Bennett Bar Length (l)	0.635m
# of Collapsible Segments (v)	5
# of Units per Segment (u)	1
Primary Skew Angle (α)	13.49°
Member Outer Diameter	69mm
Member Thickness (t)	3.2mm
Pin Diameter	32mm

A snow load of 50kg/m^2 was applied in addition to dead loading for structural analysis and design. For numerical analysis the members were composed of 6061-T6 aluminium and the pinned connections of ASTM-A242 steel.

There were a number of discrepancies between the numerical analysis and the model. The pin diameter used in the prototype was 20mm rather than the 32mm specified in the design. The materials used in the model were different as well. The material for the members was 6082-T6 aluminium and for the pinned connections grade 8.8 steel bolts. ABLY decreased the size of the structural pin and used a stronger bolt. The manner of loading the prototype was different than the numerical model as well. In the numerical model, snow and dead loads were applied evenly across all nodes of the arch. When conducting load testing, as shown in Fig. 4.13, a point load was applied at mid-span.

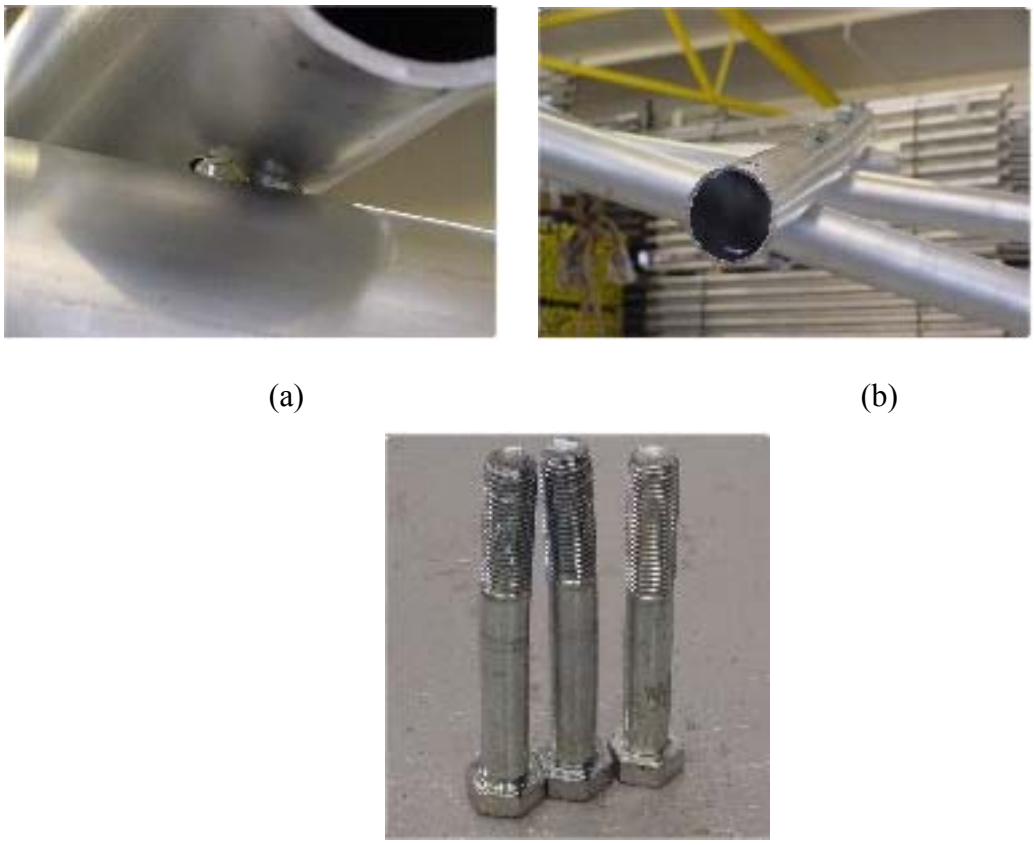


(a) (b)

(c)

Fig. 4.13 Pictures of the ABLY Prototype from the (a) side, (b) front and (c) compacted.

Testing of the prototype validated the geometric design procedure but provided little information about the structure's behaviour under load. As shown in the above figure, the prototype deployed and folded as expected. Load testing resulted in unacceptably large deflections for any given load. Structural components, to include both members and joints, also deformed plastically, as shown in Fig. 4.14.



(a) (b)

(c)

Fig. 4.14 (a) Space between the bolt and the bar in a pinned connection, (b) Deformation along a bar during load-deflection testing and (c) Deformed bolts from the prototype.

There are a number of reasons for these large deflections and deformation of the structural components. Manufacturing has to be undertaken to very high accuracy for overconstrained mechanisms. For the ABLY prototype, bolt holes were drilled larger than necessary, which contributed to large deflections. The discrepancy between the bolt size used in the structural analysis and the one used in the prototype is, also, significant. Using a smaller diameter bolt undoubtably contributed to the bending of the pins. Localised crushing of the aluminium tube wall at the pin also allowed the ends of the tube to move significantly. As shown in Fig. 4.13(a), the *spread* of the Bennett arch was

large during the load testing. Thus, the structure transmitted the loads both flexurally and axially, which increased the bending stresses in the pins.

Though the ABLY prototype is a different design than the one detailed in this chapter, lessons can be drawn from it. First, material types and dimensions specified in the design must be adhered to in prototype construction and method of loading the structure must be consistent. Next, the manufacture of components must be accurate. Drilled joints require accurate dimensions to avoid excessive clearance between the members and the pin. The *spread* of the Bennett Shelter must also be considered. The smaller the value of φ is the more flexural stress will be present in both members and joints. Finally, the member diameter must be minimised. Excessive offsets in the joint introduce larger bending stresses in the pins.

4.9 Conclusions about the Deployed Configuration

The completed design dimensions for the Bennett Shelter for aluminium and steel are shown in Table 4.22.

Table 4.22 Bennett Shelter Component Dimensions

Material	Member Dimensions		Pin Diameter (mm) (A490 Bolts)
	Outer Diameter (mm)	Wall Thickness (mm)	
6061-T6 Aluminium	88.9	9	38.1
ASTM-A242 Steel	88.9	5	38.1

The above results demonstrated that the Bennett Shelter is viable for large-scale applications. Small variations in the proposed deployed dimensions of the shelter allowed the generation of a number of possible configurations. Serviceability analysis then provided the most efficient configuration for both structure weight and stiffness.

Member and joint stress analysis sized the member cross-section and the joint required for the application. The materials to be used in the frame were also determined during this process. The design was then verified by checking if it was susceptible to buckling failure or excessive vibrations. For the Apache Longbow Helicopter shelter, total structure weight when using aluminium was 7473kg. This weight was comparable to the 6800kg weights for both the ABLY LVRE Shelter and the DRASH J Shelter. If CFRP, which is used in both the LVRE and J Series Shelter, is used as a structural material for the Bennett Shelter it would further decrease the structure weight and design dimensions.

Analysis of the Bennett Shelter, also, provided information about how the frame behaves when loaded. Loading due to structure self-weight and snow loading led to failure at mid-span. Uplift pressures due to wind loading counteracted dead loads and actually decreased the total structure load for some load cases. Overall, the combination of dead load and wind loading into the long axis of the structure was the controlling load case. The Bennett Shelter's behaviour is different than that of existing deployable scissors structures. The buckling modes shown in Langbecker's study of deployable scissors structures are characterised by individual deformed members or deformed members radiating out of a single node. Frequency analysis also revealed that the structure has a low natural frequency for both steel and aluminium. This could affect its application in situations with significant vibratory loading. The smooth modal shapes indicate that the Bennett Shelter behaves more like a membrane than multi-layer deployable bar structures.

5 Imperfection Analysis

Because the Bennett Shelter is overconstrained, any violation of the geometric compatibility conditions governing its mobility causes elastic interference to its deployment. As some error in fabrication can be expected during the manufacturing process, it is essential to understand the effect of imperfections on the deployment of the shelter. This can be accomplished through the consideration of internal energy due to the presence of manufacturing imperfections. In Section 5.1 energy methods are reviewed and equations for the calculation of strain energy and complementary strain energy are determined. Section 5.2 addresses the application of energy methods to statically indeterminate structures and overconstrained mechanisms. In Section 5.3 energy methods derived in Section 5.1 are validated using an indeterminate structure. Section 5.4 details the calculation of the internal energy in a simple, overconstrained mechanism. Section 5.5 presents different optimisation methods. In Section 5.6 an explicit method for determining the internal energy maximising pattern of imperfections for the simple overconstrained mechanism is developed. Finally, approximate methods for optimising overconstrained mechanisms are found in Section 5.7 and results are compared to those determined explicitly.

5.1 Energy Methods

5.1.1 Strain Energy and Complementary Strain Energy

Consider the deformation of an elastic structure subjected to a set of applied loads. Assuming that the process of loading is adiabatic (no energy is lost through heat absorbed by surroundings), the work done applying the forces is converted to stored energy within the structure. This is called strain energy. It can be further understood if one considers a stress-strain plot, as shown in Fig. 5.1.

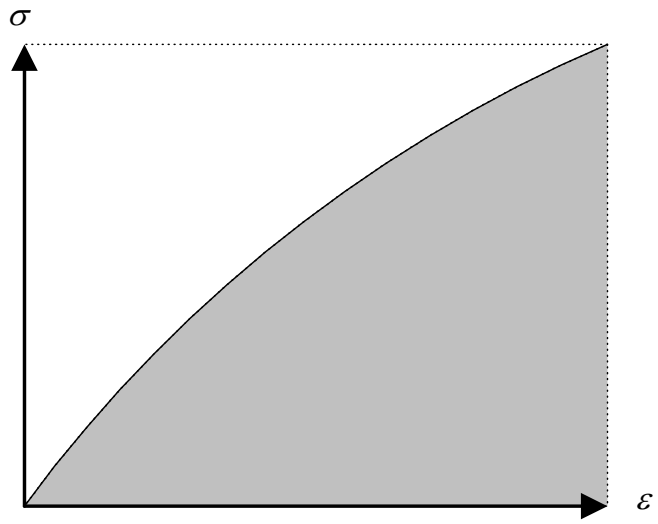


Fig. 5.1 Stress-strain diagram

The area beneath the stress-strain curve is known as the strain energy density, U_0, which is the strain energy per unit volume. If the stress-strain relationship is linear, the strain energy density can be expressed as

$$U_0 = \frac{1}{2}\sigma\varepsilon$$

The strain energy can be obtained by integrating the strain energy density over the volume of the structure.

$$U = \int U_0 dV \tag{5.1}$$

The area above the stress-strain curve is known as complementary strain energy density, U_0^*, which has the same units as strain energy density but no physical meaning. Integration with respect to volume yields the complementary strain energy of the system, U^*. The strain energy of a system equals the complementary strain energy if material used in the structure is linear elastic.

Environmental effects, such as initial strain, ε_0, or an initial temperature distribution, ε_T, will alter the stress-strain curve. The total strain is, therefore, equal to

$$\varepsilon = e + \varepsilon_0 + \varepsilon_T \tag{5.2}$$

where *e* is equal to the elastic strain. This is shown in Fig. 5.2 below (Przemieniecki, 1968).

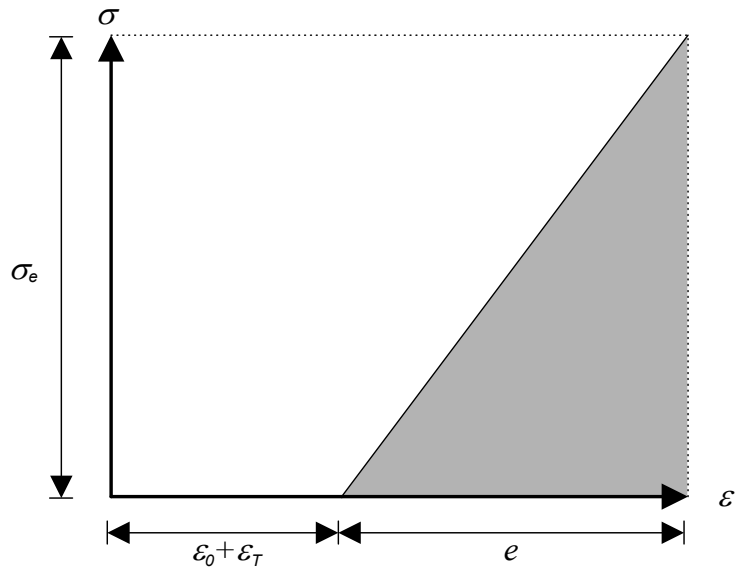


Fig. 5.2 Linear elastic stress-strain diagram with initial strain

To determine the strain energy or complementary strain energy in a body due to an initial imperfection, ε_0, and no initial temperature distribution, it is necessary to derive the energy functions. This can be accomplished using Fig. 5.2. The strain energy density can be expressed as

$$U_0 = \frac{1}{2}\sigma_e(\varepsilon - \varepsilon_0) \tag{5.3}$$

where

$$\sigma_e = E(\varepsilon - \varepsilon_0) \tag{5.4}$$

Substituting Eqn. (5.3) into Eqn. (5.4) yields

$$U_0 = \frac{1}{2}E\varepsilon^2 - E\varepsilon\varepsilon_0 + \frac{1}{2}E\varepsilon_0^2 \tag{5.5}$$

where E is Young's modulus. For a structure made of linear elastic material, the strain energy density for a single member is

$$U_0 = \frac{1}{2}\varepsilon^T D\varepsilon - \varepsilon^T D\varepsilon_0 + \frac{1}{2}\varepsilon_0^T D\varepsilon_0 \tag{5.6}$$

where D is the material constant relating stress and strain. Strain energy can then be found by integrating with respect to volume. The total potential energy, Π, is expressed as

$$\Pi = U - W \tag{5.7}$$

where work, W, is composed of the work due to body forces, surface forces, and any concentrated forces applied to the structure.

The complementary strain energy function can also be derived from Fig. 5.2. Complementary strain energy density can be expressed as

$$U_0^* = \sigma_e\varepsilon_0 + \frac{1}{2}\sigma_e(\varepsilon - \varepsilon_0) \tag{5.8}$$

rearranging Eqn. (5.4) and substituting into Eqn. (5.8) yields

$$U_0^* = \sigma_e\varepsilon_0 + \frac{{\sigma_e}^2}{2E} \tag{5.9}$$

For a structure made of linear elastic material, the complementary strain energy density for a single member is

$$U_0^* = \sigma_e\varepsilon_0 + \frac{1}{2}{\sigma_e}^T D^{-1}\sigma_e \tag{5.10}$$

As with strain energy, complementary strain energy equals the integral of complementary strain energy density with respect to volume.

$$U^* = \int U_0^* dV \tag{5.11}$$

Furthermore, for a structure consisting of more than one member, the total complementary strain energy is equal to the sum of the complementary strain energy in each member. The total complementary energy can be expressed as

$$\Pi^* = U^* - W^* \tag{5.12}$$

where the complementary work, W^*, is composed of the complementary work due to body forces, surface forces and any concentrated forces applied to the structure.

5.1.2 Relationships derived from Virtual Work and Virtual Complementary Work

In deriving Eqns. (5.1-5.7), it was assumed that any infinitesimal variation in displacement, δu, would be accompanied by corresponding variation in stresses and forces such that both equilibrium and compatibility relationships are satisfied for the structure. It can be observed, however, that the first variations of W and U are independent of forces and stresses in the structure. It is valid to assume that forces and stresses in the structure will remain constant while displacements are varied. Thus, a variation of displacement δu gives rise to strains that must satisfy equations of compatibility but not necessarily equations of equilibrium. Displacements δu can be any infinitesimal displacements as long as they are geometrically possible, continuous within the structure boundaries, and satisfy all boundary conditions. Such displacements are referred to as *virtual displacements*.

The principle of virtual work states that an elastic structure is in equilibrium under a given system of loads or temperature distribution if for any virtual displacement δu from a compatible state of deformation u the virtual work is equal to the virtual strain energy. This can be expressed as

$$\delta W = \delta U$$

This can also be expressed as

$$\delta \Pi = \delta (U + W) = 0 \tag{5.13}$$

This is the principle of the stationary values of total potential energy. It states that of all compatible virtual displacements satisfying the given compatibility conditions, the ones

that also satisfy equilibrium make the total potential energy Π assume a stationary minimum. If virtual displacements are selected such that they do not coincide with any applied loads, then Eqn. (5.12) can be simplified to

$$\delta U = 0 \tag{5.14}$$

The physical significance of stationary minimum energy is that a structure under a system of loads and initial strains resulting in minimum energy with the application of any virtual displacement is stable (Przemieniecki, 1968).

Definition of the principle of complementary virtual work also provides useful relationships. Derivation of Eqns. (5.8-5.12) assumed variation in the strain distribution accompanying a variation in stress $\delta\sigma$. It can be shown, however, that complementary strain energy and complementary work are independent of elastic strain, *e*, and displacement. It can, therefore, be assumed that displacement and total strain remain constant while the forces and stresses are varied. Thus, virtual stresses, $\delta\sigma$, can be any stresses that are statically possible and satisfy all equations of equilibrium throughout the structure.

The principle of complementary virtual work states than an elastic structure is in a compatible state of deformation under a given set of loads and temperature distribution if for any virtual stresses $\delta\sigma$ away from the equilibrium state-of-stress the virtual complementary work equals the virtual complementary strain energy. This can be expressed as

$$\delta W^* = \delta U^*$$

This can be expressed also as

$$\delta\Pi^* = \delta(U^* + W^*) = 0 \tag{5.15}$$

The principle of the stationary value of total complementary strain energy, as shown in Eqn. (5.15), states that of all statically equivalent stress states that satisfy geometrical compatibility conditions, the ones that satisfy equilibrium make Π^* assume a stationary minimum value (Tauchert, 1974). If there are no external virtual forces but only virtual stresses that are zero at the boundaries, the variation in complementary work equals zero. Thus, Eqn. (5.15) can be rewritten as

$$\delta U^* = 0 \tag{5.16}$$

It is important to note that, since virtual stresses are kept zero on the boundaries, this theorem can be applied only to redundant structures where variation of internal stresses is possible (Przemieniecki, 1968).

Using the principles defined above, as well as the strain energy and complementary strain energy functions incorporating initial strains, it is possible to define two methods for determining the internal stress and strain distributions in statically indeterminate structures and overconstrained mechanisms.

5.2 Application of Energy Methods to Indeterminate Structures

There are two methods for determining internal stress and displacement distributions in statically indeterminate structures. They will be referred to as the total potential energy method and the total complementary energy method. The total potential energy method involves variation of internal displacements. Application of this method requires that initial imperfections applied to the statically indeterminate structure meet the requirements for *virtual displacements*. In applying the total potential energy method, the first step is to apply compatibility relationships to relate member displacements. Next, a structure strain energy function incorporating initial imperfections can be expressed using Eqns. (5.1-5.7). The principle of stationary value

of total potential energy, Eqn. (5.14), is then applied to determine expressions for member displacements in terms of initial imperfections, ε_0. These expressions are then inserted into the strain energy expression to provide a function for strain energy with initial imperfections as the independent variables.

The total complementary energy method involves variation of internal stresses. Application of this method requires that initial internal stresses meet the requirements for *virtual stresses*, as detailed in Section 5.1.2. Additionally, this method is only applicable to redundant structures. The first step is to apply equilibrium to relate member internal stresses. Next, a complementary strain energy function can be expressed incorporating initial strains, as shown in Eqns. (5.8-5.12). The principle of stationary value of total complementary energy, Eqn. (5.16), is then applied to determine expressions for internal stresses in terms of initial strains. These expressions are then inserted into the complementary strain energy function to provide a function for complementary strain energy with initial imperfections as the independent variables.

As overconstrained mechanisms become redundant structures when their mobility is restrained, it is possible to apply both methods to analyse the effect of initial imperfections on them. Using either the total potential energy or total complementary energy methods provides a single expression describing the internal energy in a structural system. Including a configuration parameter in the energy expression incorporates the point in deployment of the mechanism. An explicit relationship for the internal energy in the mechanism with initial imperfections as the independent variables is useful because energy can be directly related to the initial imperfection variables. Application of mathematical optimisation methods to the internal energy function provides the pattern of initial imperfections corresponding to the maximum internal energy. As smooth, energy-free deployment of a mechanism is desired, the pattern of

initial imperfections yielding the largest value of internal energy is the worst-case. It is useful to know this pattern so that it can be avoided in the manufacturing process. Determination of the worst-case pattern of imperfections also provides the largest possible energy required to articulate the structure.

Once the worst-case pattern of imperfections is known, it is possible to examine how internal energy changes through deployment. Kuznetsov (1991) stated that the presence of any variation in geometry in an overconstrained mechanism induces a self-stress. The system will spontaneously move to the configuration where the *global* energy is minimised and acquire elastic resistance to any displacements. To illustrate this phenomenon clearly, two concepts are introduced: *global* minimum energy and *local* minimum energy. For each specific configuration of an overconstrained mechanism, a *local* minimum energy has to be achieved to maintain equilibrium. Among these minimum energies, the smallest one is defined as the *global* minimum energy. Statically analysing different configurations of the mechanism with the initial imperfections and calculating the local internal energy at each configuration can find this *global* minimum energy state. The point during the deployment of the mechanism that has the minimum energy for a given set of imperfections is the stable configuration.

5.3 Validation of Energy Methods

Before applying energy methods to overconstrained mechanisms, it is useful to validate the energy functions derived in Section 5.1 for a simple, statically indeterminate three-bar structure, like the one shown in Figure 5.3 below.

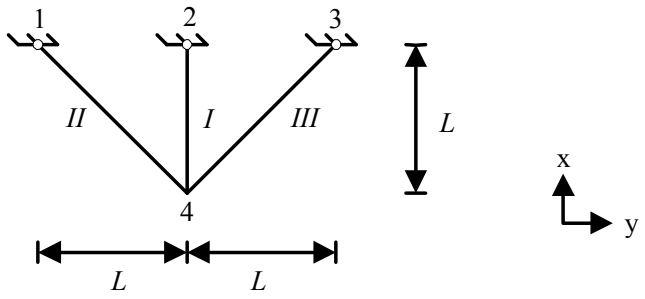


Fig. 5.3 Simple, statically indeterminate structure

For this analysis, each bar has an initial strain value. The type of imperfection to be considered is member length either longer or shorter than the ideal value. The sign convention for this type of imperfection is positive if the bar is initially shorter and negative if the bar is initially longer. For convenience, it is assumed that bars *II* and *III* have the same initial axial strain ε_{20}. Bar *I* has an initial strain, ε_{10}.

Total potential energy method is applied first. Eqns. (5.5) and (5.6) are used to express the strain energy in the structure due to imperfections:

$$\begin{aligned} U = &\left(\frac{1}{2}E\varepsilon_I^2 - E\varepsilon_I\varepsilon_{10} + \frac{1}{2}E\varepsilon_{10}^2\right)AL \\ &+ 2\left(\frac{1}{2}E\varepsilon_{II}^2 - E\varepsilon_{II}\varepsilon_{20} + \frac{1}{2}E\varepsilon_{20}^2\right)A\sqrt{2}L \end{aligned} \tag{5.17}$$

where $\varepsilon_I = \frac{\delta_I}{L}$ and $\varepsilon_{II} = \frac{\delta_{II}}{\sqrt{2}L}$ are the total strain in members *I* and *II* and δ_I and δ_{II} are total bar elongations. To relate elongations in bars *I*, *II*, and *III*, it is necessary to use compatibility. Assuming small deformations, it can be derived that

$$\delta_I = \sqrt{2}\delta_2 \tag{5.18}$$

Eqn. (5.17) can then be rewritten using bar elongations as

$$U = \frac{EA\delta_2^2}{L} - \sqrt{2}EA\delta_2\varepsilon_{10} + \frac{EAL}{2}\varepsilon_{10}^2 + \frac{EA\delta_2^2}{\sqrt{2L}} - 2EA\delta_2\varepsilon_{20} + \sqrt{2}EAL\varepsilon_{20}^2 \tag{5.19}$$

Application of the principle of the stationary values of total potential energy allows determination of an expression for the total bar elongation δ_2 in terms of initial strains ε_{10} and ε_{20}.

$$\frac{\partial\Pi}{\partial\delta_2} = 0 = \frac{2EA\delta_2}{L} - \sqrt{2}EA\varepsilon_{10} + \frac{\sqrt{2}EA\delta_2}{L} - 2EA\varepsilon_{20} \tag{5.20}$$

The above expression is an equilibrium equation. This can be rearranged, such that

$$\delta_2 = \frac{\left(\sqrt{2}\varepsilon_{10} + 2\varepsilon_{20}\right)L}{2+\sqrt{2}} \tag{5.21}$$

It is then possible to solve for the ε_2 and N_2

$$\varepsilon_{II} = \frac{\delta_2}{\sqrt{2}L} = \frac{\sqrt{2}\varepsilon_{10} + 2\varepsilon_{20}}{2\sqrt{2}+2} \tag{5.22}$$

$$N_2 = E\left(\varepsilon_{II} - \varepsilon_{20}\right)A = \frac{\sqrt{2}\varepsilon_{10} - 2\sqrt{2}\varepsilon_{20}}{2\sqrt{2}+2}EA \tag{5.23}$$

Calculation of numerical values for the strain and internal forces in bars *II* and *III* using Eqns. (5.22) and (5.23) allowed comparison with results from the numerical model. Using ABAQUS, it was possible to calculate the stress and strain in the structure, as well as the internal energy. The variables were defined as follows: L=2m, E= $70*10^9$ Pa, A=$6.155*10^{-4}$ m^2, ε_{10}=-0.05, and ε_{20}=0. It was determined using the analytical method that U= 44616J, N_2 = -630965N, and ε_{II} =-0.0146. ABAQUS and analytical results matched exactly. Thus, the strain energy derivation is correct.

The same values can be calculated using the total complementary energy method. If the values match the results from ABAQUS and the total potential energy method,

then the complementary strain energy values are valid. Applying Eqns. (5.10) and (5.11), the complementary strain energy function for the structure is

$$U^* = \left(\frac{N_1}{A} \varepsilon_{10} + \frac{N_1^2}{2EA^2} \right) AL + 2\left(\frac{N_2}{A} \varepsilon_{20} + \frac{N_2^2}{2EA^2} \right) A\sqrt{2}L \tag{5.24}$$

A relationship between the internal forces in the structure is found using equilibrium. It can be determined that $N_1 = -\sqrt{2}N_2$. Eqn. (5.24) can be rewritten as

$$U^* = \left(\frac{-\sqrt{2}N_2}{A} \varepsilon_{10} + \frac{\left(-\sqrt{2}N_2\right)^2}{2EA^2} \right) AL + 2\left(\frac{N_2}{A} \varepsilon_{20} + \frac{N_2^2}{2EA^2} \right) A\sqrt{2}L \tag{5.25}$$

Applying the principle of stationary values of total complementary energy provided a compatibility equation. It was possible to determine an expression for N_2 in terms of initial strains. It is

$$N_2 = \frac{\left(\sqrt{2}\varepsilon_{10} - 2\sqrt{2}\varepsilon_{20}\right)EA}{2 + 2\sqrt{2}} \tag{5.26}$$

Using the above expressions, it was found that U^* equals -44616J and N_2 equals -630950N. It is not possible to determine complementary strain energy using ABAQUS, but the internal force result matches those of the total potential energy method and ABAQUS. It should be noted that the negative sign on the complementary strain energy value is not an issue. The sign convention relates to whether or not the initial imperfection lengthens or shortens the bar. The first term in Eqn. (5.10) contains the initial imperfection term and, if negative, can result in a negative energy value. Thus, the energy functions derived in Section 5.1 are correct.

For a simple structure, compatibility relationships are easily deduced. They are more difficult to determine for large structures. It is possible to calculate strain energy for different configurations using matrix methods, but a single strain energy expression cannot be formulated. Without an explicit expression, it is not possible to apply mathematical optimisation techniques and find the internal energy maximising pattern of imperfections. Thus, further explicit analysis will use the total complementary energy method.

5.4 Imperfection Analysis of an Imperfect Overconstrained Parallelogram Linkage

With energy functions correctly derived, it is possible to consider the calculation of energy in an overconstrained mechanism with initial imperfections. The mechanism to be considered is the one first analysed by Kuznetsov, as described in Section 2.4.2 and shown in Fig. 5.4.

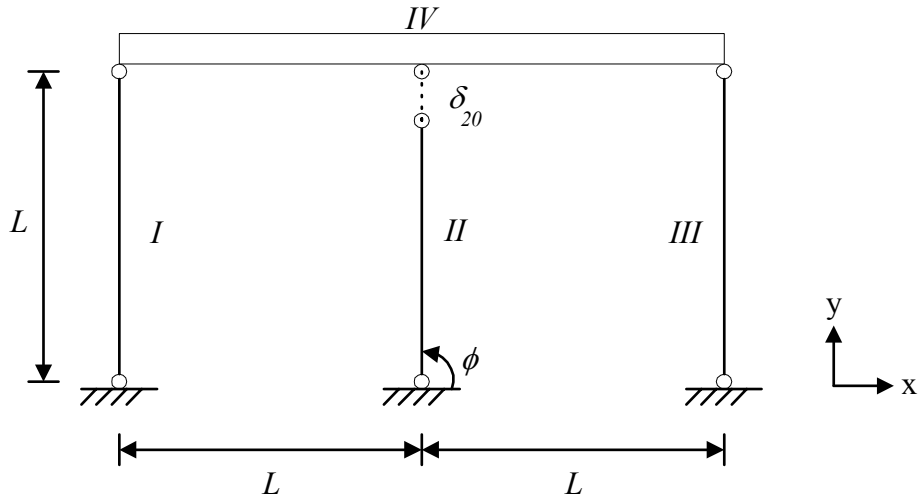


Fig. 5.4 Overconstrained parallelogram linkage

It is a two-dimensional, single degree-of-freedom linkage with an additional bar. The parallelogram four-bar linkage is overconstrained, and when in the ideal geometry can

displace without stresses and strains. In cases where there is an initial imperfection in the geometry of the mechanism, such as a shortened bar, stresses and strains develop and the mechanism becomes a statically indeterminate structure that requires an input of energy to regain mobility.

Analysis of this mechanism begins with the consideration of the fully open configuration (ϕ=90°). In his analysis, Kuznetsov assumed that bar *IV* is perfectly rigid in bending ($EI=\infty$). As bending stresses vary through the cross-section of a beam, calculation of strain energy in bar *IV* due to bending stresses is an approximation. Axial stresses are constant throughout the cross-section and, therefore, allow the determination of the internal energy accurately. To analyse the relationship between the internal forces in the structure, it is useful to apply equilibrium to bar *IV*. The sum of internal forces in the global y direction equals

$$\sum F_y = N_1 + N_2 + N_3 = 0 \tag{5.27}$$

where N_1, N_2, and N_3 are the internal forces in bars *I*, *II*, and *III* respectively. Using symmetry, it can be found that $N_1 = N_3$. From this, it follows that

$$N = N_1 = N_3 = -0.5N_2 \tag{5.28}$$

and

$$N_2 = -2N \tag{5.29}$$

Applying Eqns. (5.9) and (5.10), the complementary strain energy function is

$$U^* = \int U_0^* dv = \frac{N_1^2 L}{2EA} + N_2\delta_{20} + \frac{N_2^2 L}{2EA} + \frac{N_3^2 L}{2EA} \tag{5.30}$$

Substituting in Eqns. (5.28) and (5.29) yields

$$U^* = \frac{3N^2 L}{EA} - 2N\delta_{20} \tag{5.31}$$

The principle of the stationary value of total complementary strain energy, Eqn. (5.16), is next applied

$$\frac{\partial U^*}{\partial N} = \frac{6NL}{EA} - 2\delta_{20} = 0 \tag{5.32}$$

It is then possible to solve for the internal forces in the members due to an initial imperfection, δ_{20}.

$$N = \frac{\delta_{20} EA}{3L} \tag{5.33}$$

Eqn. (5.34) can be substituted into Eqn. (5.31) to find the expression for the complementary strain energy in the structure due to initial imperfections.

$$U^* = \frac{-\delta_{20}^2 EA}{3L} \tag{5.34}$$

The same result can be determined using strain energy through matrix displacement methods.

Kuznetsov's assumption that bar *IV* is infinitely rigid is meant to simplify the calculation of internal energy in the overconstrained, parallelogram mechanism. This assumption, however, excludes the internal energy that is developed in bar *IV* due to the initial imperfection. If the infinitely rigid beam, bar *IV*, is replaced with a multi-bar truss, then the structure is the same as the one with the beam but only axial stresses develop in it.

Formulation using multi-bar truss also includes consideration of a configuration variable, ϕ, as defined in Fig. 5.5 below. In deriving the complementary strain expression, it is useful to consider the possibility of multiple imperfections in the mechanism. Therefore, three initial length imperfections are introduced into the mechanism (δ_{10}, δ_{30}, and δ_{50}).

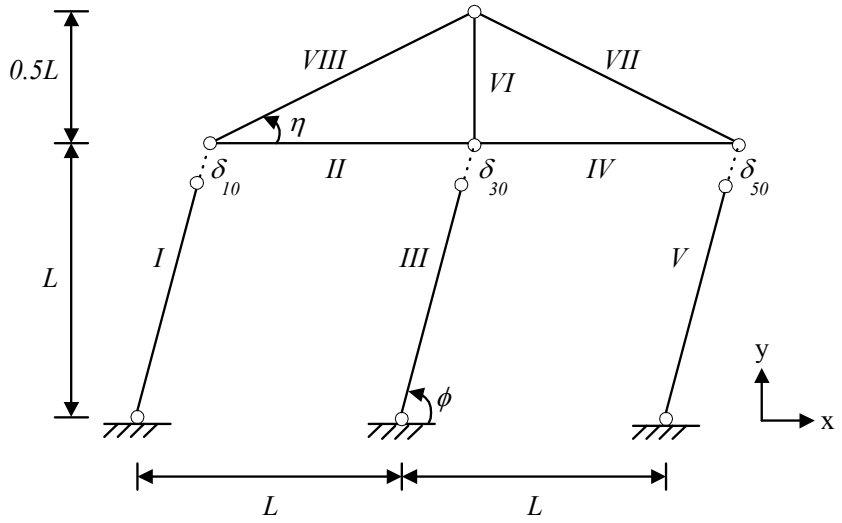


Fig. 5.5 Overconstrained parallelogram linkage with truss cap

The first step to determining the internal energy in the mechanism at any point in deployment is to apply equilibrium at each joint and solve for the internal forces in the mechanism in terms of a single force variable, *N*. They are as follows:

$$N_I = -0.5N \tag{5.35}$$

$$N_{II} = -0.5N\cos\phi + 0.5N\sin\phi\cot\eta \tag{5.36}$$

$$N_{III} = N \tag{5.37}$$

$$N_{IV} = 0.5N\cos\phi + 0.5N\sin\phi\cot\eta \tag{5.38}$$

$$N_V = -0.5N \tag{5.39}$$

$$N_{VI} = N\sin\phi \tag{5.40}$$

$$N_{VII} = -0.5N\frac{\sin\phi}{\sin\eta} \tag{5.41}$$

$$N_{VIII} = -0.5N\frac{\sin\phi}{\sin\eta} \tag{5.42}$$

It is next possible to write the complementary strain energy equation for the mechanism. For simplicity, initial imperfections will be expressed in the complementary energy function as strains.

$$\begin{aligned} U^* &= \frac{2(-0.5N)^2 L}{2EA} - 0.5NL\varepsilon_{10} - 0.5NL\varepsilon_{50} + \frac{N^2 L}{2EA} + NL\varepsilon_{30} \\ &+ \frac{(-0.5N\cos\phi + 0.5N\sin\phi\cot\eta)^2 L}{2EA} + \\ &\frac{(0.5N\cos\phi + 0.5N\sin\phi\cot\eta)^2 L}{2EA} + \frac{2\sqrt{5}\left(-0.5N\dfrac{\sin\phi}{\sin\eta}\right)^2 L}{2EA} \\ &+ \frac{(N\sin\phi)^2 L}{4EA} \end{aligned} \tag{5.43}$$

This can be simplified to

$$\begin{aligned} U^* &= \frac{1.5N^2 L}{2EA} + NL(-0.5\varepsilon_{10} - 0.5\varepsilon_{50} + \varepsilon_{30}) \\ &+ \frac{N^2 L\sin^2\phi\cot^2\eta}{4EA} + \frac{N^2 L\cos^2\phi}{4EA} + \frac{\sqrt{5}N^2 L\sin^2\phi}{4EA\sin^2\eta} \\ &+ \frac{N^2 L\sin^2\phi}{2EA} \end{aligned} \tag{5.44}$$

This is the complementary strain energy function for a single value of ϕ. Application of the principle of stationary value of total complementary energy provides an expression for the internal force variable in terms of the configuration variable and initial imperfections.

$$N = \frac{(0.5\varepsilon_{10} + 0.5\varepsilon_{50} - \varepsilon_{30})EA}{\left(1.5 + \dfrac{\sin^2\phi\cot^2\eta}{2} + \dfrac{\cos^2\phi}{2} + \dfrac{\sqrt{5}\sin^2\phi}{2\sin^2\eta} + \dfrac{\sin^2\phi}{2}\right)} \tag{5.45}$$

This expression can be substituted into Eqn. (5.44) to calculate the complementary strain energy at any point in the deployment of the mechanism. By setting L=2m, ε_{10}=0,

ε_{30}=-0.05, ε_{50}=0, E = 70*10^9 Pa, A = 6.155*10^{-4} m^2 and varying the configuration variable ϕ from 0 to 180°, it was possible to graph the complementary strain energy of the mechanism deployment. For reference, the strain energy distribution was calculated using matrix displacement methods as well. The results are shown in Fig. 5.6.

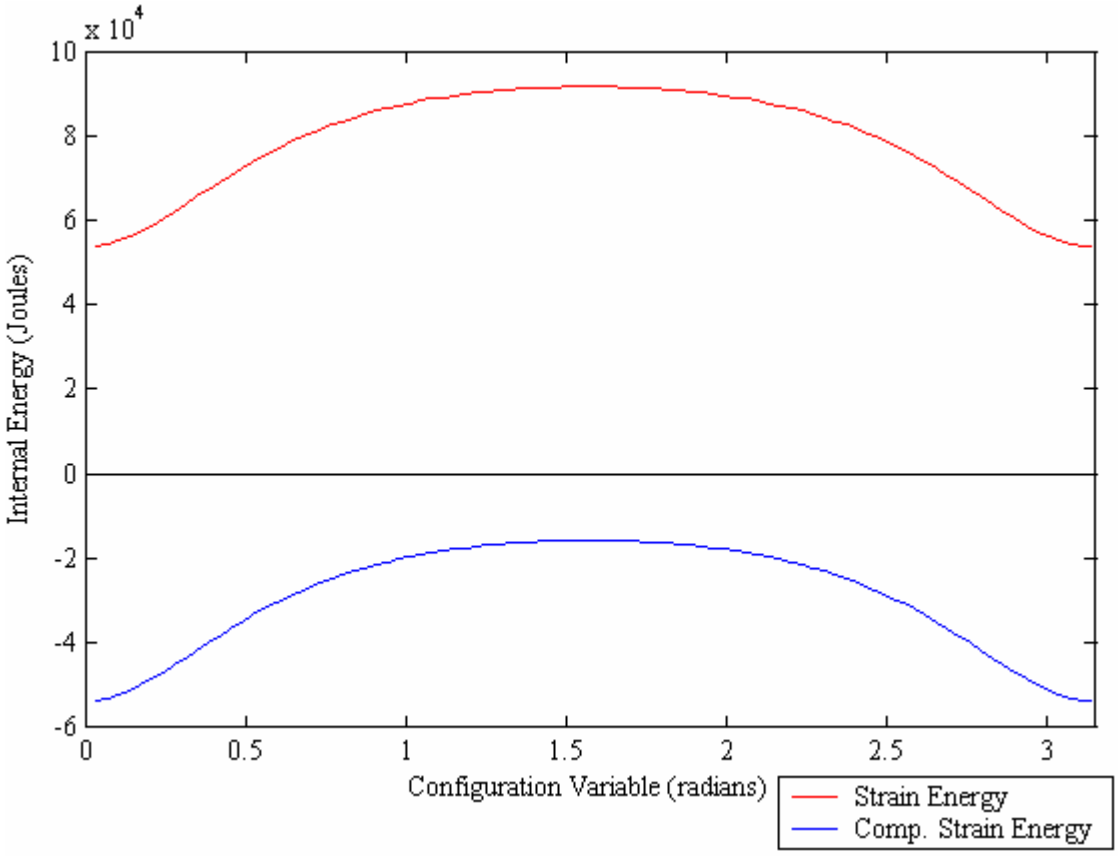


Fig. 5.6 Internal energy vs. deployment angle for a single imperfection

As detailed in Section 5.3, the negative value of the complementary strain energy through deployment is not an issue. The sign convention relates to whether or not the initial imperfection lengthens or shortens the bar. It is useful to note that for both strain energy and complementary strain energy the minimum energy state occurs at $\phi = 0$ or π radians (0 or 180°). The mechanism will jump to the horizontal position (bars *I*, *III* and *V* parallel to the ground) and elastically resist any change in configuration. The maximum energy state during deployment is the fully open configuration, $\phi = \pi/2$

radians (90°). These results shows that the complementary energy result, which has no physical significance, corresponds to the strain energy result and can therefore be used to determine the variation of internal energy through deployment for more complicated mechanisms. The mechanism's behaviour was further verified through the construction of a small model, which behaved in the same manner as shown above.

The expressions derived for complementary strain energy are suitably general so that the figure above can be generated for sets of multiple imperfections. Knowing the magnitude of the internal energy throughout deployment for a given pattern of imperfections, it is possible to determine whether an equilibrium state is stable, neutral or unstable. These states have the same definition as those detailed in stability theory (Ugural and Fenster, 1995). Additionally, it indicates the amount of energy that must be input to articulate the mechanism. The above analysis prompts an obvious question. What is the worst-case (internal energy maximising) pattern of imperfections in an overconstrained mechanism? To answer this question, it is necessary to consider methods of optimising explicit functions.

5.5 Optimisation Techniques

In most structural analysis and design problems, there are a number of feasible solutions for the problem. It is desirable to select the solution that will meet some set of design criteria while achieving an optimum value for some key parameters, such as structural strength or material cost. A great deal of work has focused on methods of determining optimum values for design criteria. To understand these methods, it is necessary to provide the basic definitions used in optimisation problems. There are three types of variables in optimisation problems: pre-set, design, and behavioural. Pre-set variables are constants, such as the modulus of elasticity or π. Design variables are

independent, and generally express some aspect of the topology of the structure, its configuration or cross-section. Behavioural variables are dependent on variation of the design variables and behavioural relationships such as elasticity. Examples of behavioural variables for a structural system are stress, strain, and strain energy (Kirsch, 1981).

The possible values for variables can be limited by constraints on the design or behavioural variables. These constraints define the design space, which encompasses all feasible designs. This can be shown using the simple, overconstrained mechanism shown in the previous section. If there are two initial imperfections, ε_{10} and ε_{30}, that have constraints of +/- 0.05, the design space for the structure is shown in Figure 5.7 below.

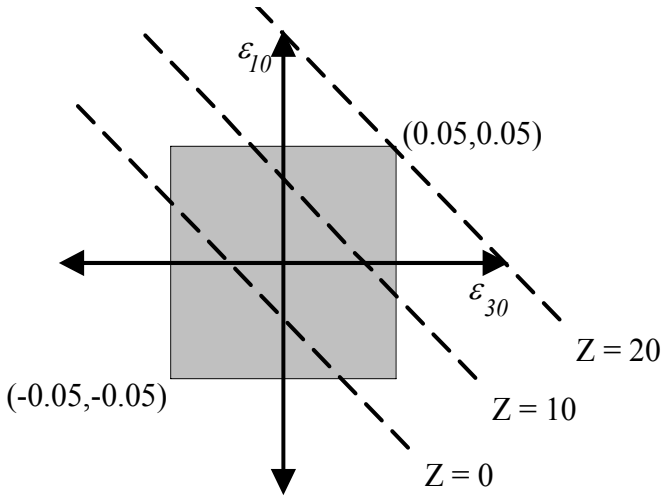


Fig. 5.7 Design space for simple mechanism with two imperfections

Definition of an objective function that relates the design variables, $Z(\varepsilon_{10}, \varepsilon_{30})$, allows a method of comparing different combinations of design variables. The combination yielding the optimum solution lies within the shaded region, while those outside of the region violate the constraints. This can be visualised using Fig. 5.7. If lines or curves composed of patterns of imperfections with constant Z values are plotted,

the intersection between the contour line with the desired value of Z and the design space yields the optimum combination or combinations of imperfections. The combination of imperfections yielding the largest or smallest value for the objective function, depending upon what is desired, is either the best or the worst combination (Kirsch, 1981).

A number of methods exist for determining the optimum combination of imperfections. The first is iteration. By calculating the value of the objective function for a large number of possible combinations of the design variables, it is possible to find an approximate optimum value. Another method used for analysis is the pre-selection of constraints believed to be critical (active) at the optimum and solution of the optimisation problem based upon these constraints. This method can be accurate if the correct constraints are chosen. If not, then the method yields a false optimum (Kirsch, 1981). Optimality criteria approaches assume that some criterion based upon the behaviour of the structure is satisfied at optimum. Fully stressed design in structural weight optimisation is an example of this method. It assumes that the members of a structure will be at their limiting stresses for at least one load case combination at optimum. Repeated analysis is conducted, with modification of variables based upon simple computational rules. This method can yield accurate solutions, but they are generally specialised (Kirsch, 1981).

The general method of optimisation used with mechanisms is mathematical programming. It is intended to solve a generally defined problem using numerical search algorithms. This method is efficient in solving problems with a single, global optimum value for the objective function within the design space. It is possible for multiple, relative optima to exist. The more complex the objective function, the greater the possibility of relative optima. Good approximations of the global optimum can,

however, be made. The specific procedures considered in this analysis are linear programming, quadratic programming, and sequential quadratic programming.

Linear programming is a method of determining the optimum values for an objective function and set of constraints that are expressed linearly in terms of design variables. Constraints can be either equalities or inequalities, and the objective function can be maximised or minimised. The general problem statement for linear programming is

$$Z = \sum_{j=1}^{n} C_j X_j \rightarrow \min \tag{5.46}$$

subject to

$$\sum_{j=1}^{n} a_{ij} X_j \langle \leq, =, \geq \rangle b_i \qquad i = 1,...,m \tag{5.47}$$

and

$$X_j \geq 0 \qquad j = 1,...,n \tag{5.48}$$

where X_j are the design variables, C_j are the constants on design variables in the objective function, a_{ij} are the constants on design variables in the constraints, b_i are the constants in the constraint statement, i equals the number of constraints and j equals the number of design variables. It is necessary that all design variables be positive, and that b_i be nonnegative as well. If the objective of the analysis is maximising the objective function, it is only necessary to multiply it by –1. Similarly, if a constraint has a negative b_i one can multiply both sides of the constraint by –1 to meet the non-negativity requirement specified above (Fletcher, 1981).

A solution is defined as any set of values for the design variables that satisfies Eqn. (5.46). A feasible solution is any solution that satisfies Eqn. (5.47) as well. An optimum feasible solution is one that minimises the objective function, and a basic

feasible solution is a feasible solution with no more than m nonzero X_j. The first step in setting up the solution is to write the system of equations Eqns. (5.46) and (5.47) in standard form.

$$\begin{aligned} &a_{11}X_1 + a_{12}X_2 + ... + a_{1n}X_n = b_1 \\ &a_{21}X_1 + a_{22}X_2 + ... + a_{2n}X_n = b_2 \\ &a_{m1}X_1 + a_{m2}X_2 + ... + a_{mn}X_n = b_m \\ &C_1X_1 + C_2X_2 + ...C_nX_n = Z \end{aligned} \tag{5.49}$$

These expressions can be simplified by linearly combining the equations in a manner that yields a resultant set of equations with the same values as the initial ones. This can be repeated until there are m columns, each containing zeros and a single one. When rearranged such that the matrix of coefficients is an identity matrix, the system can be said to be in canonical form. The solution of the equations in this form is a basic, feasible solution. The optimal set of design variable values is found by moving from one canonical form to an improved one until the objective function value can no longer be improved (Fletcher, 1981).

Quadratic programming also applies the simplex method. The standard form for a quadratic programming problem is

$$Z = cx + \frac{1}{2}x^T Qx \tag{5.50}$$

subject to

$$Ax \le b \text{ and } x \ge 0 \tag{5.51}$$

where c is a n-dimensional row vector describing coefficients of the linear terms in the objective function, Q is a (n x n) symmetric matrix describing the coefficients of the quadratic terms, A is a (m x n) matrix and b is a m-dimensional column vector. If the objective function is strictly convex, then the problem has a unique global minimum. This condition is met when the Q matrix is positive definite (the eigenvalues of the

matrix are greater than zero). If the objective function is not positive definite, then there is a possibility of multiple, relative minima (Kirsch, 1981).

The solution process, if constraints are present, begins by combining the objective function and constraints into a lagrangian function, as shown below.

$$L(x,\mu) = cx + \frac{1}{2}x^T Qx + \mu(Ax - b) \tag{5.52}$$

where μ is an m-dimensional row vector. From here, the Karush-Kuhn-Tucker conditions for a local minimum are introduced (Kirsch, 1981):

$$\frac{\partial L}{\partial x_j} \geq 0,\ j = 1,\ldots, n \qquad c + x^T Q + \mu A \geq 0 \tag{5.53}$$

$$\frac{\partial L}{\partial \mu_j} \leq 0,\ j = 1,\ldots, m \qquad Ax - b \leq 0 \tag{5.54}$$

$$x_j \frac{\partial L}{\partial x_j} = 0,\ j = 1,\ldots, n \qquad x^T\left(c^T + Qx + A^T\mu\right) = 0 \tag{5.55}$$

$$\mu_i g_i(x) = 0,\ i = 1,\ldots, m \qquad \mu(Ax - b) = 0 \tag{5.56}$$

$$x_j \geq 0,\ j = 1,\ldots, n \qquad x \geq 0 \tag{5.57}$$

$$\mu_j \geq 0,\ i = 1,\ldots, m \qquad \mu \geq 0 \tag{5.58}$$

Eqns. (5.53) to (5.58) provide a set of linear equations that can be optimised using the simplex method. Each x column vector determined using this method is substituted back into Eqn. (5.52) and then the Karush-Kuhn-Tucker conditions are reapplied until an optimum is found. This process requires the use of a computer utility to conduct the analysis. Matlab has an optimisation toolbox that can perform quadratic optimisation. For the analysis of the explicit quadratic complementary strain energy function, this utility was used.

Sequential linear or quadratic programming is simply the expression of a non-linear or non-quadratic function either linearly or quadratically and optimising of this expression using one of the methods shown above. The design variable values found during each iteration are re-entered into the original function, and the value of the function determined. When the function value can no longer be improved or the constraints of the design variables are reached, it is optimised.

5.6 Optimisation of the Simple Overconstrained Mechanism using Explicit Methods

Substituting Eqn. (5.45) into Eqn. (5.44) yields the complementary strain energy function for the simple, overconstrained mechanism in terms of initial imperfections.

$$U^* = \frac{-LEA}{4+\sin^2\phi\cot^2\eta+\dfrac{\sqrt{5}\sin^2\phi}{\sin^2\eta}}\left(0.5\varepsilon_{10}+0.5\varepsilon_{50}-\varepsilon_{30}\right)^2 \tag{5.64}$$

It is possible to simplify this equation by defining an additional variable, *J*.

$$J = \frac{-LEA}{4+\sin^2\phi\cot^2\eta+\dfrac{\sqrt{5}\sin^2\phi}{\sin^2\eta}} \tag{5.65}$$

Next, Eqn. (5.64) can be expanded and placed into the proper form to conduct the quadratic optimisation. When completed, the complementary strain energy function is of the form

$$U^*\left(\varepsilon_{10},\varepsilon_{30},\varepsilon_{50}\right) = \frac{1}{2}\begin{bmatrix}\varepsilon_{10} & \varepsilon_{30} & \varepsilon_{50}\end{bmatrix}\begin{bmatrix}0.5J & -1J & 0.5J\\ -1J & 2J & -1J\\ 0.5J & -1J & 0.5J\end{bmatrix}\begin{bmatrix}\varepsilon_{10}\\ \varepsilon_{30}\\ \varepsilon_{50}\end{bmatrix} \tag{5.66}$$

This is the objective function for the optimisation. The design variables are ε_{10}, ε_{30} and ε_{50}. The vector of design variables, ε_{0i}, is constrained by the following relationships

$$\varepsilon_{0i} \geq -0.05$$

$$\varepsilon_{0i} \leq 0.05$$

Setting L=2 meters, $\varepsilon_{10n}=\varepsilon_{30n}=\varepsilon_{50n}=0$, $E = 70*10^9$ Pa, $A = 6.155*10^{-4}$ m^2 and $\phi = 45°$, it is possible to use the quadratic optimisation tool in Matlab. The result is $\varepsilon_{10}= 0.05$, $\varepsilon_{30}= -0.05$ and $\varepsilon_{50} =0.05$. The value of the objective function for these imperfections is –97975J.

The above optimisation of the explicit complementary strain energy function provides the pattern of imperfections that causes the most complementary strain energy to develop in the mechanism. It is then possible to calculate the mechanism's internal energy through deployment for the set of imperfections. A graph of both strain energy and the complementary strain energy through deployment for this pattern of imperfections is shown in Fig. 5.8 below.

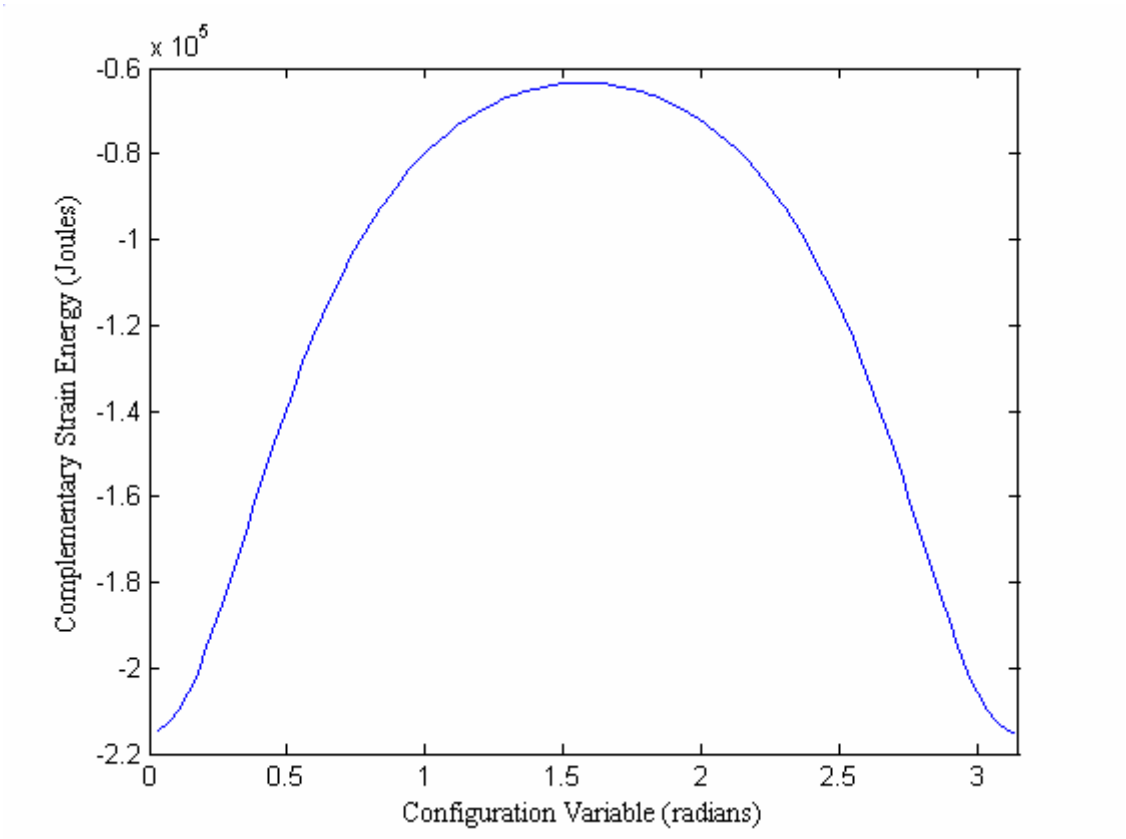


Fig. 5.8 Graph of complementary strain energy through deployment

Internal energy is at a maximum when $\phi = \pi/2$ radians (90°) and a minimum when $\phi = 0$ or π radians (0 or 180°). In the absence of restraining forces, the mechanism will move to the horizontal position and assume a state of stable equilibrium.

5.7 Approximate Expressions of Energy Functions

There are instances when the derivation of an explicit function for the internal energy in terms of initial imperfections is not practical. In cases of combined loading or calculation in three dimensions, it can be prohibitively complex to express the strain energy or complementary strain energy of the mechanism in a single expression. In these cases, the variation of the internal energy is considered implicit, and it is necessary to develop a method to approximate its value for different patterns of initial

imperfections. If the internal energy in the mechanism, U_n, is known for a set of imperfections, ε_{0n}, and a set value of the configuration variable, then a Taylor series expansion of the internal energy with respect to the initial imperfections can be used to approximate the internal energy function over a step-size λ. An example is shown below, as a function of two initial imperfections, ε_{10} and ε_{30}.

$$U(\varepsilon_{10},\varepsilon_{30}) = U_n + \frac{\partial U}{\partial \varepsilon_{10}}(\varepsilon_{10}-\varepsilon_{10n}) + \frac{\partial U}{\partial \varepsilon_{30}}(\varepsilon_{30}-\varepsilon_{30n}) + \frac{1}{2!}\left(\begin{array}{l} \dfrac{\partial^2 U}{\partial \varepsilon_{10}^2}(\varepsilon_{10}-\varepsilon_{10n})^2 + 2\dfrac{\partial^2 U}{\partial \varepsilon_{10}\partial \varepsilon_{30}}(\varepsilon_{10}-\varepsilon_{10n})(\varepsilon_{30}-\varepsilon_{30n}) \\ + \dfrac{\partial^2 U}{\partial \varepsilon_{30}^2}(\varepsilon_{30}-\varepsilon_{30n})^2 \end{array}\right) \tag{5.62}$$

where U_n is the strain energy for the current set of design variables, ε_{10n} and ε_{30n} are the initial imperfections, and $\frac{\partial U}{\partial \varepsilon_{10}}$, $\frac{\partial U}{\partial \varepsilon_{30}}$, $\frac{\partial^2 U}{\partial \varepsilon_{10}^2}$, $\frac{\partial^2 U}{\partial \varepsilon_{30}^2}$ and $\frac{\partial^2 U}{\partial \varepsilon_{10}\partial \varepsilon_{30}}$ are the first and second-order sensitivities of the objective function to the design variables. These sensitivities express the effect of changing a specific design variable or set design variables on the objective function. Finite differences can be used to calculate the sensitivity of the implicit energy function over the step-size λ. The first-order sensitivities are

$$\frac{\partial U}{\partial \varepsilon_{10}} = \frac{1}{2\lambda}\left(U(\varepsilon_{10n}+\lambda,\varepsilon_{30n}) - U(\varepsilon_{10n}-\lambda,\varepsilon_{30n})\right) \tag{5.63}$$

$$\frac{\partial U}{\partial \varepsilon_{30}} = \frac{1}{2\lambda}\left(U(\varepsilon_{10n},\varepsilon_{30n}+\lambda) - U(\varepsilon_{10n},\varepsilon_{30n}-\lambda)\right) \tag{5.64}$$

Calculation of internal energy using ABAQUS for small variations in the initial imperfection values provides the sensitivity of the function to variation of the independent variables. The second-order sensitivities are

$$\frac{\partial^2 U}{\partial \varepsilon_{10}^2} = \frac{1}{\lambda^2}\left(U\left(\varepsilon_{10n}+\lambda, \varepsilon_{30n}\right) - 2U_n + U\left(\varepsilon_{10n}-\lambda, \varepsilon_{30n}\right)\right) \tag{5.65}$$

$$\frac{\partial^2 U}{\partial \varepsilon_{30}^2} = \frac{1}{\lambda^2}\left(U\left(\varepsilon_{10n}, \varepsilon_{30n}+\lambda\right) - 2U_n + U\left(\varepsilon_{10n}, \varepsilon_{30n}-\lambda\right)\right) \tag{5.66}$$

$$\frac{\partial^2 U}{\partial \varepsilon_{10}\partial \varepsilon_{30}} = \frac{1}{4\lambda^2}\begin{pmatrix} U\left(\varepsilon_{10n}+\lambda, \varepsilon_{30n}+\lambda\right) - U\left(\varepsilon_{10n}-\lambda, \varepsilon_{30n}+\lambda\right) \\ + U\left(\varepsilon_{10n}-\lambda, \varepsilon_{30n}-\lambda\right) - U\left(\varepsilon_{10n}+\lambda, \varepsilon_{30n}-\lambda\right) \end{pmatrix} \tag{5.67}$$

If λ is sufficiently small, the sensitivities will accurately approximate the continuous value of the gradient of the internal energy function within the step-size.

Using ABAQUS, it is possible to determine the internal energy for an initial set of imperfections. Of the two available energy methods, it is necessary to use strain energy because ABAQUS does not output complementary strain energy values. A Taylor expansion of the internal energy can be developed using the initial values for strain energy and imperfections. A step size, λ, is chosen and sensitivities are then calculated. The smaller the step-size, the more accurate the approximation of the strain energy function. The quadratic strain energy function can then be optimised within the maximum imperfection constraints using the fmincon routine in Matlab. A pattern of imperfections is found and an accompanying strain energy value. The process of determining the Taylor expansion for strain energy is then repeated using the results of the first optimisation as the initial set of imperfections. The iteration of the procedure continues as long as strain energy values continue to increase. If the results are the same after two consecutive optimisations, the procedure has converged on a strain-energy maximising pattern of initial imperfections for a single value of the configuration variable. If the internal energy results from iteration of the procedure oscillate between two values, then λ should be decreased and iteration of the procedure should continue.

After all values of the configuration variable have been considered, the pattern of imperfections resulting in the largest internal energy is the worst-case.

Once the strain energy maximising pattern of imperfections has been found, the variation of internal energy through deployment is then determined by running successive ABAQUS models using different values for the configuration variable. This reveals the stable configuration of the mechanism. This procedure, which will be referred to as approximate sensitivities optimisation, is summarised in Fig. 5.9 below.

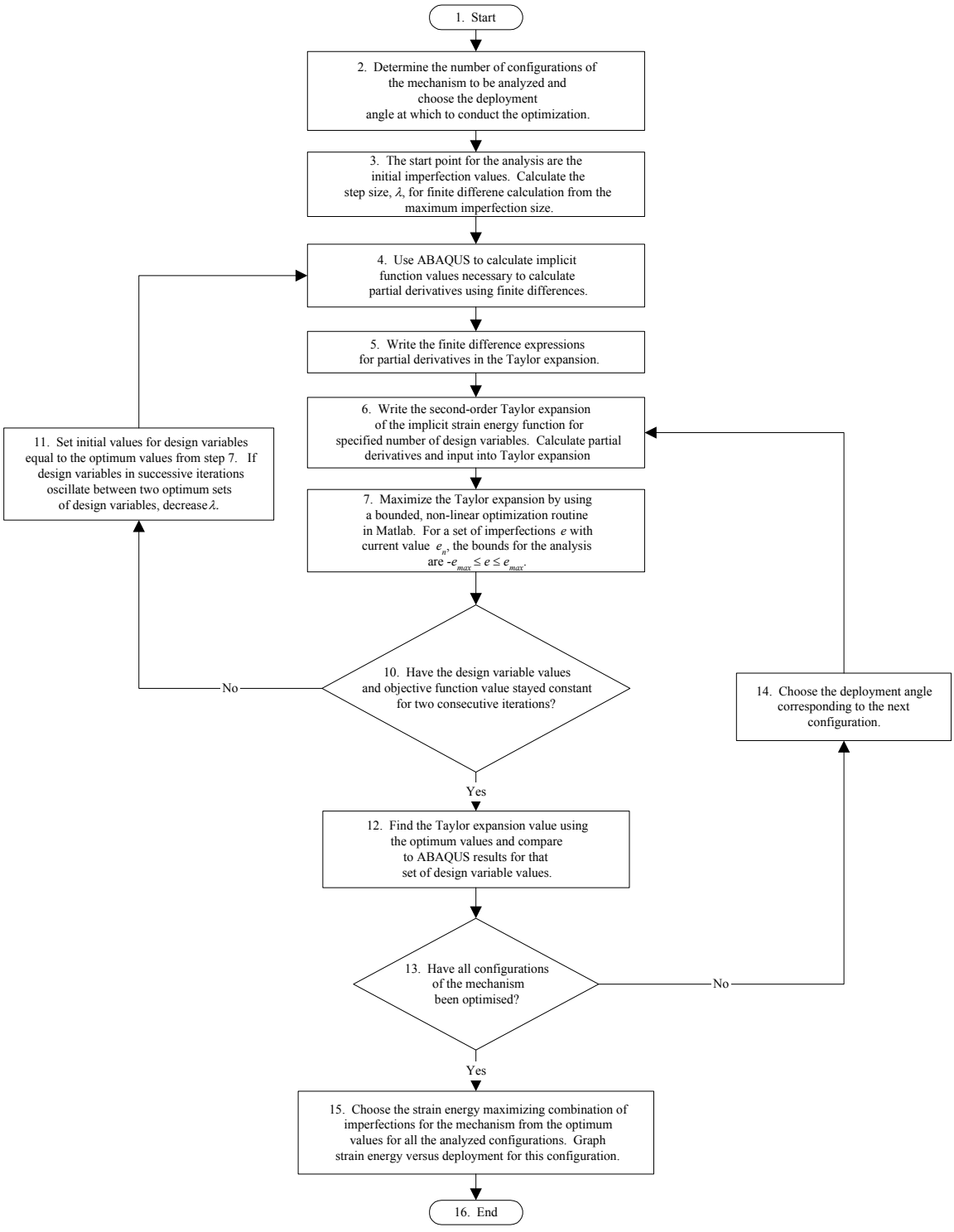


Fig. 5.9 Approximate sensitivities optimisation flowchart

This method was applied to the simple, overconstrained mechanism using the same set of variable definitions as in the explicit optimisation. The step size used for the

analysis was 0.01, which is 10% of the difference between the maximum and minimum possible imperfections. In order to calculate the sensitivities, 19 ABAQUS runs were required per iteration. The initial imperfection values used for each ABAQUS run are shown in Table 5.1 below.

Table 5.1 ABAQUS runs for each iteration of approximate sensitivities optimisation

ABAQUS Run	ε_{10}	ε_{30}	ε_{50}
1	ε_{10n}	ε_{30n}	ε_{50n}
2	$\varepsilon_{10n}+\lambda$	ε_{30n}	ε_{50n}
3	$\varepsilon_{10n}-\lambda$	ε_{30n}	ε_{50n}
4	ε_{10n}	$\varepsilon_{30n}+\lambda$	ε_{50n}
5	ε_{10n}	$\varepsilon_{30n}-\lambda$	ε_{50n}
6	ε_{10n}	ε_{30n}	$\varepsilon_{50n}+\lambda$
7	ε_{10n}	ε_{30n}	$\varepsilon_{50n}-\lambda$
8	$\varepsilon_{10n}+\lambda$	$\varepsilon_{30n}+\lambda$	ε_{50n}
9	$\varepsilon_{10n}+\lambda$	$\varepsilon_{30n}-\lambda$	ε_{50n}
10	$\varepsilon_{10n}-\lambda$	$\varepsilon_{30n}-\lambda$	ε_{50n}
11	$\varepsilon_{10n}-\lambda$	$\varepsilon_{30n}+\lambda$	ε_{50n}
12	ε_{10n}	$\varepsilon_{30n}+\lambda$	$\varepsilon_{50n}+\lambda$
13	ε_{10n}	$\varepsilon_{30n}+\lambda$	$\varepsilon_{50n}-\lambda$
14	ε_{10n}	$\varepsilon_{30n}-\lambda$	$\varepsilon_{50n}-\lambda$
15	ε_{10n}	$\varepsilon_{30n}-\lambda$	$\varepsilon_{50n}+\lambda$
16	$\varepsilon_{10n}+\lambda$	ε_{30n}	$\varepsilon_{50n}+\lambda$
17	$\varepsilon_{10n}+\lambda$	ε_{30n}	$\varepsilon_{50n}-\lambda$
18	$\varepsilon_{10n}-\lambda$	ε_{30n}	$\varepsilon_{50n}-\lambda$
19	$\varepsilon_{10n}-\lambda$	ε_{30n}	$\varepsilon_{50n}+\lambda$

As it took three iterations for the procedure to reach a stable, optimum imperfection set, 57 ABAQUS runs were required in total. The iterations of the approximate sensitivities method are shown in Table 5.2.

Table 5.2 Approximate sensitivities method results

Iteration	ε_{10}	ε_{30}	ε_{50}	U (Joules)
1	-0.000111	0.000111	0.000111	22.1
2	-0.05	0.05	-0.05	98005
3	-0.05	0.05	-0.05	98005

The pattern of imperfections resulting from the application of the approximate sensitivities method is equivalent to that found with the total potential energy method. The percent error was 0.003, which is insignificant for this analysis. Thus, the approximate sensitivities method is valid.

When approximating a function, accuracy is a concern. The accuracy of the approximation is governed by the sensitivities. The finite differences method of determining the sensitivity of a function to an independent variable, as shown above, is calculated by varying the function value by a small amount, λ. The smaller one makes the value of λ, the more accurate the approximation. If an explicit method for calculating sensitivities could be determined, the accuracy of the approximation would increase. To determine an explicit expression for sensitivity, it is necessary to express the strain in an element as

$$\varepsilon = Bu \tag{5.68}$$

where B is the strain displacement matrix and u is the nodal displacement vector of the element. Determining the shape function for each member and taking the partial with respect to the displacement variable accomplishes calculation of the B matrix. The strain energy in an element can be written using Eqns. (5.6) and (5.68) as

$$U = \int \left(\frac{1}{2} u^T B^T D B u - u^T B^T D \varepsilon_0 \right) dV + \int \left(\frac{1}{2} {\varepsilon_0}^T D \varepsilon_0 \right) dV \tag{5.69}$$

It is important to note that u is the nodal displacement in the local coordinate system. To calculate the strain energy in the structure, it is necessary to write the strain energy in terms of the global nodal displacements, Δ. The conversion from local to global coordinates simply requires multiplying the u by a transformation matrix, T. As the volume of the members in the structure are not always equal, the strain energy

expression must be written as a sum the strain energy in the members. The global strain energy expression is therefore

$$U = \sum_{i=1}^{m} \begin{pmatrix} \int \left(\frac{1}{2} \Delta^T T^T B^T DBT\Delta - \Delta^T T^T B^T D\varepsilon_0 \right) dV_i \\ + \int \left(\frac{1}{2} \varepsilon_0{}^T D\varepsilon_0 \right) dV_i \end{pmatrix} \tag{5.70}$$

where *m* is the number of members in the structure. The remainder of the derivation will consider a single member. Taking the partial derivative with respect to the initial strain vector provides an explicit expression for the sensitivity of the strain energy function with respect to the initial strain vector. This is the first order sensitivity vector for the strain energy function.

$$\begin{aligned} \frac{\partial U}{\partial \varepsilon_{0i}} &= \int \left(\Delta^T T^T B^T DBT \frac{\partial \Delta}{\partial \varepsilon_{0i}} \right) dV - \\ &\int \left(\Delta^T T^T B^T D \frac{\partial \varepsilon_0}{\partial \varepsilon_{0i}} + \frac{\partial \Delta^T}{\partial \varepsilon_{0i}} T^T B^T D\varepsilon_0 \right) dV + \int \left(\frac{1}{2} \varepsilon_0{}^T D \frac{\partial \varepsilon_0}{\partial \varepsilon_{0i}} \right) dV \end{aligned} \tag{5.71}$$

From this equation, there are two unknown quantities. It is necessary to determine $\frac{\partial \varepsilon_0}{\partial \varepsilon_{0i}}$ and $\frac{\partial \Delta}{\partial \varepsilon_{0i}}$. The partial derivative of the initial strain vector with respect to an initial strain value is simply a vector containing zeros in all positions except for a one in the position held by the initial strain value. For example, the partial of the strain vector $(\varepsilon_{10}\ \varepsilon_{30}\ \varepsilon_{50})^T$ with respect to ε_{10} is simply $(1\ 0\ 0)^T$.

It is possible to find the global displacement sensitivity vector by setting the partial derivative of the strain energy function with respect to global displacement, Δ, equal to zero. This can be done because there are no external forces applied to the mechanism.

$$\frac{\partial U}{\partial \Delta} = \int \left(T^T B^T DBT\Delta - T^T B^T D\varepsilon_0 \right) dV = 0 \tag{5.72}$$

This can be rearranged, yielding

$$\int \left(T^T B^T DBT\,\Delta \right) dV = \int \left(T^T B^T D\,\varepsilon_0 \right) dV \tag{5.73}$$

The global structure stiffness matrix, *K*, can be expressed as shown below.

$$K = \int \left(T^T B^T DBT \right) dV \tag{5.74}$$

Substituting this expression into Eqn. 5.79 yields

$$K\Delta = \int \left(T^T B^T D\varepsilon_0 \right) dV \tag{5.75}$$

The expression now takes the form of the global stiffness equation. The right-hand side of the equation is the load vector caused by initial imperfections in the members. Taking the partial derivative with respect to ε_0 and rearranging yields

$$\frac{\partial \Delta}{\partial \varepsilon_{0i}} = K^{-1} \left(\int \left(T^T B^T D \frac{\partial \varepsilon_0}{\partial \varepsilon_{0i}} \right) dV \right) \tag{5.76}$$

Applying Eqns. (5.71) and (5.76), it is possible to explicitly determine the first-order sensitivities for the strain energy function. It is necessary to determine the global stiffness matrix, the nodal deflection for each element, the strain-displacement matrices for each member, and the transformation matrices for each member. For simple mechanisms, it is easy to find the global stiffness matrix and strain displacement matrices. Determination of the nodal displacements is done using ABAQUS.

Explicit calculation of second-order sensitivities is prohibitively complex. Thus, optimisation using explicit sensitivities will use a first-order Taylor expansion rather than Eqn. (5.62).

$$U(\varepsilon_{10}, \varepsilon_{30}) = U_n + \frac{\partial U}{\partial \varepsilon_{10}} (\varepsilon_{10} - \varepsilon_{10n}) + \frac{\partial U}{\partial \varepsilon_{30}} (\varepsilon_{30} - \varepsilon_{30n}) \tag{5.77}$$

The procedure, which will be referred to as explicit sensitivities optimisation, is otherwise the same as shown in Fig. 5.9 (See Fig. 5.10 below).

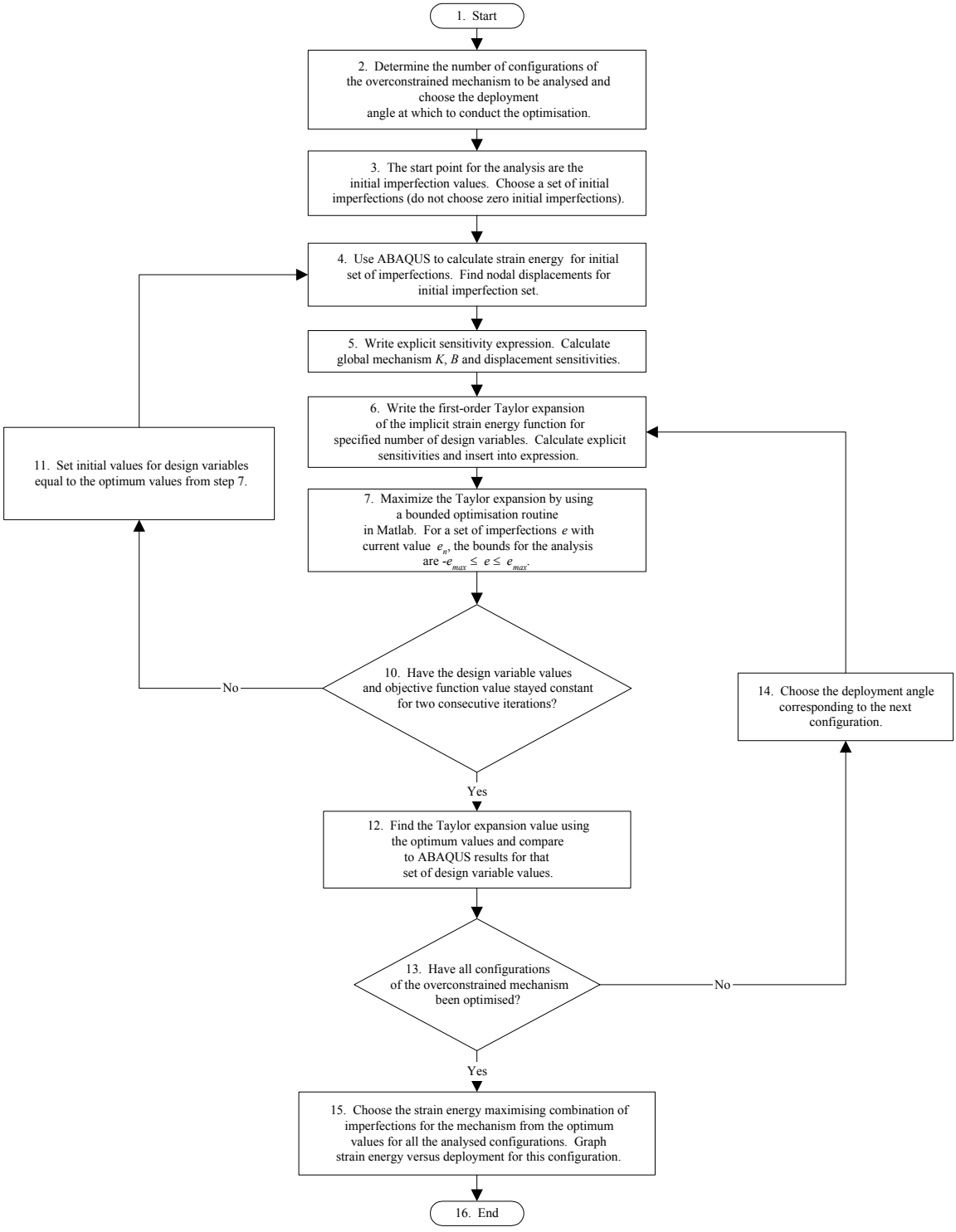


Fig. 5.10 Explicit sensitivities optimisation flowchart

This method was validated using the simple, overconstrained mechanism. Variable definitions were the same as with the explicit method and implicit method with approximate sensitivities. The starting point of the analysis was, however, different. Because the sensitivities are explicitly determined, it is not possible to start the analysis with no imperfections. The sensitivity expressions are continuous and zero-valued when initial imperfections equal zero. It is possible to use a zero-valued initial imperfection set when using finite differences to approximate sensitivities because expressions are discrete. Before analysis could begin, it was necessary to determine the global stiffness matrix, K, the member strain displacement matrices, B, and the transformation matrices, T. For the simple overconstrained mechanism these matrices could be calculated directly.

Analysis of the initial imperfection set using ABAQUS provided the set of nodal deflections and the initial strain energy value. The deflection sensitivities, and in turn the first-order energy sensitivities could then be calculated using Eqns. (5.77) and (5.82). The first order Taylor expansion of the strain energy was then defined and optimised, as shown in Table 5.3 below.

Table 5.3 Explicit sensitivities method

Iteration	ε_{10}	ε_{30}	ε_{50}	U (Joules)
1	0.005	-0.005	0.005	3132.5
2	-0.05	0.05	-0.05	98071
3	-0.05	0.05	-0.05	98071

The solution took only three iterations to converge. The pattern of imperfections resulting from the application of the explicit sensitivities optimisation method was the same as that found using the approximate sensitivities optimisation method. The difference in strain energy was insignificant.

The use of both explicit and approximate sensitivities optimisation methods provides accurate results when considering overconstrained mechanisms. The major advantage of the approximate method is that very complex mechanisms can be analysed. It is not necessary to structurally analyse the mechanism or explicitly determine the internal energy expression. With an accurate finite element model of the mechanism, one can approximate the internal energy expression of the mechanism. Determination of the strain energy sensitivities require repeated analysis of the finite element model. For three initial imperfections, a total of 57 ABAQUS runs are required. As more initial imperfections are introduced as variables, the number of finite element runs required to calculate the sensitivities at each optimisation iteration increases and computational effort becomes an issue.

The explicit sensitivities optimisation method requires only one ABAQUS run per iteration to determine the nodal displacements. Despite having to calculate the strain energy sensitivity as a sum of the members rather than as a whole mechanism, the determination of the explicit sensitivities is more direct and requires less computational effort than the approximate sensitivities optimisation method. The difficulty is determining the global stiffness matrix, K, and the strain displacement matrices for a complex mechanism. Calculation of these constants for the simple, overconstrained mechanism was straightforward because the mechanism is two-dimensional. The distribution of internal stresses allowed the use of truss elements. For three-dimensional mechanisms, such as the Bennett mechanism, the distribution of internal stresses is complicated, and K difficult to analytically determine. This process becomes more difficult with more complex tilings of the Bennett mechanism. Because ABAQUS does not output stiffness matrices as a result of processing, it can be concluded that the explicit sensitivities optimisation method is impractical for use with the Bennett Shelter.

The approximate sensitivities optimisation method requires a large number of analyses using ABAQUS, but can be applied to large, complicated mechanisms. Additionally, generating input programs in large numbers and writing a program to run analyses more quickly streamlines the computational process. This is the method that is used when analysing the Bennett Shelter.

6 Analysis of the Bennett Shelter with Imperfections

Understanding of the behaviour of the Bennett Shelter during deployment requires consideration of imperfections. Imperfections in the geometry of Bennett mechanisms violates the compatibility conditions discussed in Chapter 2 and leads to the development of internal stresses. These stresses are not restricted to the imperfect member. Rather, they distribute through the mechanism and can lead to stiff deployment. The procedure detailed in Chapter 5 provides a systematic method for determining the effect of imperfections on overconstrained mechanisms. Application of this procedure to the Bennett Shelter will allow the determination of the combination of imperfections resulting in the largest internal stresses. In Section 6.1 the numerical model for a single Bennett segment is developed. Different types of initial imperfections are explored, and methods for applying them to the model are examined. A single unit segment of the Bennett Shelter is analysed in Section 6.2. A two-unit Bennett segment is analysed in Section 6.3. Section 6.4 then discusses the results of the analysis.

6.1 Model Definition

Execution of the approximate sensitivities optimisation procedure detailed in Section 5.7 requires the development of a numerical model. Model generation can be broken down into three parts: development of nodal locations at different points in deployment, boundary condition definition and application of imperfections. Articulation of a single segment of the Bennett Shelter is described using the configuration variable ξ, as shown in Fig. 6.1 below:

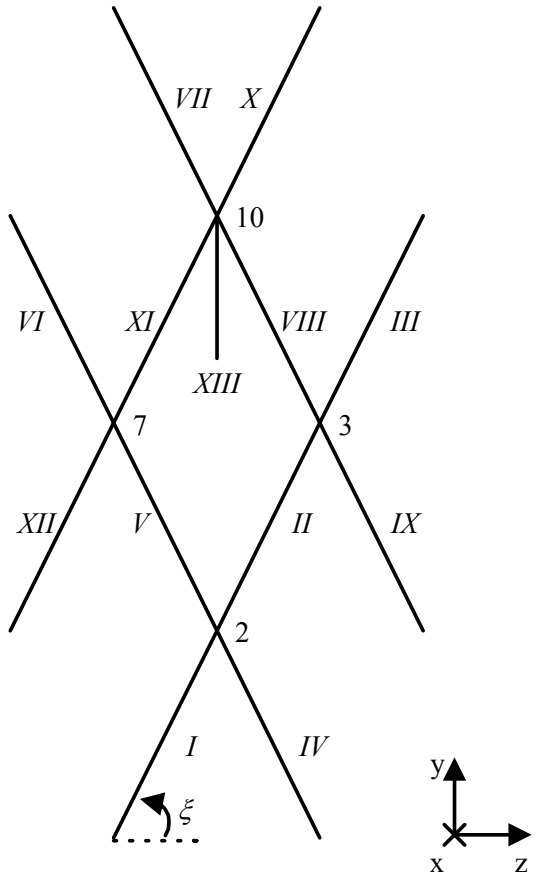


Fig. 6.1 One-unit Bennett segment

As ξ changes, the nodal locations change as well. To model this in ABAQUS, the members consisting of elements *I, II, III, IV, V,* and *VI* are defined in the y-z plane. They translate in plane for different values of the configuration variable and are, therefore, easily determined. Members defined by elements *VII, VIII, IX, X, XI* and *XII* both translate and rotate about joint axes 3 and 7. Application of the compatibility conditions of the Bennett mechanism provides the relationships needed to calculate nodal locations for these members at any point during articulation. The accuracy of this modelling process was visually verified using a physical model of the segment and the ABAQUS CAE postprocesser. Beam elements were used for the analysis in ABAQUS rather than the frame elements used in the structural analysis model. The analysis results are the

same, but use of beam elements allows for output of member internal energy by the postprocesser.

With member definition and nodal locations through deployment defined, it was necessary to determine boundary conditions that allow articulation of the mechanism and static analysis using ABAQUS. This was done by restraining all degrees of freedom of joints except those involved with the ideal motion of the mechanism. The boundary conditions for the one-unit Bennett segment were defined as follows: joints 3 and 7 were restricted in the x and y directions, nodes 2 and 10 were restricted in the z direction. These boundary conditions did not impede the motion of the mechanism. ABAQUS would not analyse the Bennett segment using these conditions because it identifies a singular stiffness matrix. For ABAQUS to statically analyse the model, it was necessary to add an extra member with a pinned support oriented in the direction of motion (element *XIII* in Fig. 6.1). This enabled the program to assess the mechanism as a statically indeterminate structure. During analysis of the mechanism, there should be zero forces in the extra bar. Otherwise, the structure being analysed will be different than the actual one.

The motion of the segment during deployment is quite complex. The correct orientation of the extra bar for each value of the configuration variable, ξ, was determined incrementally by rotating the extra member at node 10 about the z-axis. If the bar is correctly oriented, no stresses should develop in this extra bar. One orientation of the extra bar is shown in Fig. 6.2 below:

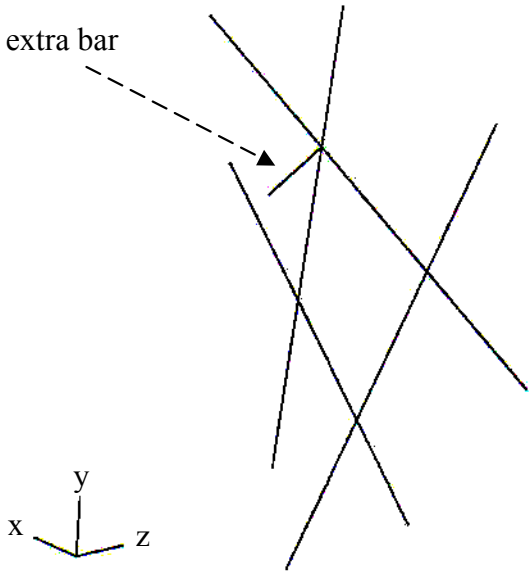


Fig. 6.2 Orientation of extra bar for ξ=60 °

Because it is difficult to determine the orientation exactly, residual stresses in the extra bar are unavoidable. The stress minimising orientation was found iteratively for each configuration. Forces carried by the extra bar and not the mechanism decrease the accuracy of the stress distribution in the mechanism. Lowering the stiffness of the extra bar decreases these stresses. When the modulus of elasticity of the bar is set equal to one, internal stresses in the member resulting from initial imperfections are approximately zero. They are accompanied by large deformations, but this is logical considering the change in stiffness. ABAQUS provides accurate member strain energy results when using the boundary conditions detailed above.

There are a number of possible manufacturing imperfections in the Bennett Shelter. They are skew angle error, joints aligned at an angle other than 90° with respect to the connected members and joints positioned incorrectly along the bar. Skew angle error consists of alignment error between drilled holes along bars to be connected at a joint. To allow connection of the bars and to meet compatibility conditions, it is

necessary to deform one of the bars by twisting to align the holes. Initial deformation of this type causes torsional stresses in the imperfect member. This can be defined as

$$\tau = \frac{\phi_i G r}{L} \tag{6.1}$$

where τ is the torsional stress, G is the shear modulus, r equals the inner or outer radius of the cross-section and L is the element length. This source of error is complicated because twisting a bar to correct an alignment error at one joint changes the alignment of the other pinholes along the bar. Thus, the initial stresses added to the numerical model are a function of two or more independent variables. For simplicity, this type of imperfection will not be considered.

Another type of imperfection arises from the incorrect inclination of joint holes with respect to the connected member. Revolute, pin jointed connections are oriented at 90 ° with respect to the connected member. Joint orientation varying from this will cause elastic interference in the mechanism. Internal bending stresses will develop if the mechanism is deformed to meet compatibility conditions. The strain induced in the imperfect member due to inclination of the joint with respect to the connected member is

$$\varepsilon = \frac{\delta}{L} = \frac{y}{r} = y\kappa \tag{6.2}$$

The initial stress that could be introduced into the perfect geometry of the numerical model is

$$\sigma = E\varepsilon = E\frac{\delta}{L} = E\frac{y}{r} \tag{6.3}$$

This type of imperfection is difficult to model numerically because bending stresses vary through the cross-section. The final type of possible imperfection is the incorrect positioning of a joint along the member. This would result in elements being either too

long or too short to meet compatibility. The stress induced in the element due to this type of imperfection is

$$\sigma = \frac{E\delta}{L} \tag{6.4}$$

Axial stresses are constant through the cross-section. They can be easily introduced to the cross-section, but the consideration of multiple imperfections in a single member introduces additional complexity into the numerical model. The imperfections used for the optimisation procedure are, therefore, single joint placement imperfections in each member.

The model for the one-unit Bennett segment is complete. Optimisation of imperfections in the one-unit segment and then consideration of a two-unit segment will allow the determination of whether or not it is possible to consider a larger structure. The computational effort of examining larger portions of the Bennett shelter and more imperfections makes consideration of the whole shelter infeasible. Application of the approximate sensitivities optimisation procedure to the one-unit model requires 33 ABAQUS runs for each iteration. Increasing the complexity of the model to two units increases the number of ABAQUS runs to 129. Even with programs to expedite this process, it is not possible to analyse larger segments. Generalising the results for repetitive subunits of the shelter may provide a method for estimating the worst-case set of imperfections for the entire shelter.

6.2 Analysis of Single Unit

The approximate sensitivities optimisation method was applied to the numerical model shown in Fig. 6.1. The element length was set at 0.775m and the cross-sectional area at $6.155*10^{-4}$ m^2. The material used was 6061-T6 aluminium, where $E=70*10^9$ Pa.

Four initial length imperfections were introduced in elements *II, V, VIII,* and *XI*. These initial strains, ε_{20}, ε_{50}, ε_{80}, and ε_{110}, are zero-valued initially and are restricted to +/- 0.10. Large initial strain ranges were chosen to provide observable energy variation during deployment. The step-size, λ, was set at 0.02, which is 10% of the difference between the maximum and minimum possible imperfections. Optimisation was conducted for ξ = 5, 15 and 30°. The results of the optimisations are shown in Tables 6.1-6.3 below.

Table 6.1 Approximate sensitivities optimisation for ξ=5°

Iteration	ε_{20}	ε_{50}	ε_{80}	ε_{110}	U (Joules)
1	$-1.29*10^{-5}$	$7.51*10^{-5}$	$8.88*10^{-6}$	$4.20*10^{-5}$	0.3571
2	-0.1	0.1	0.1	-0.1	$9.1251*10^{5}$
3	-0.1	0.1	0.1	-0.1	$6.6782*10^{5}$
4	-0.1	0.1	0.1	-0.1	$6.6782*10^{5}$

Table 6.2 Approximate Sensitivities Optimisation for ξ=15°

Iteration	ε_{20}	ε_{50}	ε_{80}	ε_{110}	U (Joules)
1	$-0.11*10^{-9}$	$0.0286*10^{-9}$	$-0.05*10^{-9}$	$0.122*10^{-9}$	$1*10^{-4}$
2	$-0.1343*10^{-6}$	$0.1323*10^{-6}$	$3.943*10^{-6}$	$-0.3928*10^{-6}$	$1.09*10^{-4}$
3	-0.1	0.1	0.1	-0.1	$6.6782*10^{5}$
4	-0.1	0.1	0.1	-0.1	$6.6782*10^{5}$

Table 6.3 Approximate Sensitivities Optimisation for ξ=30°

Iteration	ε_{20}	ε_{50}	ε_{80}	ε_{110}	U (Joules)
1	$-0.61*10^{-8}$	$0.5984*10^{-8}$	$0.0662*10^{-8}$	$-0.0567*10^{-8}$	$1*10^{-4}$
2	$-0.51*10^{-6}$	$0.23*10^{-6}$	$2.81*10^{-6}$	$-0.56*10^{-6}$	$2.3*10^{-4}$
3	-0.1	0.1	0.1	-0.1	$6.6782*10^{5}$
4	-0.1	0.1	0.1	-0.1	$6.6782*10^{5}$

For all three configurations, the solution converged after four iterations. For these points in deployment, the pattern of imperfections, as well as the strain energy values, were identical.

These results were unexpected. It was anticipated that there would be a variation of strain energy as ξ changed. Instead, both the pattern of imperfections and magnitude of the total strain energy remained constant. Additionally, the mechanism had negligible deformations. Optimisation of other configurations showed that the above results were the same for all values of the configuration variable. In order to clarify the behaviour of the numerical model, static equilibrium analysis was conducted using the member internal forces outputted by ABAQUS. Element internal forces in their local coordinate systems are shown in Table 6.4 below.

Table 6.4 Local element internal forces for ξ=15°

Element	Internal Forces (N)			Internal Moments (N-m)		
	shear n_1	shear n_2	axial	bending n_1	bending n_2	torque
II	58.1	-1.28	$-4.31*10^6$	78.96	0	40.33
V	-58.89	2.28	$4.31*10^6$	79.06	45.64	-46.55
VIII	-30.17	-5.34	$4.31*10^6$	81.17	21.1	45.83
XI	59.36	21.89	$-4.31*10^6$	79.69	-46.01	-45.09
XVII (extra bar)	77.63	35.15	6.55	6.8	25.88	-6.504

Note: directions n_1 and n_2 correspond to the local cross-sectional axes

This analysis showed that internal stresses in the bars were balanced. The axial forces corresponded, in fact, to the stresses caused by the maximum initial length imperfections imposed on each bar. In order to verify that the mechanism was in equilibrium, it was useful to conduct equilibrium analysis of joints 2 and 6 (see Fig. 6.1). The results of this analysis are shown in Table 6.5 below.

Table 6.5 Global Forces and Moments at the Top and Bottom of Joints 2 and 7

Joint	Global Forces (N)			Global Moments		
	shear n_1	shear n_2	axial	bending n_1	bending n_2	torque
Top of 2	1.2780	$-2.15*10^6$	$-3.73*10^6$	90.21	-1.67	0
Bottom of 2	-2.27	$2.15*10^6$	$3.73*10^6$	-90.21	1.6702	0
Top of 7	2.27	$-2.15*10^6$	$3.73*10^6$	45.64	91.73	0
Bottom of 7	-2.27	$2.15*10^6$	$-3.73*10^6$	-45.64	-91.73	0

The above results show that the forces and moments in the pins are in equilibrium. Analysis of other configurations yielded identical results. The conclusion to be drawn from the above results is that a pattern of imperfections exists such that internal stresses are balanced throughout deployment and there is no variation of internal stresses. Thus, the strain energy in the mechanism is constant for any value of the configuration variable.

To determine if this result was correct, it was useful to look at how stress distributed through the mechanism due to a single imperfection. A single length imperfection, ε_{20} = -0.0286, was introduced and static analysis was conducted using ABAQUS. The results at equilibrium, for ξ=15°, were ε_2 = -0.00715, ε_5 = 0.00715, ε_8= 0.00715 and ε_{110} = -0.00715. It can be seen that the initial stress due to the imperfection distributed through all interior elements in the mechanism (those without a free end). The pattern is the same as the maximum set of imperfections. To further investigate if the pattern of imperfections was, in fact optimal, static ABAQUS analyses were run for different values of the configuration variable using imperfection values as depicted in Fig. 6.3 below.

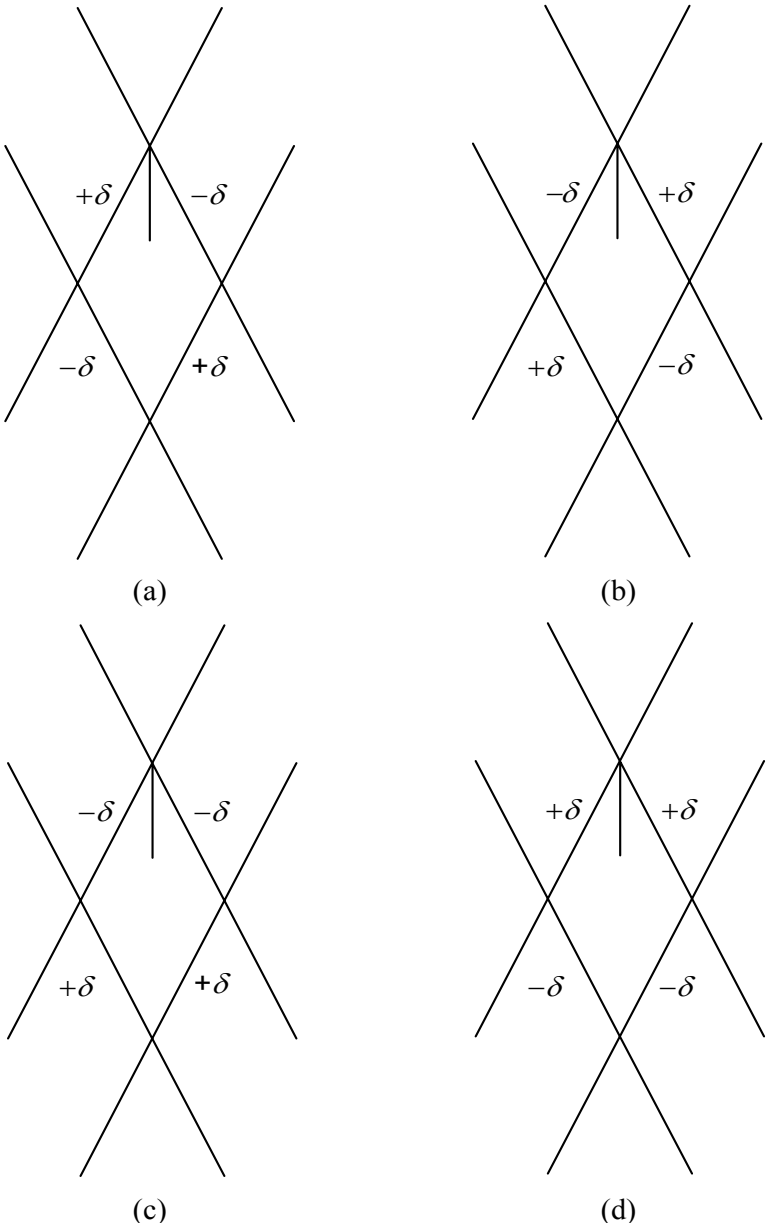


Fig. 6.3 Test patterns

Analysis of imperfection patterns (a) and (b) should both result in balanced internal stresses. If the patterns do not change and the strain energy results are the same for all analyses, then the proposition that there is a pattern of imperfections resulting in balanced internal stresses for any value of the configuration variable is validated. Analysis of both (a) and (b) resulted in a strain energy of $6.672 * 10^5$ J and negligible

deformations. Variation of the configuration variable did not alter these results, as was expected.

The results of analysing imperfection patterns (c) and (d) in ABAQUS should be equal to each other but less than the results from (a) and (b). This is because the patterns shown in (c) and (d) do not correspond to the balanced patterns of internal stresses shown in (a) and (b). Analysis of (c) and (d) yielded a strain energy value of 1196J for both patterns and was accompanied in both cases by large deflections. Additionally, there was variation in strain energy during deployment for both (c) and (d).

It can be concluded that when the pattern of initial imperfections matches the sign of the equilibrium pattern of deformations, there is a constant state of stress through deployment. This may occur because the boundary conditions restrict the deformation to the theoretically correct direction of deployment. These results could be valuable. If they hold for larger segments, the worst-case pattern of imperfections could be approximated.

6.3 Analysis of Two Units

The setup of the two-unit segment is similar to that of the single Bennett. The model is defined as shown in Fig. 6.4 below:

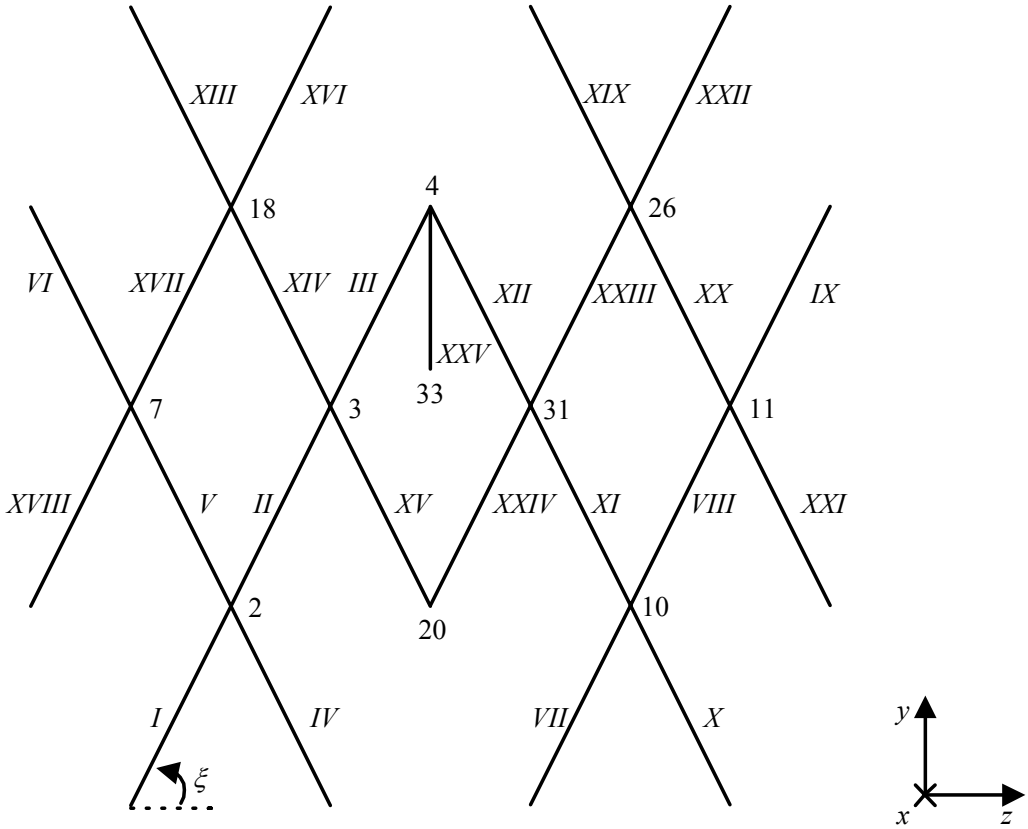


Fig. 6.4 Two-unit Bennett segment

The boundary conditions used initially for this model are as follows: nodes 3 and 31 are restricted in the x and y directions, nodes 4 and 20 are restricted in the z direction, and node 33 is pinned. For this analysis, only the middle Bennett mechanism comprised of elements *III, XII, XV* and *XXIV* was restrained to ideal motion. Length imperfections were introduced initially to members *II, V, VIII, XI, XIV, XVII*, *XX* and *XXIII*. These initial strains, ε_{20}, ε_{50}, ε_{80}, ε_{110}, ε_{140}, ε_{170}, ε_{200} and ε_{230} are restricted to +/- 0.10. Analysis of eight imperfection variables greatly increased the complexity of the analysis and the required computational effort. Consideration of larger segments is not practical, due to excessive processing time to analyse each optimisation step.

The results of analysis for eight imperfections were different than the one-unit Bennett segment. Extremely large deformations were observed, accompanied by small

strain energy values. Optimisation was not realistically possible, due to the poor results of the analysis. The reason for this result is the choice of boundary conditions. Restricting the middle members connecting the two units and introducing imperfections in unrestricted members caused the mechanism to deform almost without bound. This indicates that the mechanism was improperly restrained and ABAQUS identified it as an unstable structure. The boundary conditions were, therefore, redefined as follows: nodes 3, 7, 11 and 31 are restricted in the x and y directions, and nodes 4, and 20 were restricted in the z direction. Imperfections were introduced in the same manner as for the first set of boundary conditions.

Results of this analysis followed logically from the one-unit optimisation. The member strains were ε_2 = -0.067, ε_3 = -0.067 ε_5 = 0.067, ε_8= -0.067, ε_{11} = 0.067, ε_{12} = 0.067, ε_{14} = 0.067, ε_{15} = 0.067, ε_{17} = -0.067, ε_{20} = 0.067, ε_{23} = -0.067 and ε_{24} = -0.067. The total structure strain energy equaled $1.3356*10^6$ J. The pattern of imperfections in the shelter mirrored the one-unit solution for each segment and the strain energy result was twice that found in Section 6.2. These results stayed the same throughout the deployment of the two-unit segment.

6.4 Discussion and Conclusion

The results of the analysis of one-unit and two-unit Bennett segments can be generalised to larger tilings of the Bennett mechanism. As shown with the one-unit segment, when all constrained elements have initial imperfections and the pattern of imperfections matches the sign of the equilibrium pattern, strain energy is constant through deployment. Elements in the mechanism without free ends can be considered constrained. Analysis of a single imperfection in the one-unit Bennett segment showed that when the pattern of imperfections does not match the equilibrium pattern, internal

stresses distribute equally through all constrained elements with signs matching the equilibrium pattern.

Analysis of the two-unit segment validated the above conclusions. When boundary conditions were correctly configured, stress distributed evenly through the constrained elements in the mechanism. The internal energy due to eight initial imperfections in the two-unit mechanism was twice that due to four imperfections in the one-unit mechanism. This energy was constant for all values of the configuration variable. Thus, the internal energy due to initial imperfections in a large structure can be accurately determined through analysis of a segment of the mechanism and multiplication of the strain energy result by the number of segments. The strain energy in a constrained element in a large mechanism is equal to the total strain energy determined for the large mechanism, through analysis of a sub-unit, divided by the number of constrained elements. Using the above relationships, the strain energy within the Bennett Shelter due to initial length imperfections can be accurately determined.

7 Concluding Remarks

The aim of this dissertation was to develop a new type of deployable, long-span shelter frame called the Bennett Shelter because it is based upon tiled Bennett linkages. Consideration was given to both the deployed configuration and behavior during deployment. This chapter details the main achievements in the development of the shelter concept and highlights future work needed.

7.1 Achievements

The first effort of this dissertation was to determine the geometric properties of the deployed configuration of the Bennett Shelter. The configuration of the mechanism most applicable to shelter applications has a barrel vault profile with end members at 90° with respect to the ground. The required length, width, and height of the shelter can be specified for a given application. A procedure to determine the geometrical properties of a Bennett Shelter for any set of user dimensions has been developed and validated through the construction of a large prototype.

In order to demonstrate the usefulness of the Bennett Shelter for long-span applications, extensive structural analysis has been conducted. This included consideration of serviceability, stress in both members and joints and the structure's response to buckling and frequency. The example used for the analysis was a shelter capable of accommodating the Apache Longbow Helicopter. Its dimensions are 20.55m long by 7m high by 12.61m long. It was found that serviceability was the controlling design criterion. As there are a number of geometrically possible configurations of the shelter that meet design requirements, it was necessary to determine the most efficient configuration. Weight and the density of the tiling of Bennett mechanisms are the variables used to evaluate different possible shelters. Conducting serviceability analysis

for the family of geometrically possible shelters allowed the determination of the most efficient shelter for the given set of user-defined dimensions.

Successful stress analysis of both member and joints demonstrated that the Bennett Shelter was viable using steel, aluminum or carbon fibre composite laminates. The shelter was not susceptible to failure due to buckling. Frequency analysis revealed that the structure had a natural frequency of 0.677Hz, which is lower than the standard excitation of 2 to 6Hz. Additional reinforcement is needed in order to increase the stiffness of the structure for applications with vibratory loading. Examination of mode shapes from frequency and buckling analysis revealed that the frame behaves under load in a manner similar to membrane structures. Unlike other deployable shelters, the Bennett Shelter is single-layer. In large applications, numerical analysis demonstrated that it behaves more like a reticulated shell structure.

The deployment of the Bennett Shelter was explored using analytical and numerical methods. As a foldable structure, it should be ideally stress-free. The presence of manufacturing imperfections causes internal stresses that lead to stiff deployment or even a loss of mobility. Using energy methods, explicit functions describing the variation of internal energy during deployment were derived for a simple overconstrained mechanism. These functions, which are dependent only on the initial imperfections, were then optimised using mathematical programming. The results of the optimisation provided the pattern of imperfections causing the maximum internal energy in the simple, overconstrained mechanism.

In cases of combined loading or calculation in three dimensions, it can be difficult to express the strain energy or complementary strain energy of the mechanism in a single expression. For these instances, it was necessary to develop a procedure for

approximating internal energy through deployment. The approximate energy expressions could then be optimised using mathematical programming.

Two methods were developed to approximate the internal energy of an overconstrained mechanism during deployment: the approximate and explicit sensitivities optimisation methods. Both methods make use of a Taylor expansion to express the energy function. The approximate sensitivities optimisation method uses finite differences to approximate the sensitivity of the function to the independent variables, while the explicit sensitivities optimisation method derives expressions for the sensitivities analytically. It was found that both methods accurately approximated the energy function for simple overconstrained mechanisms. Due to the complexity of the analytical derivations, the explicit sensitivity method was impractical for large, complicated mechanisms.

For this reason, the approximate sensitivity method was applied to the Bennett Shelter. Analysis of the variation of internal energy within a single-unit segment showed that a pattern of imperfections exists that leads to a constant, maximum internal energy value throughout deployment. This pattern results in balanced internal forces within constrained elements of the mechanism. Analysis of a two-unit segment yielded similar results. These results for sub-units of the Bennett Shelter can be generalised across the entire structure to determine the worst-case internal energy and pattern of imperfections.

The construction of a large prototype of an arch composed of tiled Bennett mechanisms by ABLY Shelters provided insight into the behavior of the Bennett Shelter. It was found that inaccuracies in fabrication have a large effect on the stiffness of the frame. Holes drilled for pinned connections that were larger than the specified joint sizes resulted in inordinately large deflections. It was established that the presence of imperfections did lead to an internal energy minimising shelter configuration. The

model's behaviour showed that imperfections would cause the structure to move towards a particular configuration. Although the equilibrium and compatibility are achieved throughout the deployment, the value of the minimum strain energy at each configuration is different. The stable configuration has the smallest internal energy.

The analysis completed in this thesis provides an understanding of the behaviour of the Bennett Shelter during deployment and when deployed. It combines practical design considerations of the shelter as a deployed structure with more theoretical considerations of geometry and the effect of imperfections. These results show that the Bennett Shelter is viable as a long-span deployable shelter.

7.2 Future Work

The research conducted in this study opens up many areas for future study. Geometrical analysis of configurations of the Bennett Shelter where ground-level segments are not at 90° with respect to the ground is necessary. This will allow application of the concept to shallow vaulted structures that are often used in more permanent applications, such as roof structures. As new tile patterns for the Bennett mechanism continue to be developed at Oxford University, geometrical analysis of deployed configurations should be expanded. This will allow for flexibility in the shape of the deployed configuration.

Construction of a large prototype of the shelter is necessary. Performance of load testing will validate and improve the numerical model. Design and testing of joints will allow joint rigidities to be integrated into the numerical model. The performance of different types of joints, such as pinned connections and swivel couplers, in prototypes will provide information about which type of joint to use in the shelter and what

manufacturing tolerance is required to ensure smooth deployment and avoid structural deflection due to loose joints.

Specific carbon fibre composite designs should be developed for the Bennett Shelter. As internal forces in the shelter are known, the lay-up of the member cross-section can be developed. Practical considerations involved with building these shelters and the procedure for deploying them can also be determined through the construction of a prototype.

Finally, compilation of statistical information about the actual occurrence of imperfections in manufactured components will allow the determination of a probability distribution for imperfections in the Bennett Shelter. This can then be used to find a representative number of imperfections that can be expected in a shelter and a design variation of internal energy through deployment.

References

ABLY Shelters, LVRE Shelter-Lightweight, Very Rapid Erect Shelter, http://www.ablyshelters.co.uk/.

American Institute of Steel Construction (AISC) (1980), *Manual of Steel Construction: Allowable Stress Design*, 5-18 to 5-28.

American Institute of Steel Construction (AISC) (1998), *Load & Resistance Factor Design*, Volume 1, 2-5 to 2-7 and 6-30 to 6-31.

American Institute of Steel Construction (AISC) (1998), *Load & Resistance Factor Design,* Volume 2, 8-7 to 8-25.

AMC Pamphlet 36-1 (1995), U.S. Army Air Mobility Command.

ASCE 7-95: Minimum Design Loads for Buildings and Other Structures (1996), American Society of Civil Engineers, 15-45.

Ashby, Michael F. (1999), *Material Selection in Design*, Butterworth-Heinemann, 2nd Edition.

Baker, E.J. (1979), The Bennett, Goldberg, and Myard Linkages - in perspective, *Mechanism and Machine Theory*, 14, 239-253.

Baker, E.J. and M. Hu (1986), On spatial Networks of overconstrained Linkages. *Mechanism and Machine Theory*, 21(5), 427-437.

Beggs, J. (1966), *Advanced Mechanism*, Macmillan, New York.

Belda, E.P. (1996), Constructive Problems in the Deployable Structures of Emilio Perez Pinero, in: *Mobile and Rapidly Assembled Structures II*, Computational Mechanics Publications, 1996, 23-34.

Bennett, G.T. (1903), A new Mechanism, *Engineering*, 76, 777-778.

Bricard, R.: Leçons de cinématique. *Tome II Cinématique Appliquée*, Gauthier-Villars, Paris, 1927, 7-12.

British Standard BS1139: Metal Scaffolding (1991), British Standards Institution.

Carradine, D.M. (1998), Experiments on the Response of Arch-Supported Membrane Shelters to Snow and Wind Loading, Masters Thesis, Virginia Polytechnic Institute and State University.

Crawford, R. and J. Hedgepeth: Effects of Initial Waviness on the Strength and Design of Built-up Structures. *AIAA Journal*, Vol. 13, No. 5, 1975.

Dhande S.G. and J. Chakraborty (1973), Analysis and Synthesis of Mechanical Error in Linkages - A Stochastic Approach, *Journal of Engineering for Industry, Transactions of ASME*, Series B, Vol 95, No 3, 672-676.

Chatterjee, G.B. and A. K. Mallik (1997), Mechanical error of a four-bar linkage coupler curve, *International Journal of Mechanism and Machine Theory*, 22, 85-88.

Chen, Y. (2003), Design of Structural Mechanisms, Doctoral Dissertation, University of Oxford.

Chen Y. and Z. You (2001), Network of Bennett Linkages as Deployable Structures, presentation paper, AIAA 2001-4661 by AIAA Space 2001 Conference and Exposition, 28-30.

Chen Y. and Z. You (2001), Deployable Structural Element Based on Bennett Linkages, presentation paper, 2001 American Society of Mechanical Engineers International Congress, 11-15.

Cook, R.D. (1981), *Concepts and Applications of Finite Element Analysis, Version 2,* John Wiley & Sons, New York.

Delassus, E. (1922), Les chaînes articulées fermées et déformables à quatre membres, *Bulletin des SciencesMathématiques*, 2nd series, 46, 283-304.

Denavit, J. and R.S. Hartenberg (1955), A Kinematic Notation for Lower Pair Mechanisms, in Journal of Applied Mechanics, Vol. 22, 215-221.

Dent, R.N. (1970), *Principles of Pneumatic Architecture*, The Architectural Press, London.

Derby, B., D.A. Hills and C. Ruiz (1992), *Materials for Engineering*, Longman.

DHS Systems LLC: DRASH, Deployable Rapid Assembly Shelter, http://www.drash.com.

Drabble, G.E. (1990), *Dynamics*, MacMillan Press, Ltd.

Escrig F. and J.P. Valcarcel (1986), Analysis of Expandable Space Bar Structures, in: Heki, H.: IASS Symposium on Membrane Structures and Space Frames, Elsevier Science Publishers, 269-284.

Escrig, F. (1996), General Survey of Deployability in Architecture, in: *Mobile and Rapidly Assembled Structures II*, Computational Mechanics Publications, 3-21.

Escrig, F. and J.P. Valcarcel (1998), Roofing Geometry of Deployable X-Frames, *International Journal of Space Structures*, 13(1), 1-12.

Fletcher, R. (1981), *Practical Methods of Optimization*, John Wiley & Sons, Ltd., New York.

Gantes, C. (1996), A Creative Aspect of a Destructive Phenomena: Using Snap-through Buckling as a form of Prestressing, *IASS/IABSE International Symposium on Conceptual Design of Structures*, vol. I, Stuttgart, Germany, 222-229.

Gantes, C., J.J. Connor, and R.D. Logcher (1991), Geometric and Structural Design Considerations for Deployable Space Frames, in: Bulson, P.S., *Rapidly Assembled Structures*, Computational Mechanics Publications, U.K., 249-259.

Gantes, C. (2001), *Deployable Structures: Analysis and Design*, WIT Press, Boston.

Gea, H. and Jianhui Luo (2001), Topology Optimization of Structures with Geometrical Nonlinearities, *Computers and Structures, 79*, 1977-1985.

Gioncu, V. (1995), Buckling of Reticulated Shells: State-of-the-Art, in: *International Journal of Space Structures*, 10(1), 1-46.

Goh, J.K.S. (1998), Analysis of Pressurized Arch Shells, Masters Thesis, Virginia Polytechnic Institute and State University.

Goldberg, M. (1943), New Five-bar and Six-bar Linkages in three Dimensions, *Transactions of the ASME*, 65, 649-663.

Hernandez, C. H. (1996), New Ideas on Deployable Structures, in: Escrig, Felix, *Mobile and Rapidly Assembled Structures II*, Computational Mechanics Publications, U.K., 63-72.

Hibbitt, Karlson, and Sorenson (2002), *ABAQUS, version 6.3, User's Manual*. Pawtucket, RI, USA.

Hummel, S.R. and Chassapis, C. (2000), Configuration design and optimization of universal joints with manufacturing tolerances, *Mechanism and Machine Theory*, Vol 35, 463-476.

Kaveh, A. and A. Davaran (1996), Analysis of Pantograph Foldable Structures, *Computers and Structures*, 59(1), 131-140.

Kennedy H. (2001), Combat Troops Pitch a New Generation of Field Shelters, National Defense Magazine, http://www.nationaldefensemagazine.org/article.cfm?Id=573.

Kim, J.Y., R.H. Plant and T.-J. Kwun (1998), Analysis of Tent-Like Structures supported by Pressurized Fabric Arches, in: *Lightweight Structures in Architecture, Engineering and Construction* (LSA98), Vol. 2, 821-829.

Kirsch, Uri (1981), *Optimum Structural Design*, McGraw-Hill Book Company, New York.

Krishnapillai, S. and W.P. Zalewski (1985), *The Design of Deployable Structures*, Unpublished Research Report, Department of Architecture, MIT, Cambridge, Massachusetts, USA.

Kuznetsov, E. (1991), *Underconstraint Structural Systems*, Springer-Verlag, New York.

KFOR Online News Archive (1999), http://www.kforonline.com/news/archive_1999.htm.

Langbecker, T. (2000), Kinematic and Non-Linear Analysis of Foldable Scissor Structures, DPhil diss., University of Queensland.

Lee, S.J. and B.J. Gilmore (1991), Determination of the probabilistic properties of velocities and accelerations in kinematic chains with uncertainty, *Journal of Mechanical Design*, 113(1), 84–90.

Manfield, P. (2000), Modeling of a Cold Climate Emergency Shelter Prototype and a Comparison with the United Nations Winter Tent, MPhil diss., University of Cambridge.

Mavroidis, C. and B. Roth (1994), Analysis and Synthesis of Overconstrained Mechanisms, Mechanism Synthesis and Analysis, Proceedings of the 1994 ASME Design Technical Conferences, Minneapolis MI, DE- 70, 115-133.

Mavroidis C. and M. Beddows (1997), A Spatial Overconstrained Mechanism That Can Be Used In Practical Applications, Proceedings of the 5th Applied Mechanisms and Robotics Conference, Cincinnati, OH.

Melin, N. and R. Workman (2000), Large Area Maintenance Shelter Foundation Design: CE489 Project Report, United States Military Academy.

Mohan, P. and R.K. Kaponia (1998), Analysis of General Shells under Deformation Dependent Pressure Loads using a Flat Triangular Shell Element, in: Proceedings of the 39th Structures, Structural Dynamics and Materials Conferences, AIAA, Reston, VA, 534-541.

Myard, F.E. (1931), Contribution à la géométrie des systèmes articulés, *Societe mathématiques de France*, 59, 183-190.

Pellegrino, S. (1995), Large Retractable Appendages in Spacecraft, *Journal of Spacecraft and Rockets*, 32(6), 1006-1014.

Perez, A. and J.M. McCarthy (2000), Dimensional Synthesis of Bennett Linkages, Presentation Paper, 2000 ASME Design Engineering Technical Conference, 1-8.

Army Soldier Biological and Chemical Command (2001), Performance Specification: Modular General Purpose Tent System (MGPTS), U.S. Natick, MA.

Phillips, J. (1990), *Freedom in Machinery*, Volume 2, Cambridge University Press, Cambridge.

Przemieniecki, J.S. (1968), *Theory of Matrix Structural Analysis*, Dover Publications, Inc., New York.

Raghavan, M. and B. Roth (1990), A general solution for the inverse kinematics of all series chains, *RoManSy 8*,Warsaw, Nowowiejska, 24-31.

Roark, Raymond J. (1976), *Formulas for Stress and Strain*, McGraw-Hill, London.

Rosenfeld, Y., Y. Ben-Ami and R.D. Logcher (1993), A Prototype "Clicking" Scissorlink Deployable Structure, *International Journal of Space Structures*, 8 (1,2), 85-95.

Sanchez, J., F. Escrig, and J.P. Valcarcel (1996), The Adventure of Covering a Swimming-Pool with an X-Frame Structure, in: *Mobile and Rapidly Assembled Structures II*, Computational Mechanics Publications, 113-122.

Sarrus, P.T. (1853), Note sur la transformation des mouvements rectilignes alternatifs, en mouvements circulaires, et reciproquement, *Académie des Sciences*, 36, 1036-1038.

Shan, W. (1992), Computer Analysis of Foldable Structures, *Computers and Structures*, 42(6), 903-912.

Shigley, J. E. and J. J.Uicker, Jr. (1980), *Theory of Machines and Mechanisms*, McGraw-Hill, New York.

Tauchert, T. R.(1974), *Energy Principles in Structural Mechanics*, McGraw-Hill, Tokyo.

Teal, M.J. (1996), Deployable Roof Structure, Fourth Year Project in Group A, University of Cambridge.

Ting, K. (2000), The Effects of Joint Clearance on Position and Orientation Deviation of Linkages and Manipulators, *Mechanism and Machine Theory*, 35, 391-401.

Ugural, A.C. and S.K. Fenster (1995), *Advanced Strength and Applied Elasticity*, Prentice Hall PTR, Upper Saddle River, New Jersey 07458.

U.S. Army Soldier and Biological Chemical Command-Natick Soldier Center: Department of Defense Standard Family of Tactical Shelters (Rigid/Soft/Hybrid) (1999), Joint Committee on Tactical Shelters (JOCOTAS) Brochure, 24-34.

Waldron, K.J. (1968), Hybrid overconstrained Linkages, *Journal of Mechanism*, 3, 158-164.

Zeigler, T.R. (1976), Collapsible Self-Supporting Structure, U.S. patent 4026313, issued May 31, 1977.

Appendix 1: Standards for Shelter Structure

Pallet Size Limits
U.S. 463L Pallet
2.4616m L x 2.1336m W x 2.4384m H
104" L x 84" W x 96" H
(height varies based on aircraft)
U.K. Palletized System
Type 1: 1.3208m L x 1.0922m W x 1.524m H
52" L x 43" W x 60" H
Type 2: 2.4616m L x 1.0922m W x 1.524m H
104" L x 43" W x 60" H

Environmental Loads
Snow Load: 10 lb/ft^2 for max. 12 hours
Wind Load: 55 mph for 5 minutes
65 mph in any direction for 10 seconds
Setup in winds up to 25 mph
Rain: 2" per hour for 30 min w/o leakage (w/o liner)
Wind Driven Rain: 2" per hour for 30 min w 55mph winds
Sunlight: Withstand exposure to direct sunlight for 18 months
Temp 160 degrees Fahreheit w/o degradation
Temperature: -60 to 120 degrees Fahrenheit

Army Ergonomic Requirements
Stovepipe Shield: A stovepipe shield shall permit the passage of a 4" diameter stovepipe through the roof. The fabric must be able to withstand temperatures up to 600 degrees Fahrenheit. The opening shall be no less than 48" from the side walls, end walls, or liner partitions.

Liner system: The liner subsystem shall provide an air gap between the liner and the fabric subsystem to improve the thermal performance of the system.

Flame resistance: The fabric elements shall be flame resistant, self-extinguishing and shall have no flaming melt drip or molten pieces when exposed to flame.

Zippers and Lanyards: The MGPTS shall be inspected for any components attached by lanyards or any loose nuts, bolts, or pins. Also, no zippers shall be used with the MGPTS.

Mechanical Shock and Vibration/Rough handling: The MGPTS must withstand rough handling by military personnel, to include being stepped on by soldiers, components being dropped or thrown from trucks onto hard ground.

Varying Terrain: Must be useable on both prepared and unprepared surfaces, and be useable on uneven terrain with local variations in ground elevation up to 6 inches.